Molecular Inflammation Research Group
Department of Medical Biology
University of Tromsø

Oncolytic Activity and Mechanisms of Action by a small $\beta^{2,2}$-amino acid derivative LTX-401

—

Brynjar Mauseth

Master Thesis in Medical Biology [Master in Biomedicine] May 2015

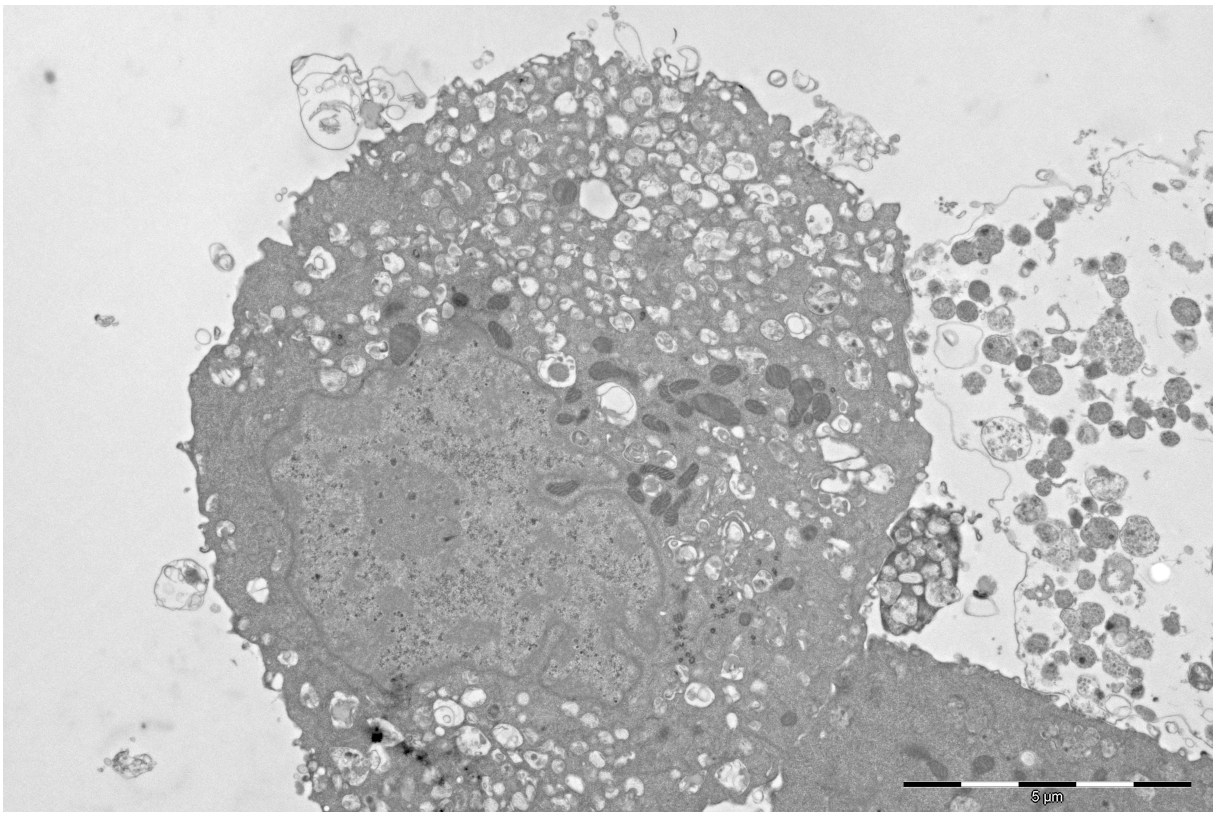

Intentionally left blank

Front cover: B16F1 murine melanoma cell succumbing to death by treatment with LTX-401

Acknowledgement

The work presented in this thesis has been carried out in the period March 2014 to May 2015 at the Molecular Inflammation Research group, Institute of Medical Biology, The Arctic University of Norway, Tromsø.

I would first like to express my gratitude towards my supervisor and mentor Professor **Baldur Sveinbjørnsson** for believing in me and allowing me to work in such an exciting area of cancer research. Your guidance, encouragement and availability throughout the course of my master's degree project have been most appreciated.

Ketil. A. Camilio, my co-supervisor. Thank you for always keeping your door open to answer any of my questions regarding work in the laboratory. Your critical reading and pointers has greatly shaped and influenced my scientific writing and way of thinking.

Liv-Marie Eike, thank you for your collaboration, valuable discussions and support.

To the rest of my group – **Ugo Moens, Conny Tümmler, Igor Snapkov, Maria Ludvigsen, Gianina Dumitriu, Kashif Rasheed** and **Nannan Yang –** thank you for being so welcoming, enjoyable and helpful.

Finally I would like to thank **Randi Olsen** and **Tom Ivar Eilertsen** at the Electron Microscopy Department for providing me necessary skills to pursue this field independently.

Brynjar Mauseth

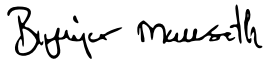

Tromsø, May 2015

Abstract

Antimicrobial peptides are part of the innate immune defence of many organisms and represent a novel class of therapeutics due to their broad-spectrum activities, including cytotoxic activity against cancer cells. It has recently been reported that small antimicrobial $\beta^{2,2}$-amino acid derivatives (Mw<500), such as LTX-401, possess potent anticancer activity against Ramos human Burkitt's lymphoma cells. In the present thesis, the anticancer properties displayed by LTX-401 became subject for a continued investigation. *In vitro* cytotoxicity studies revealed that LTX-401 was highly active against a panel of malignant cells including murine and human cancer cell lines. Moreover, LTX-401 was found to induce known features of immunogenic cell death as shown by the release of Damage-Associated Molecular Pattern molecules such as High-Mobility Group Box-1 protein, adenosine triphosphate and cytochrome *c in vitro*. Intralesional administration of LTX-401 into intradermally established B16 melanomas in syngeneic mice resulted in complete regression of the tumor. Moreover, cured animals that were given a second tumor challenge with live B16F1 cells did not develop tumor and displayed immune protection against the cancer. Altogether, these results underscore the therapeutic potential of LTX-401 in conveying local tumor control and generation of protective immunity, presumably by the engagement of immunogenic cell death.

Table of contents

Abbreviations

ACP	Anticancer peptide
AMP	Antimicrobial peptide
APCs	Antigen-presenting cells
ATP	Adenosine triphosphate
CRT	Calreticulin
CTLs	Cytotoxic T cells
DAMPs	Damage-associated molecular pattern molecules
DCs	Dendritic cells
DMSO	Dimethyl sulfoxide
DTT	Dithiothreitol
EDTA	Ethylene diamine tetraacetic acid
EGTA	Ethylene glycol tetraacetic acid
ER	Endoplasmic reticulum
EM	Electron microscopy
EtOH	Ethanol
FA	Formaldehyde
FBS	Fetal bovine serum
GA	Glutaraldehyde
HCl	Hydrochloric acid
HEPES	(4-(2-hydroxyethyl)-1-piperazineethanesulfonic acid)
HMGB1	High-mobility group box protein 1
HRP	Horseradish peroxidase
ICD	Immunogenic cell death
i.d	Intradermal
IFN-γ	Interferon-gamma
IL	Interleukin
LfcinB	Lactoferricin
MTT	3-(4,5-dimethylthiazol-2-yl)-2,5-diphenyltetrazodium bromide
MyD88	Myeloid differentiation primary-response protein 88
NLRP3	NOD-like receptor family pyrin domain containing-3 protein
NLRs	NOD-like receptors
PAMPs	Pathogen-associated molecular pattern molecules
PBS	Phosphate buffered saline
PDVF	Polyvinylidine fluoride
PHEM	PIPES, HEPES, EGTA, $MgCl_2$
PIPES	[Piperazine-N,N′-bis(2-ethanesulfonic acid)]
RAGE	Receptor for advanced glycation end products
RBCs	Red blood cells
RLU	Relative luciferase units
ROS	Reactive oxygen species
RPMI	Roswell park memorial institute medium
SAR	Structure-relationship
SDS	Sodium dodecyl sulphate
TBS-T	Tris buffered saline (with tween)
TEM	Transmission electron microscopy
TLRs	Toll-like receptors
TNF-α	Tumor-necrosis factor alfa
Tregs	Regulatory T cells

Intentionally left blank

1. Introduction – Antimicrobial peptides

Multicellular organisms fend off a broad spectre of pathogens in a variety of ways resolving around immunological detection followed by protective immune responses. As an adaptive immune response requires the delayed actions of antigen-presentation and clonal proliferation of immunocytes, the evolutionary conserved mechanisms exerted by the innate immune system functions as an initial barricade, thus establishing a front line defence against foreign organisms. Integrated in this barricade are antimicrobial peptides (AMPs), which are highly evolutionary conserved molecules with broad antimicrobial activity, capable of eliciting early non-specific immune reactions towards a large spectre of pathogens such as bacteria, fungi, viruses and parasites [1-3]. In mammals, AMPs are often referred to as host-defence peptides based on their ability to modulate innate immune responses in addition to exert direct antimicrobial killing [4, 5]. Additionally, they are found in lower vertebrates such as amphibians, but also crustaceans, insects and even plants and fungi [6, 7]. To date, the Antimicrobial Peptide Database contains almost 2500 entries of naturally isolated AMPs displaying a wide variety of cytotoxic activities [8] and numbers are growing. Common features of AMPs include being relatively short, between 12-50 amino acid residues in length [1, 9], possessing the ability to adopt diverse amphipathic structures containing both hydrophobic and cationic regions [10, 11]. The elevated portions of basic amino acids such as lysine, arginine and histidine contrary to acidic residues (e.g glutamate or aspartate), yields a positive net charge typically varying between +2 and +9 [2, 12-14]. These characteristics enable AMPs to non-specifically interact with negatively charged microbial membranes, thus leading to membrane permeabilization/destabilization and lysis [15]. The swift mode-of-action also decreases the probability of resistance development, which is why AMPs, either naturally occurring or synthetic, are considered a highly promising approach towards the issue of antibiotic resistant bacteria [16-18].

Despite extensive sequence variability making up for a diversity of structurally different motifs, AMPs are normally divided into three classes based on their three-dimensional conformation (fig. 1.1) [19-21]; The first class is composed of linear peptides capable of adopting an amphipatic α-helical structure in a hydrophobic environment. Well-studied peptides from this class include the cecropins and magainins found in the Cecropia moth and

the African clawed frog, respectively [22]. Both peptides possess broad antimicrobial properties against a panel of both Gram-negative and positive microorganisms [22]. The human cathelicidin LL-37 also exhibits potent antimicrobial activity in addition to aid in regulation of the inflammatory response, chemoattraction of immune effector cells to wound sites and neutralization of the lipopolysaccharide component of Gram-negative bacterial cell walls [23]. As with cecropins and magainins, LL-37 also adopts an α-helical structure in a hydrophobic environment [24], a property believed to be responsible for their spontaneous insertion into membranes followed by membrane disruption [11, 25].

The second class of AMPs consists of β-sheet peptides rich in cysteine residues that aid in stabilization by forming disulphide bonds. A well-known example from this class include the defensins, an evolutionary conserved group of vertebrate peptides that has received considerable attention and appreciation for its widespread ability to either suppress growth or exert direct killing of various bacterial strains [24, 26]. Defensins are further categorized into the subfamilies of α-and β-defensins according to structural differences deriving from alignment of the disulphide bridges [27, 28].

Finally, the third class of AMPs involve peptides containing high proportions of certain amino acids such as proline, histidine, arginine and tryptophan that make up for highly variable secondary structures differing from the regular α-helical and β-sheet peptides [19, 29]. AMPs of this class are normally linear, although some may form extended coils [19]. However, as the available literature regarding this subject is rather limited, the structural behaviour of this class along with the mechanisms and selectivity criteria by which they kill target cells, is still a controversial subject. Nevertheless, one of the few well-documented examples include the AMP indolicidin, a small molecules of only 13 amino acids containing 5 tryptophan residues. Indolicidin has been shown to form an extended “boat-shaped” conformation upon interaction with biological membranes, including dodecylphosphocholine, a lipid often used in model membrane systems such as micelles [30].

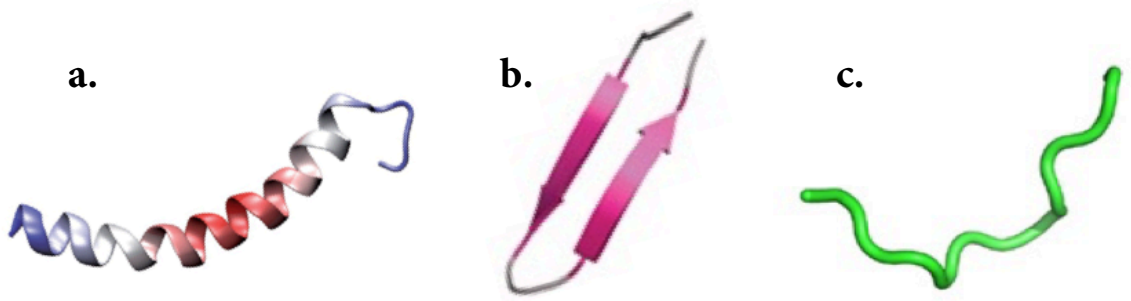

Fig. 1.1 Secondary structural overview of the major classes of antimicrobial peptides including **(a)** α-helices, **(b)** β-sheets and **(c)** linear/extended structures. Figure was designed by adapting partial images from [35-37].

Along with the numerous studies establishing a membrane-disrupting and permeating role of AMPs, emerging evidence also describes a potential immunomodulatory role, such as the stimulation of pro-inflammatory cytokines, suppression of anti-inflammatory mediators and modulation of both innate and adaptive immune cell differentiation [31-34]. In addition to their widespread bactericidal effects, a growing number of studies also suggest that several AMPs display cytotoxic activity against cancer cells, and are consequently referred to as anticancer peptides (ACPs).

1.1 Anticancer peptides – Determinants of efficacy

The ability of ACPs to kill cancer cells is a property believed to derive from biochemical features such as amphipathicity, cationicity and the secondary structure, allowing for membrane interactions that potentially causes loss of integrity and cell death [38, 39]. Most ACPs adopt either an α-helical (α-ACPs) or β-sheet (β-ACPs) conformation, albeit some linear and extended forms (E-ACPs) exist such as PR-39 (table. 1.1) [38, 40, 41]. Moreover, ACPs are divided into two major categories depending on their cell specificity. The first category includes ACPs that are only active against cancer cells, while not being cytotoxic against normal mammalian cells. The second category encompasses APCs that display cytotoxic activity against both cancer and non-cancerous cells alike [42]. Despite still being a subject of debate, the mechanisms that allow for selective killing by ACPs seems to rely on fundamental differences in the plasma membrane composition on cancer cells compared to normal cells. The former often carries a higher net negative charge of their plasma membrane, thus rendering them susceptible for the potential electrostatic interaction with membrane disruptive cationic peptides. Components that contribute to the higher than normal anionicity

of cancer cells include elevated expression of phosphatidylserine [43, 44], sulfated glycosaminoglycans like heparin sulfate [45, 46] and O-glycosylated mucins [45, 47,]. In contrast, the plasma membrane of normal mammalian cells predominantly consists of zwitterionic components such as sphingomyelin and phosphatidylcholine [48, 49], thus conferring them an overall neutral charge that reduces the capacity of ACPs to bind via electrostatic forces. Moreover, cancer cells often have a greater membrane fluidity and increased surface area due to an abundance of microvilli on their plasma membrane [50, 51], which enables both membrane insertion and binding of more ACP molecules. It has been suggested that elevated levels of cholesterol-rich lipid rafts in normal eukaryotic cell membranes decreases the rate of peptide insertion, thereby reducing the cytolytic effect of membrane active peptides in general as membrane fluidity is reduced [52]. Consistent with this suggestion, recent studies have provided evidence of certain breast and prostate cancer cell lines possessing high levels of plasma membrane cholesterol [53-55], which may potentially inhibit binding and lysis by ACPs. To summarize, the interaction of ACPs with cancerous and non-cancerous cells is governed by differences in membrane composition resulting in a net negative charge and higher transmembrane potentials, increased membrane fluidity and surface area of neoplastic cells. These characteristics may collectively account for the specificity of some ACPs against cancer cells, while simultaneously sparing the healthy counterpart.

Table. 1.1. Naturally occurring ACPs

	Peptide name	Selectivity[1]	References
α-helical peptides	Cecropin A	Yes	59
	Cecropin B	Yes	58
	Dermaseptin B2	Yes	57
	LL-37	No	60
	Magainin 2	Yes	61
	Temporin-1CEa	Yes	62
β-sheet peptides	HNP 1-3	No	38
	LfcinB	Yes	56
	Tachylepsin	No	63, 64
Linear peptides	PR-39	Nd[2]	65, 66

1=normal vs cancer cells

2=not determined

1.2 Mode of action of ACPs – Membranolytic and non-membranolytic

The negatively charged outer surface of cancer cell membranes is also an inherit characteristic displayed by bacterial cells, which led to the assumption that ACPs interact with target membranes in a similar manner to AMPs. Thus, the different models that have been developed to explain the membrane-disrupting properties of AMPs are also applied for ACPs. It should be noted, however, that the majority of available literature on the subject revolve around experiments conducted with α-helical peptides on bacterial membranes and it is therefore unknown whether the proposed mechanisms of action are transferable to ACP-cancer cell membrane interactions.

Any case involving ACP-membrane interactions, it is necessary to reach a critical threshold concentration for the induction of membranolytic events. The threshold concentration is not only dependent on the peptide-to-lipid ratio, but also involves other parameters such as the peptides' molecular weight, amphipathicity, propensity to self-assemble, overall net charge, as well as membrane composition and fluidity of the target membrane [14, 67-70]. Possible alterations in membrane structure may include pore formation (barrel-stave or torodial pore

models), altered curvature (carpet/detergent model) and thinning of the lipid bilayers (molecular electroporation and sinking rafts models) (fig. 1.2) [41, 71]. In the "barrel-stave model", monomers of amphipatic peptides (presumably α-helices) bind to the cell membrane and self-aggregate in bundles, ultimately forming cylindrical transmembrane pore channels whose inner lumen consists of the hydrophilic portions of the peptide with the lipophilic side aligned against the hydrophobic membrane bilayer [72]. It has been proposed that the "barrel-stave" model cannot be used to explain the cytotoxic activity of peptides containing less than 23 amino acids due to insufficient length to span cell membranes [39], but evidence indicates otherwise as illustrated by the amphipatic α-helix alamethicin (20-residues), a peptide widely agreed to conform to the forespoken model [73, 74]. The "torodial pore model" differs from the latter in that the peptides are initially oriented parallel to the membrane surface, but once inserted induce a continuous bend of phospholipid head groups of the monolayer. Consequently, the membrane curves inwards resulting in a pore lined by both inserted peptides and lipid headgroups [75]. As a result, cell death proceeds by the loss of transmembrane electrochemical gradients and metabolites. In the "carpet/detergent model", peptides are thought to not insert themselves into the hydrophobic core of the lipid bilayer, but rather become aligned in parallel to the cells' surface upon binding to anionic membrane components, thereby creating a carpet-like appearance. When the curvature stress exceeds the membrane's ability to maintain physical integrity, typically upon reaching a critical threshold concentration, the membrane collapses causing cellular lysis [76]. The final modes of actions have received less attention but nonetheless demonstrate non-membranolytic mechanisms; in the "molecular electroporation model", binding of cationic peptides to a target membrane generates membrane pores due to differences in electrical potential [77] while in the "sinking raft model", bound peptides are believed to aggregate on the surface (like rafts) leading to a mass imbalance and local curvature as they sink into the membrane [78, 79]. In general, due to the direct and rapid membranolytic effect exerted by many ACPs, cell death is often accompanied by distinct cellular morphological alterations associated with necrosis, such as cell shrinkage, swelling and chromatin condensation [80-83]. However, cell death as induced by ACPs is not entirely restricted to necrotic cell death features, but may also proceed to induce apoptosis or a combination of the two [50, 84], presumably by interaction with intracellular targets such as mitochondria (outlined in the following section).

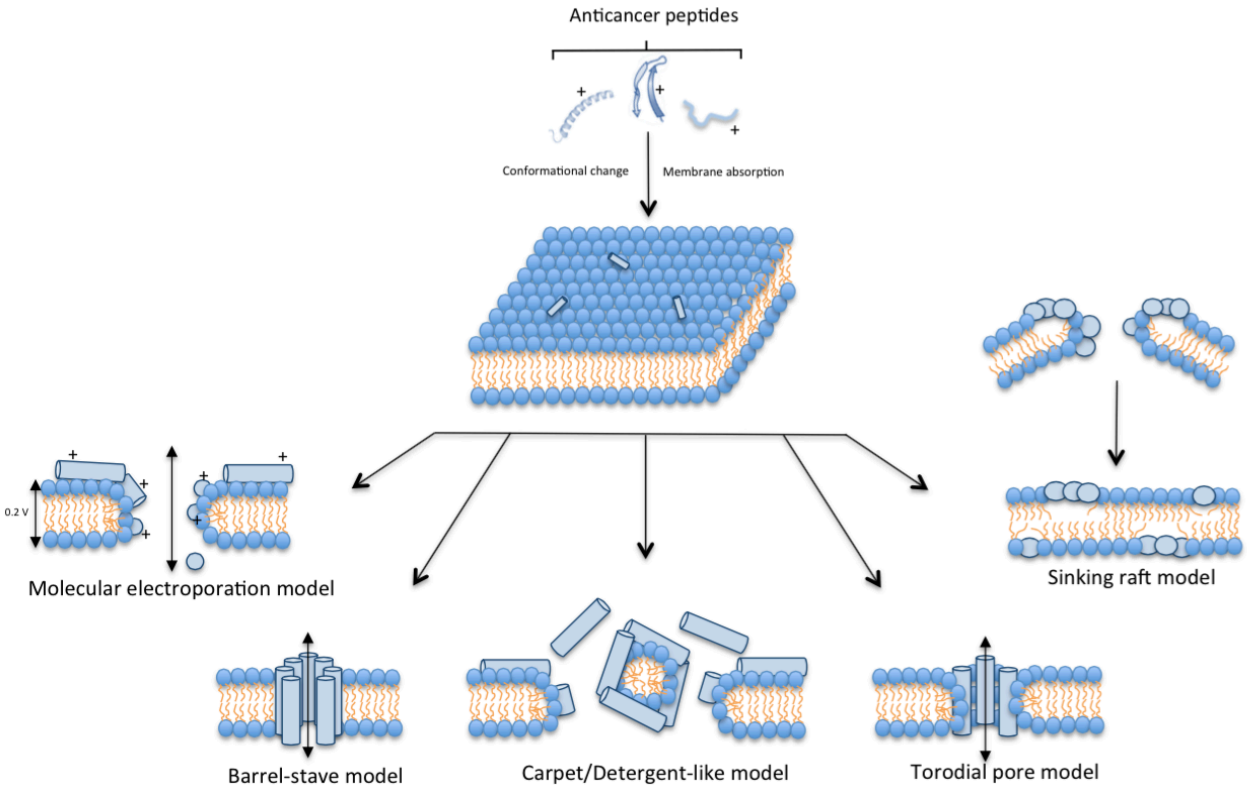

Fig. 1.2. Anticancer peptides – proposed models of cancer cell membrane permeabilization. Many ACPs are unstructured in aqueous solution and only adopt their secondary structure upon interaction with lipid bilayers. Interaction is driven by electrostatic differences in the positively charged peptides and negatively charged cancer cell membranes. Once reaching a critical threshold concentration, the peptide can exert its activity by a variety of mechanisms, e.g the "barrel-stave model", the "carpet/detergent-like model", the "torodial pore model", the "molecular electroporation model" and the "sinking raft model". The models were generated using Microsoft® PowerPoint® for Mac 2011.

1.3 Intracellular targets

Considering the nature of amphipatic molecules and their detergent-like properties at sufficiently high concentrations, it is tempting to assume an exclusively membrane-disrupting role of ACPs, or AMPs in general. However, recent studies suggest that cell death may also be accompanied by penetration of ACPs into the cytoplasmic compartment, thus targeting intracellular components and finally interfere with both necrotic and apoptotic pathways [50, 85-87]. The well-studied β-ACP bovine lactoferricin (LfcinB), produced from lactoferrin by pepsin cleavage [88], is known to exhibit anticancer activity against a wide variety of cancer cell lines *in vitro*, including fibrosarcoma, melanoma, colon carcinoma [89] and neuroblastoma [90]. Furthermore, LfcinB inhibits growth of several tumor models *in vivo* [90, 91]. The capacity of LfcinB to kill cancer cells has been shown to occur by induction of

apoptotic pathways associated with the production of intracellular ROS (reactive oxygen species) and activation of Ca^{2+}/Mg^{2+}-dependent endonucleases [92]. In another study, LfcinB was concluded to kill cancer cells by triggering the mitochondrial pathway of apoptosis [93], although a later report demonstrated induction of necrosis in neuroblastoma cells treated with LfcinB *in vitro* [90]. Another ACPs, buforin IIb, a synthetic analog of buforin II, displays cytotoxic activity against over 60 cancer cell lines *in vitro*, presumably via mitochondria-dependent apoptosis [94, 95]. The α-ACP dermaseptin B2 derived from frog skin has been shown to aggregate and penetrate the cell surface of several human tumor cell types, and that cell death proceeds by necrotic means contrary to apoptosis, as indirectly demonstrated by no activation of caspase-3 and changes in mitochondrial transmembrane potential [57]. Considering the negative charge of mitochondrial membranes [96], it represents a preferential intracellular target for internalized cationic peptides whose actions may induce release of cytochrome c, followed by activation of downstream caspases that ultimately ends in apoptosis and death of the cell.

1.4 Anticancer peptides and their therapeutic potential

Despite several promising anticancer therapeutic approaches reaching the clinic, cancer is still among the leading causes of mortality worldwide, accounting for 8.2 million deaths in 2012 [97]. The therapeutic arsenal against cancer has grown progressively more complex and includes treatments such as DNA alkylating antineoplastic agents, hormonal therapy, antitumor antibiotics, all of which may be utilized in concert with surgical procedures and radiation therapy [98-100]. Unfortunately, many conventionally used chemotherapeutics display poor selectivity towards transformed cells and rather impose immunosuppressive side effects due to unspecific targeting of rapidly dividing host cells (e.g myelosuppresion). More importantly, several chemotherapeutic drugs are known to eradicate tumor cells by induction of tolerogenic apoptosis, i.e silencing of immunological responses [101-103]. Therefore, much effort has been devoted in developing anticancer therapies with improved selectivity and preferably immunostimulatory properties. As previously shown, ACPs represents a novel class of therapeutics with selective cytotoxic activity and mode of actions that are independent of proliferative status, thus being capable of terminating both slowly growing and dormant neoplastic cells [41, 104-106]. Besides killing via disruption of plasma and/or mitochondrial membranes, ACPs have been found to display alternative mechanisms including anti-

angiogenic effects [107], engagement of plasma membrane receptors [108] and inhibition of DNA polymerase [109]. Finally, it has become evident that some ACPs [110, 111], along with a small minority of chemotherapeutics and oncolytic viruses [112] are capable of inducing a type of cancer cell death associated with the release of endogenous danger molecules, notably immunogenic cell death (ICD). This scenario may help orchestrate an immune response in which the patients' own dying cancer cells functions as an *in situ* vaccine, thus stimulating antitumor immune responses and generation of tumor-specific immunological memory.

1.5 The 'danger signal' concept and DAMPs

According to the 'danger theory' postulated by Polly Matzinger in 1994, self-constituents may trigger potent immune responses if perceived in the presence of endogenous danger signals [113, 114]. Nowadays, the 'danger signal' concept help explain why the immune system becomes activated upon situations such as tissue transplantation, autoimmunity or various cases of cellular stress and/or abnormal cell death [115-117], in the apparent absence of microbial infection. Danger signals, otherwise known as damage/danger-associated molecular patterns (DAMPs) are normally sequestered within cells where they perform non-immunogenic functions, but acquire immunomodulatory properties once released and/or expressed by stressed or dying cells [118]. DAMPs may activate the immune system by similar means as the microbe-derived pathogen-associated molecular patterns (PAMPs) via corresponding/cognate pathogen-recognition receptors (PRRs) such as the toll-like receptors (TLR), NOD-like receptors (NLRs) and RIG-I-like receptors [119, 120]. Albeit argued to interact with different co-receptors resulting in a divergence of downstream effects [121], receptor ligation by either DAMPs or PAMPs on antigen presenting cells (APCs) collectively dictate the recruitment of immune effector cells, thus initiating innate responses.

1.6 Immunogenic cell death

Cell death can either be perceived as immunogenic or non-immunogenic, depending on the initial stimuli [112]. The concept of ICD was originally introduced to describe a new form of cell death that particullary occurred in cancer cells succumbing to/in response to conventional cytotoxic drugs such as doxorubicin, oxaliplatin and mitoxantrone, all of which may induce immunogenic apoptosis [122-124]. Due to these findings, the dogma that apoptosis is a non-immunogenic (or at least poorly immunogenic) form of cell death compared to necrosis was

naturally invalidated [125]. In the context of cancer immunotherapy, ICD is characterized by the presence of DAMPs that, in company with cancer cell constituents (i.e tumor antigens), provide immunostimulatory APCs with maturation stimuli/signals necessary for activating and priming both $CD4^+$ helper T cells and tumor-specific $CD8^+$ cytotoxic T cells (CTLs) [101, 126]. Studies have also shown that inducers of ICD may even favor an increased count of CTLs over $FOXP3^+$ regulatory T cell (Tregs) [127, 128], the latter which in several types of cancer is linked to a poor prognosis [129]. Kroemer et al. has proposed that ICD must satisfy the following criteria; first, cancer cells that undergo ICD *in vitro* should, when administered in the absence of any adjuvant, elicit an immune response that protects mice against a re-challenge with live and equivalent tumor cells. Secondly, *in vivo* ICD must drive an immune response featuring both innate and adaptive immunity that should contribute to direct anticancer effects (e.g inhibition/reduction of tumor growth), and in turn control and even eradicate residual cancer cells [130]. Biochemical analysis has revealed that in order for cell death to be perceived as immunogenic, cells must display distinct morphological and biochemical hallmarks. These include alterations in plasma membrane components caused by endoplasmic reticulum (ER) stress and subsequent trafficking and exposure of the pre-apoptotic protein calreticulin (CRT) or other ER proteins, pre-apoptotic secretion of adenosine triphosphate (ATP) and the post-mortem release of the nuclear protein high-mobility group box 1 (HMGB1) as membrane integrity becomes lost [131-133] (fig 1.3). These are to date considered hallmarks of ICD. As the work of this thesis partly dealt with screening for the release of ATP and HMGB1 from dying cancer cells, the next section will give an introduction to their role in ICD.

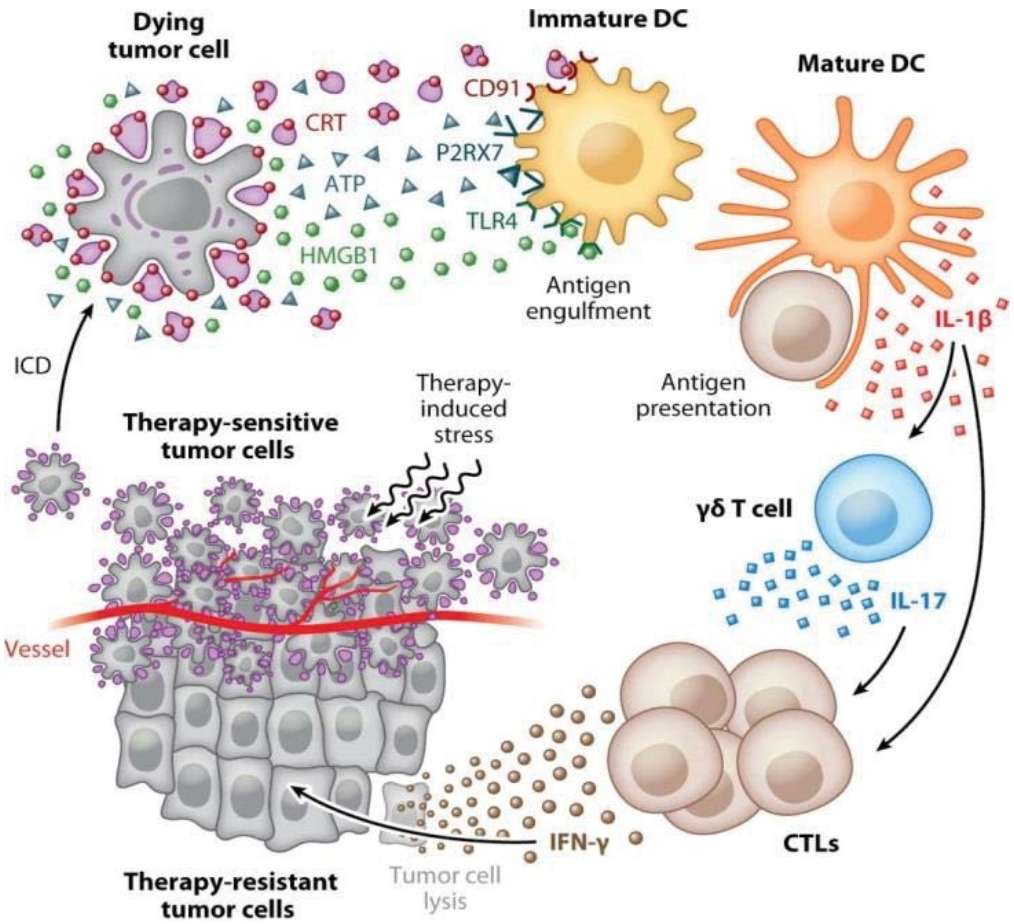

Fig. 1.3. Immunogenic cell death (ICD) and implications that follows – Various anticancer treatments induce ICD in cancer cells, which is characterized by the release and/or surface expression of DAMPs, including pre-apoptotic surface expression of CRT, apoptotic secretion of ATP and the post-mortem (after death) release of HMGB1 as membrane integrity becomes lost during secondary necrosis. DAMPs bind to their respective receptors on immature DCs, which facilitate engulfment of tumor antigens (stimulated by CRT), recruitment of immune effector cells into the tumor bed (stimulated by ATP) and up-regulation of pro-inflammatory cytokines and co-stimulatory molecules necessary for optimal antigen presentation to T-cells (stimulated by HMGB1). DC-associated cross-priming results in potent IL-17 and IFN-γ mediated immune responses involving both γδ T cells and tumor-specific CTLs that potentially may eradicate residual therapy-resistant tumor cells. (DAMPs, damage-associated molecular pattern molecules; CRT, calreticulin; ATP, adenosine triphosphate; HMGB1, high-mobility group box 1; DC, dendritic cell; IL, interleukin; IFN, interferon; CTLs, cytotoxic $CD8^+$ T lymphocyte). Figure retrieved from [130]

1.7 ATP in immunogenic cell death

In addition to its widespread involvement in countless physiological processes, ATP has additionally become one of the main determinants of cell death to be perceived as immunogenic. During phagocytic clearance of apoptotic bodies, extracellular ATP also act as a 'find-me' signal by mediating the attraction of macrophage and DC precursors, presumably

upon binding to the metabotropic P2Y2 receptors [134]. Beyond its role as a chemoattractant, ATP induces potent pro-inflammatory effects when binding to the purinergic receptors P2X7, which are abundantly expressed on immune cells such as macrophages and DCs [135]. Chemotherapy-induced release of ATP from tumor cells has been shown to trigger K^+ efflux and assembly of the NOD-like receptor family, pyrin domain containing-3 protein (NLRP3) in response to P2X7 activation on APCs. The NLRP3 inflammasome may in turn activate caspase-1, which results in proteolytic cleavage of pro-interleukin-1β into interleukin-1β (IL-1β) in addition to secretion of IL-18. After being actively secreted, IL-1β further initiates pro-inflammatory events by aiding in the maturation of tumor specific interferon-γ (IFN-γ) producing CTLs [136-139]. In mice tumor models, the immunological cross-talk between innate and adaptive immune cells leading to anti-tumor immune responses is abolished when subjecting the animals to neutralizing antibodies targeting IL-1β [133]. As accumulating evidence suggests, the release of ATP from dying cancer cells seems to be indispensible in order to establish immunogenicity against tumors.

1.8 HMGB1 in immunogenic cell death

HMGB1 is a highly conserved non-histone chromatin binding protein that is widely and abundantly expressed by nucleated cells [140]. As a nuclear protein, HMGB1 is involved in architectural operations due to its ability to facilitate chromatin remodelling during gene transcription [141]. Additionally, in response to bacterial exo- and endotoxins, TNF-α (tumor necrosis factor α), interleukin-1 (IL-1) and IFN-γ, cells of the innate immune system may actively secrete HMGB1 during regulated necrosis (i.e pyroptosis and pyronecrosis) [142-144]. Mechanically injured cells also passively secrete HMGB1 as they succumb to primary or secondary (postapoptotic) necrosis [130]. Once released extracellulary, HMGB1 occupies a critical role as a proinflammatory mediator due to its ability to engage multiple surface receptors on both innate and non-immune cells. These include TLR2, TLR4, TLR9 and the receptor for advanced glycation end products (RAGE). One if its main adverse effects is seen upon binding with TLR4 on DCs and macrophages, which stimulates the myeloid differentiation primary-response protein 88 (MyD88) pathway resulting in the transcription and active secretion of proinflammatory mediators such as TNF-α and IL-6 [145]. In cancer, the importance of a functional MyD88 pathway is highlighted by knockout experiments in which macrophages deficient in either of these proteins (i.e *TLR4*$^{-/-}$ and *MyD88*$^{-/-}$) displayed

impaired production of TNF-α [146]. Additionally, tumors established in TLR4 and MyD88 deficient mice exhibited far less responsiveness to known inducers of ICD (anthracyclines, oxaliplatin) compared to non-immunocompromised mice [147]. Other important aspects of HMGB1 as a proinflammatory mediator (in cancer) include the ability to inhibit fusion of phagosomes, possibly containing tumor-antigens, with lysosomes, thereby increasing the change of antigen processing within APCs [148], induction of both maturation and migration of immature DCs via engagement of RAGE [149] and finally recruitment of mononuclear cells when signalling through the chemokine receptor CXCR4 [150]. However, there are also contradictory observations regarding HMGB1 in cancer. For instance, secretion of HMGB1 by human malignant mesothelioma cells assisted in proliferation and prolonged their survival [151], whilst co-expression of RAGE and HMGB1 in prostate cancer is associated with poor survival rate [152]. Nonetheless, while some reports are consistent in the notion of HMGB1's contribution to carcinogenesis, the majority of information points towards a pivotal role in inflammation and especially tumor cells undergoing ICD [122, 130, 131, 133].

1.9 LTX-401

Based on structure-relationship (SAR) studies on short cationic peptides (<9 amino acid residues) it was discovered that the introduction of large lipophilic groups compensated for the length of AMPs, which are commonly composed of 12-50 amino acids. Additionally, by coupling two aromatic side-chains to the same carbon atom, length could further be reduced to a minimum without loosing cytotoxic activity (*Prof. Ø. Rekdal, personal communication*). These discoveries led to the production and synthesis of a panel of β-peptidomimetics to confirm the pharmacophore model of short cationic AMPs [153], which dictates that such compounds should contain cationic charged residues in addition to bulky and lipophilic moieties for optimal activity [154, 155]. These β-peptidomimetics contained two large bulky lipophilic groups incorporated into a single $\beta^{2,2}$-amino acid derivative and were shown to exhibit high antimicrobial activity. Moreover, some of the $\beta^{2,2}$-amino acid derivatives also displayed potent anticancer activity [153, 156], which has led to a continued investigation on one particular derivative, namely LTX-401 (fig 1.4).

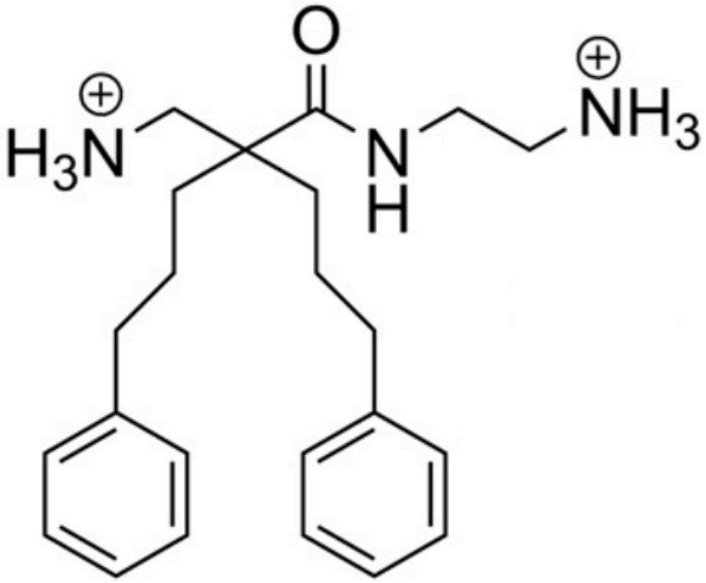

Fig. 1.4. Chemical structure of the β^{2,2}-amino acid derivative LTX-401. The molecule has an overall net charge of +2 with two lipophilic groups connected to the β-carbon (2. position).

1. 10 Aims of the study

The overall aim of this thesis was to investigate the anticancer activity and mechanisms of action of LTX-401 mainly by studying the *in vitro* effects on a hepatocellular carcinoma and melanoma cell line, but also study the *in vivo* effects against a murine B16F1 melanoma model. More specifically, the thesis aimed to:

- Evaluate the cytotoxic activity of LTX-401 against a panel of both malignant and non-malignant cells
- Determine the mechanisms of action by LTX-401
- Elucidate whether LTX-401 is capable of inducing features of immunogenic cell death by studying the release of 'danger signals' from tumor cells *in vitro*
- Investigate the *in vivo* anti-tumor effects of LTX-401 in a syngeneic melanoma mouse model (pilot-study)

2. Materials

Table 2.1 Cell lines and culture conditions

Cell line	Origin	Culture Conditions	Supplier
JM1	Rat hepatocellular carcinoma	DMEM[1]	Colleague[5]
HEPG2	Human hepatocellular carcinoma	DMEM[1]	Colleague[5]
BEL7402	Human hepatocellular carcinoma	DMEM[1]	Colleague[5]
HT-29	Human colorectal adenocarcinoma	RPMI-1640[2]	ATCC[6] (#HTB-38)
B16F1	Murine skin malignant melanoma	DMEM[1]	ATCC[6](#CRL-6323)
A375	Human skin malignant melanoma	DMEM[1]	PHE[7] (#88113005)
SK-N-AS	Human neuroblastoma	RPMI-1640[2]	ATCC[6](#CRL-2137)
MRC-5	Human lung fibroblasts	MEM[3]	ATCC[6] (#CCL-171)
HUVEC	Human vascular endothelium	EGM-2 Bulletkit[4]	ATCC[6](#CRL-1730)

[1] = With 4500 mg glucose/L, L-glutamine, $NaHCO_3$, pyridoxine HCl and 10 % FBS, Sigma, #D5796

[2] = With L-glutamine, $NaHCO_3$ and 10 % FBS, Sigma, #R8758

[3] = With 1500 mg glucose/L, 2 mM L-glutamine, 1 % non-essential amino acids and 10 % FBS, Sigma, #M4655

[4] = Lonza, MA, #CC-3162. See product site for complete list of ingredients

[5] = Kindly provided by Dr. Pål-Dag Line, Department of Transplantation Medicine, Oslo University Hospital

[6] = American Type Culture Collection, Rockville, MD, USA

[7] = Public Health England Culture Conditions, Porton, Down, Salisbury, UK

= Catalog number

Table 2.2 Commercial kits used

Kit	Purpose	Supplier
ELISA® Cytochrome c	Detection of cytochrome c	R&D Systems (#MCTC0)
ENLITEN® ATP Assay	Detection of ATP	Promega (#FF2000)

= Catalog number

Table 2.3 Antibodies

Antibody	Host	Type	Dilution	Supplier
Anti-HMGB1 (Primary)	Rabbit	Polyclonal	1/1000	ChIP Grade, Abcam, UK (#ab18256)
Anti-rabbit IgG (Secondary)	Goat	Polyclonal	1/5000	Abcam, UK (#ab6721)

= Catalog number

Table. 2.4 Chemicals and reagents used

Type	Purpose	Supplier
Heat inactivated fetal bovine serum (FBS)	Growth media	Gibco (#10500)
1x Phosphate buffered saline (PBS)	Washing of cells	Biochrom AG (#L182-05)
0.25 % Trypsin EDTA	Loosen adherent cells	Sigma Aldrich (#T4049)
3-(4,5-dimethylthiazol-2-yl)-2,5-diphenyltetrazodium bromide (MTT)	MTT[1] assay	Sigma Aldrich (#M2128)
2-Propanol	MTT assay	Sigma Aldrich (#I9516)
Hydrochloric acid (HCl), 37 %	MTT assay	Sigma Aldrich (#258148)
Triton X-100	MTT assay	Sigma Aldrich (#T9284)
Heparin	Hemolytic assay	Sigma Aldrich (#H3393)
NuPAGE LDS Sample buffer (4x)	Western blot	Invitrogen (#NP0008)
NuPAGE Sample Reducing Agent (DTT)	Western blot	Invitrogen (#NP0009)
NuPAGE Running Buffer (20x), diluted 1:20	Western blot	Life Technologies (#NP0002)

(Continued)

Table. 2.4 Continued

Type	Purpose	Supplier
1x TBS-T (Tris buffered saline with Tween 20)	Western blot	Tween 20 → Sigma Aldrich (#P9416)
Blocking buffer	Western blot	Home made (see appendix A)
Blotting buffer	Western blot	Home made (see appendix A)
Western Blotting Luminol Reagent	Western blot	Santa Cruz Biotechnology (#sc-2048)
4x 0.4 M PHEM buffer (pH = 6.9), stock solution	Sample preparation, electron microscopy	Home made (see appendix A)
1x Malachite Green fixative	Sample preparation, electron microscopy	Home made (see appendix A)
1 % Osmium reduced ferrocyanide	Sample preparation, electron microscopy	Home made (see appendix A)
1 % Tannic acid	Sample preparation, electron microscopy	Home made (see appendix A)
1 % Uranyl acetate	Sample preparation, electron microscopy	Home made (see appendix A)
Ethanol (EtOH); 25 %, 50 %, 70 %, 90 % and absolute (100 %)	Sample preparation, electron microscopy	Home made (see appendix A)
Agar resin	Sample preparation, electron microscopy	Home made (see appendix A)

1 = MTT tetrazolium reduction assay
# = Catalog number

Table 2.5 Instruments and equipment used

Instrument	Purpose	Manufacturer
Gemini XPS Spectro-photometric Microtiter Plate Reader	MTT assay, cytochrome *c* assay, hemolytic assay	ThermomaxMolecular Devices, NJ, USA
Scepter™Hanheld Automated Cell Counter	Cell counting	EMD Millipore, Darmstadt, Germany
SysmexK-1000 (haematology analyser)	Hemolytic assay	Kobe, Japan
Luminescence Microplate Reader	Luciferase assay	Luminoskan, Finland
Amicon Ultra-0.5 Centrifugal Filter + Ultracel-50 membrane	Western blot	Milipore, Norway
Immobilon®-P Transfer Membrane (0,45 μm)	Western blot	Milipore, Norway
XCell SureLock™Mini-Cell	Western blot	Invitrogen, USA
NuPAGE Novex 4-12% Bis-Tris Gels	Western blot	Invitrogen, USA
ImageQuant LAS 4000	Western blot	GE Healtcare, USA
PHM210 Standard pH Meter	PHEM buffer pH adjustment	Radiometer Analytical, Lyon, France
Pelco Biowave Pro laboratory microwave	EM sample preparation	Ted Pella, Redding, CA
Reichert Ultracut FCS	EM sample preparation	Leica Microsystems, Vienna, Austria
JEOL JEM-1010 TEM microscope	Electron microscopy	JEOL, Tokyo, Japan
Leica DMI6000 B inverted microscope	Phase-contrast microscopy	Leica Microsystem, Wetzlar, Germany

Table 2.6 Software used

Software	Purpose
SoftMax Pro 5.4.1	MTT and Hemolytic assay
ImageQuant LAS 1.1	Western blot
iTEM 5.0	Electron microscopy
Leica Application Suite 4.4.0	Phase-contrast microscopy

3. Methods

This part describes the different methods applied in the thesis, and is briefly presented in a simple flowchart (fig. 3.1).

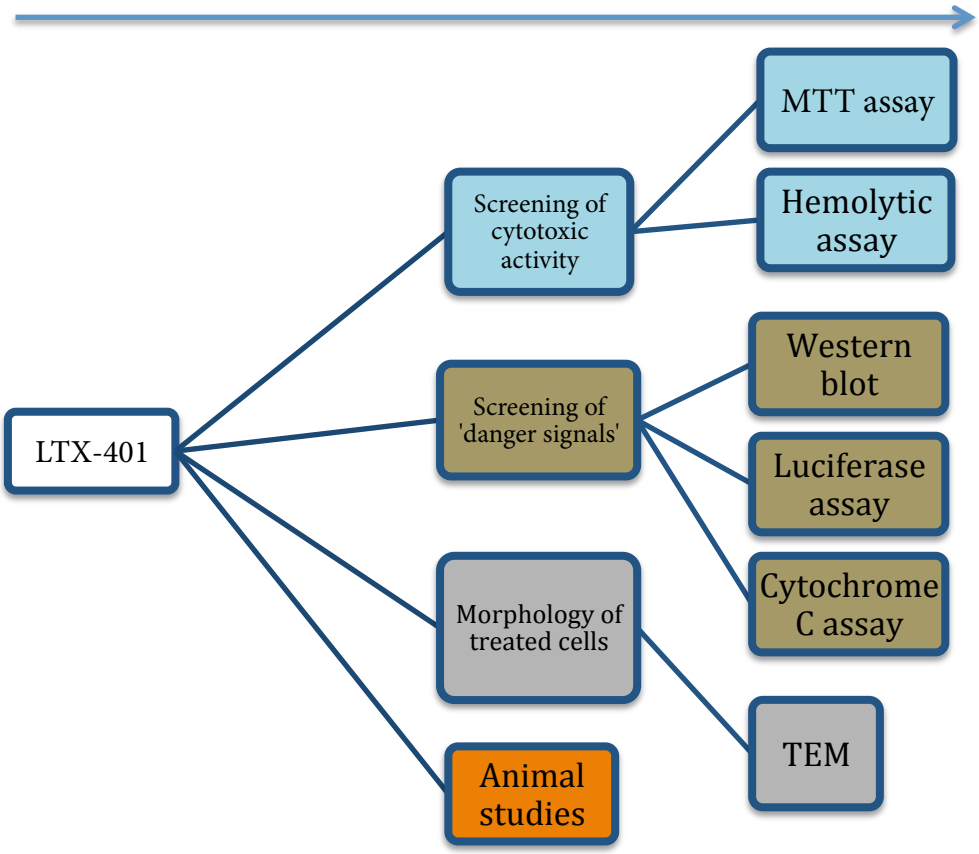

Fig. 3.1. Flowchart illustrating the experimental design and methods of this thesis.

3.1 Synthesis and origin of LTX-401

LTX-401 (2-((2-ammonioethyl)carbamoyl)-5-phenyl-2-(3-phenylpropyl)pentan-1-aminium chloride) was purchased on request from Syntethica AS (Oslo, Norway). Unless stated otherwise, LTX-401 was diluted in serum-free RPMI 1640 to yield various concentrations applied in this thesis. $Mw_{\text{LTX-401}}$ = 0.368 g/mol.

3.2 Cell counting

A preliminary task before many of the experiments conducted in this thesis was the seeding of cells into various types of flat-bottomed microtiter plates. All cell counting was performed using a Scepter™ Hanheld Automated Cell Counter with 60 μm Scepter sensors. After trypsizising cells a volume of 10 ml culture medium was added to the culture flask and distributed over the surface in order to collect as many cells as possible. 300 μl was transferred to an eppendorf tube to be used for automatic counting by the cell counter. After the count was completed, the instrument displayed a histogram of cell size or diameter on its screen in addition to cell concentration per ml. The obtained value was then multiplied with the volume of cell suspension before centrifugation in order to achieve total number of cells. The total number of cells needed was calculated using the standard equation $C_1V_1 = C_2V_2$. The unknown parameter (x) is the amount of cell suspension that needs to be extracted from the stock solution (1 ml). As followed, the number of cells needed per millilitre was multiplied with the total amount of culture medium required for a whole plate and then divided by the total number of cells obtained from cell counting. The cell suspension was then diluted in culture medium to achieve the desired concentration. An example of cell counting when needing 150 000 cells/ml, in a volume of 6 ml is shown beneath.

$$(4.897 * 10^5) * 9.7\, ml = 4.75 * 10^6$$

$$4.75 * 10^6 * X = 1.5 * 10^5 * 6\, ml$$

$$X = 0.189\, ml$$

3.3 Cell incubation conditions

All cells used for various experiments in this thesis were, unless stated otherwise, incubated in a cell incubator at 37 °C, <95% humidity and 5% CO_2 conditions.

3.4 Colorimetric MTT assay

The colorimetric 3-(4,5-dimethylthiazol-2-yl)-2,5-diphenyltetrazodium bromide (MTT) viability assay (also called MTT tetrazolium reduction assay) is a simple, yet effective method for measuring cell proliferation and testing of cytotoxic compounds. The immense number of citations towards the original article published by Tim Mosmann in 1983 reflects its major popularity in academic laboratories around the world. During normal cellular respiration by viable cells, MTT is metabolized into an insoluble purple colored formazan product. Dead cells are naturally not capable of converting MTT into formazan, and consequently the amount of color formation provides information of viability, i.e fraction of dead compared to live cells. Although still subject to debate, it is generally agreed that the conversion of MTT into formazan is likely to follow the actions by mitochondrial dehydrogenase enzymes. As formazan is only partially soluble in aqueous solution due to crystal formation, it needs to be solubilized in order to measure optical density. Preferred solvents include acidified isopropanol and dimethyl sulfoxide (DMSO), although dimethylformamide, sodium dodecyl sulphate (SDS) and other organic solvents like ethanol may also be utilized to completely dissolve formazan crystals prior to readings [157, 158].

3.4.1 *In vitro* cytotoxicity of LTX-401

The colorimetric MTT viability assay was employed to investigate the *in vitro* cytotoxic activity of LTX-401 against a panel of cancer cells and non-malignant cells. Pre-cultured cells were seeded (in triplicate) at a density between 1 x 10^4 – 1,5 x 10^4 cells/well in a volume of 100 µl in 96-well flat-bottomed microtiter plates in culture medium (see table 2.1) and left to adhere overnight. LTX-401 was usually weighed in amounts of 1 mg and dissolved in serum-free RPMI-1640 to yield a concentration of 0.4 mg/ml, which was used to prepare a series of dilutions ranging from 1-100 µg/ml. Cells were washed with 100 µl serum-free media one time before adding LTX-401 in increasing concentration at volumes of 100 µl before being

incubated for 4 hours. Cells incubated with serum-free RPMI 1640, were used as negative control, whereas cells treated with 1 % Triton X-100 diluted in serum-free media were used as a positive control. Ten µl MTT solution (5 mg MTT per ml PBS) was added to each well and incubated for an additional 2 hours. Seventy µl of solution was carefully aspired from each well before adding 100 µl of 0.04 M HCl in isopropanol to each well by thorough resuspension. The plates were put on an orbital shaker for ~30 minutes at room temperature to continue facilitation of formazan crystal solubilization. Absorbance was measured at 590 nm on a spectrophotometric microtiter plate reader (Thermomax Molecular Devices, NJ, USA). Cell survival was calculated as the A_{590} nm of peptide treated cells relative to the negative control (100% living cells) and expressed as a 50% inhibitory concentration (IC_{50}).

3.4.2 Killing kinetics study

Killing kinetics of LTX-401 was studied against JM1 hepatocellular carcinoma and B16F1 melanoma cells using both the 2 x IC_{50}^{4h} and 4 x IC_{50}^{4h} value of LTX-401 (54 µM and 108 µM, respectively). Cells were as previously described (section 3.4.1) seeded at a density between 1 x 10^4 – 1,5 x 10^4 cells/well in a volume of 100 µl in 96-well flat bottomed microtiter trays in culture media and left overnight to adhere. LTX-401 was dissolved in serum free RPMI-1640 to yield a series of dilutions ranging from 1-100 µg/ml. Cells were washed once with 100 µl serum free RPMI-1640 before being incubated with LTX-401 for specific time points (5, 15, 30, 60, 90, 120 and 240 min). Serum free RPMI-1640 and a 1 % Triton X-100 served as negative and positive controls, respectively. Cells were washed once with 100 µl serum free RPMI-1640 after incubation and further incubated in a 10 % MTT solution (diluted in serum free RPMI-1640) for an additional 2 h. Seventy µl of solution was carefully removed from each well after incubation before thoroughly resuspending the cells in 100 µl acidified isopropanol. The plates were put on an orbital shaker for ~30 minutes at room temperature to continue facilitation of formazan crystal solubilization. Absorbance was measured at 590 nm on a spectrophotometric microtiter plate reader (Thermomax Molecular Devices, NJ, USA). Cell survival was calculated as the A_{590} nm of peptide treated cells relative to the negative control (100% living cells).

3.5 Hemolytic acticity of LTX-401

The cytotoxic activity of LTX-401 against human red blood cells (hRBCs) was determined by a hemolytic assay using freshly isolated blood from healthy individuals. Eight ml of venous blood was directly transferred and divided equally into two tubes; one EDTA (ethylene-diamine-tetra-acetic acid, anti-coagulant) containing tube and one containing 40 μl heparin, to yield a final concentration of 10 U/ml. The donor's hematocrit levels were determined from the EDTA tube using a SysmexK-1000 haematology analyser, while RBCs were isolated from the heparanized blood by centrifuging at 1,500 rpm for 10 min before removing the supernatant. The RBCs were further washed three times with pre-heated PBS (37 °C) and centrifuged between each washing step at 1,500 rpm for 10 min. Supernatant was discarded after the final wash while the pellet containing RBCs was resuspended to 10 % hematocrit before being incubated for 1 h at 37 °C with LTX-401 dissolved in PBS at concentrations ranging from 50 – 500 μg/ml (136 to 1358 μM). RBCs incubated with PBS and 10 % Triton solution alone served as negative and positive control, respectively. After centrifuging the samples at 4,000 rpm for 5 min, the absorbance of the supernatant was measured at 405 nm on a spectrophotometric microtiter plate reader (Thermomax Molecular Devices, NJ, USA). The percentage of hemolysis was calculated as the [(A_{405} nm of peptide treated RBCs- A_{405} nm of buffer treated RBCs)/(A_{405} nm of Triton treated RBCs-A_{405} nm of buffer treated RBCs)] x 100 % and expressed as both an IC_{50} value (50 % inhibitory concentration) and a graphical plot.

3.6 Transmission Electron Microscopy

The use of electron microscopy (EM) has played an essential role in defining general cell biology. The high resolution (approximately 0.1 nm) makes it possible to visualize viruses, DNA and intracellular organelles. With new techniques like immune labeling of ultrathin sections of tissue or cells, one can even visualize and study cell functions at a molecular level. The electron microscope uses highly energetic electrons as an illumination source, while simultaneously exploiting its short wavelength. In transmission electron microscopy (TEM), these are accelerated from an electron gun in a column of electromagnetic fields (electromagnetic lenses) and then projected through a very thin slice of specimen to produce a 2D picture on a phosphorescent screen. Since the brightness (or darkness) of a particular area

is directly proportional to the amount of electrons passing through the specimen, the picture that forms on the screen is a result of a contrast, or "shadow image". The amount of electrons reaching the phosphorescent screen will make it send out visible light that is transferred to the computer. Since gasses may interfere with the electron beam, electron microscopes are therefore operated under vacuum conditions, and the samples used for analyses must be pre-fixed to withstand this [166].

3.6.1 Conventional specimen preparation techniques

A 2-4 % glutaraldehyde (GA) solution is often used as a fixing agent together with formaldehyde (FA) in a buffered solution for EM analyses. Regardless of its slower rate of penetration, GA is proven to inherit greater crosslinking capabilities than formaldehyde [167, 168], which partly demonstrate the widespread use of buffered solutions consisting of 4 % GA and 1 % FA. To better preserve cellular membranes and glycogen, the specimen is usually fixated a second time in an osmium tetroxide solution that is reduced with ferrocyanide (hence osmium reduced ferrocyanide). However, over the course of years other staining techniques have been developed for use with either primary fixation or during dehydrations steps. Both malachite green and tannic acid for instance can both serve as *en bloc* stains while simultaneously provide improved visualisation and structural appearance of the specimen by targeting (of) phospholipids [169-171].

The next step in the preparation scheme for EM involves step-wise dehydration with a graded series of ethanol (or acetone) to withdraw and replace water present in tissue/cells. This step, along with fixation, prevents sample distortion when subjecting the specimen for vacuum during post-analysis. As the dehydration solution is not miscible with the plastic embedding medium used in the end of the preparation process, it is normally replaced by a transitional solvent such as propylene oxide. Moreover, this will also enhance the dehydration of the specimen. The last step involves replacing the dehydrants or transition fluids with the plastic embedding medium (i.e resin infiltration) that is to permeate the specimen and form a solid matrix. Although different embedments exist (e.g araldite), an embedding medium consisting of resin, hardeners (DDSA, NMA) and accelerators (DMP-30) is used in the majority of cases.

After the resin block containing the specimen has polymerized and hardened sufficiently, it may be subjected to staining and sectioning into either ultrathin (50-100 nm) or survey/semithin sections (0.5-2 μm) by ultramicrotomy and microtomy, respectively. Routine staining and contrasting TEM samples involves using heavy metal such as uranyl acetate and lead citrate. As biological specimens are predominantly composed of atoms with low atomic number, the bulk of the electron beam will project straight through it unless it is impregnated with heavy metal salts [166].

Initially, the recently described processes for fixation and post-fixation were also utilized in this thesis. A standardized HEPES buffered solution containing 4 % GA and 1 % FA was used to fixate JM1 and B16F1 cells, while following routine post-fixation protocols including the use of osmium reduced ferrocyanide, alcohols, propylene oxide followed by traditional grid staining with uranyl acetate and lead citrate. Especially for JM1 cells, the contrast was rather poor and cell organelles such as mitochondria had little or no structural appearance. Instead of modifying the protocol by either increasing or decreasing the time samples were subjected to osmium reduced ferrocyanide, uranyl acetate and lead citrate, a new microwave-assisted staining protocol using malachite green fixation was employed. Non-treated cells were first subjected to a pilot study where it was shown that the quality and contrast of samples greatly exceeded the ones obtained with the previous protocol. This technique is described in the following section.

3.6.2 Microwave-assisted processing for Transmission Electron Microscopy

Conventional specimen preparation for TEM analysis is a time-consuming process. It has been proposed that by heating up the specimen, processing times may be decreased [172]. In this sense, the introduction of microwaves in the laboratory offered a more controlled procedure of subjecting specimens to heat during fixation. Although not fully understood, it is believed that the combination of microwaves and vacuum assists in accelerating perfusion of chemicals into the samples, thus reducing infiltration times drastically. The method is also commonly applied for paraffin embedding, antigen-retrieval and immunolabeling and *in situ* hybridization [173]. According to *Electron Microscopy: Methods and Protocol, sec. edition,*

several authors have reported equally satisfying results when comparing standardized preparation techniques to the microwave-assisted one, and some even report improved morphology and appearance of their specimens. However, some studies indicate a contradicting role of heat in the preparation process as demonstrated by subjecting specimens to microwaves in the absence of heat, and rather in a cooling environment, preparation time is yet decreased while simultaneously increasing ultrastructure [174, 175]. Modern microwave processors, including the PELCO Biowave® Pro machine used in this thesis, contain cooling systems combined with both timing of irradiation in short bursts and vacuum being enabled in cycles to minimize the risk of damage to specimens.

Moreover, cells that are to be examined by electron microscopy are usually resuspended in the fixation reagents and centrifuged between each step, thus generating a cohesive pellet within a resin block in which cells become randomly scattered and not aligned according to a surface. In contrast, cells prepared for microwave-assisted processing on standard petri dishes are not necessarily pelleted between each step of chemical fixation. As both fixation and embedding of cells may occur directly on the petri dish (*en bloc*) when using this technique, cells are sectioned according to the horizontal plane in which they are seeded onto, i.e from basolateral to apical site. The latter technique was also applied in the preparation of ultra-thin sections in this thesis.

3.6.3 Stimulation and fixation of JM1 and B16F1 cells

- *A complete overview of the PELCO Biowave® Pro program settings for malachite green fixation, as well as preparation of solutions for this experiment, are listed in appendix B and A, respectively. The EM preparation protocol used in this thesis is written by predoctoral fellow Anna Steyer, a member of the Schwab Team at the European Molecular Biology Laboratory (EMBL, Heidelberg, Germany), who kindly provided it to Randi Olsen, Head Engineer at the Electron Microscopic Department (University of Tromsø). Originally, the malachite green protocol descends from the laboratory of Dr. Raphael H. Valdivia [176].*

JM1 and B16F1 cells were seeded at a density of 1 x 10^4 cells/tissue culture dish (35 mm) in a volume of 2 ml culture media and left to adhere and proliferate until they reached a confluence of ~80 % (normally taking 3-5 days). For TEM analysis, it is more beneficial to allow cells to form a subconfluent monolayer over several days rather than stimulating them the day after seeding since this will increase their morphological characteristics and appearance. Cells were treated with the 4 x IC_{50}^{4h} value (108 μM) of LTX-401 at specific time points (5, 15, 30 and 60 min). Serum-free RPMI 1640 functioned as a negative control at 30 and 60 min. Cells were immediately fixed in a PHEM buffered (0.1 M) solution containing 0.05 % malachite green, 0.5 % GA and 4 % FA and kept on fixative until loaded in the PELCO Biowave® Pro machine (Ted Pella, Redding, CA), normally within 30 min.

3.6.4 Processing and embedding of samples

The 35 mm sterile plastic petri dishes containing the malachite green fixated cells were directly inserted into and processed with the aid of a PELCO Biowave® Pro laboratory microwave according to provided software settings. In all microwave steps, samples were kept between 23 °C – 27 °C with a set temperature of 50 °C meaning the system shuts down if the latter value was exceeded. Induction of vacuum and microwaves ranging between 100-250 W preceded either as constant or in cycles (vacuum cycles = 20 sec on, 20 sec off). While still immersed in malachite green fixative, all samples were run for an initial 14-minute cycle (2 min on, 2 min off) followed by post-fixation in a cacodyl buffered osmium reduced ferrocyanide solution (0.8 % $K_3Fe(CN)_6$, 1 % OsO_4), 1 % tannic acid and 1 % uranyl acetate. Samples were washed twice on bench with 0.1 M PHEM buffer between each fixating agent. Dehydration occurred through a graded series of ethanol starting at 25 % and ending with absolute concentration (100 %) while microwaving 40 sec at each grade. Finally, samples were subjected to a 1:2 solution of agar resin (dissolved in absolute ethanol) before immersed in pure resin. Each infiltration step lasted 3 min accompanied by constant wattage of 250 during vacuum cycles. After the program was completed, dummy blocks of resin (embedding capsules) were mounted directly onto the petri dishes now containing post-fixated cells and left in a incubator for polymerization at 60 °C overnight.

3.6.5 Ultra-thin sectioning of samples

The following morning the resin dummy blocks containing cells on the basolateral side were removed from the petri dish and carefully trimmed around the sample using a glass knife mounted on a microtome (Leica Microsystems, Vienna, Austria). The samples were next cut in ultra-thin sections of 70 nm using a DiATOME diamond knife before collected from a water surface onto standard formvar, carbon-stabilized copper grids provided by the Electron Microscope department. After the grids were sufficiently dry they were ready for post-analysis using transmission electron microscope (JEOL, Tokyo, Japan). Images were taken with an Olympus Morada side-mounted TEM CCD camera and processed with iTEM 5.0 software.

3.7 Phase-contrast imaging of JM1 and B16F1 cells treated with LTX-401

JM1 and B16F1 cells were seeded in 6-well plates at a density of 2.0 x 10^5 cells per well in a volume of 2 ml (culture media) and allowed to adhere overnight. Cells were washed once with 2 ml serum-free RPMI 1640 before treated with the 4 x IC_{50}^{4h} value of LTX-401 (108 μM) for designated time points (15, 30 and 60 min). Non-treated control cells were incubated with serum-free RPMI 1640 until experimental endpoint (60 min). Cells were examined using the Leica DMI-6000B inverted microscope (Leica Microsystem, Wetzlar, Germany) and images were taken with a side-mounted camera (DFC 310 R2, Leica Microsystems) and processed with Leica Application Suite 4.4.0 Software.

3.8 ATP bioluminescence assay

The ATP bioluminescence assay is a bioluminescence method that requires two compounds; luciferin, a complex carboxylic acid, and the enzyme luciferase. Both compounds were originally isolated from the firefly beetle, a member of the *Lampyridae* family, by McElroy and colleagues in 1947 [159]. The chemical reaction is catalyzed by luciferase, which oxidizes its substrate luciferin to oxyluciferin in the presence of oxygen, ATP and Mg^{2+} (fig. 3.2). This enzymatic process is accompanied by emission of a yellow-green light at 560 nm. In the laboratory, luciferase has been widely used as a reporter gene to study gene expression at the transcriptional level in addition to detecting minute quantities of extracellular ATP as

determined by the intensity of light produced. In this thesis the ATP bioluminescence assay served to detect ATP release from JM1 and B16F1 cells when treated with LTX-401.

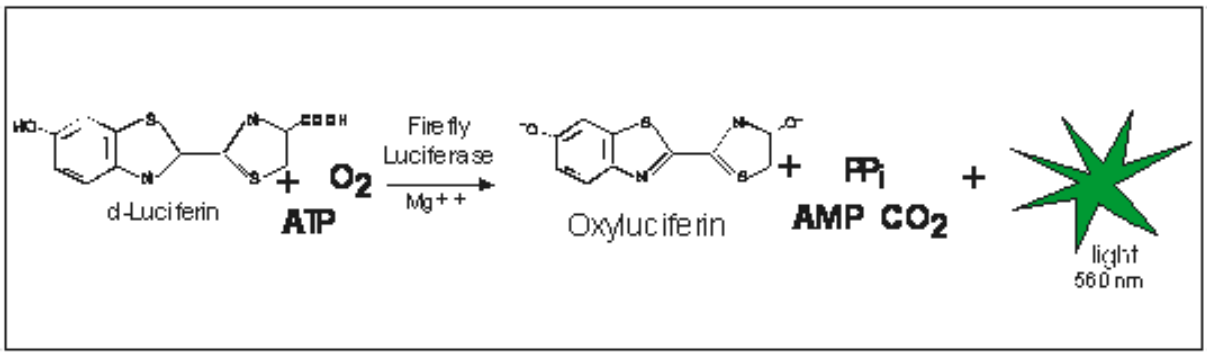

Fig. 3.2. In the presence of ATP, oxygen and Mg^{2+}, luciferin is oxidized to oxyluciferin by the enzyme luciferase in a reaction that yields light at 560 nm. Figure retrieved from [160].

3.8.1 Release of ATP from JM1 and B16F1 cells

JM1 and B16F1 cells were seeded into 96-well plates at a density of 1 x 10^4 cells/well in a volume of 100 µl (culture media) and allowed to adhere for overnight. All cells were washed twice with serum-free RPMI 1640 media before being treated with the 2 x IC_{50}^{4h} value of LTX-401 (54 µM) for designated time points (10, 30, 60, 90 and 120 min). Serum-free RPMI 1640 was used as negative control. Samples were collected by carefully transferring the supernatant to a white 96-well microtiter plate. A modified luciferin-based ENLITEN ATP assay kit (Promega, Madison, WI) was employed to measure extracellular levels of ATP by mixing 100 µl of pre-made, room temperatured, rL/L reagent with the samples and negative controls. The rL/L reagent was additionally mixed with serum-free RPMI 1640 alone in two wells to rule out unspecific ATP readings. Samples were immediately read on a Luminescence Microplate Reader (Luminoskan, Finland), in which light output was measured in relative luciferase units (RLUs). In this thesis, the extracellular levels of ATP after treatment with LTX-401 was measured by means of a modified commercial ATP assay kit (ENLITEN ATP Assay) meaning that the enclosed ATP standard was left out. Rather, extracellular levels of ATP were measured as RLUs, which is proportional to the amount of ATP in the solution. Preliminary pilot studies revealed that RPMI 1640 medium interfered with the ATP standard and inhibited the RLU signal, and could therefore not be compared to an ATP standard dissolved in ATP-free

water (all samples should be diluted in the same solution). Instead of quantifying the release of ATP, it was simply measured as RLUs.

3.9 Western blotting

The western blot (also referred to as immunoblot) is a well-established and commonly used technique to identify specific proteins from tissue extracts and cell lysates. The first step in a western blot procedure involves the separation of proteins by SDS-polyacrylamide gel electrophoresis. Next, proteins are transferred electrophoretically (blotted) from the gel to a membrane, typically being either a nitrocellulose or polyvinylidine fluoride (PDVF) membrane. The latter is achieved by assembling the gel together with the membrane, blotting pads and filter papers before an electric current is run through a blotting buffer-containing chamber. This causes the proteins to migrate from the gel to the membrane. The last step of a western blot procedure involves blocking of non-specific antibodies with a blocking buffer to reduce background interference. A blocking buffer normally contains a mixture of irrelevant proteins that binds to and block remaining binding surfaces on the membrane, thus increasing the likelihood of the primary antibody to specifically bind its target protein. In this thesis, the membranes were blocked using a solution of 5 % non-fat dried milk in TBS-T. The primary antibody may either be of monoclonal or polyclonal nature in which the main difference resides in its ability to recognize only one or multiple epitopes on an antigen, respectively. The secondary antibody is an enzyme-linked complex that binds specifically to the Fc region of the heavy chain on the primary antibody. This allows for signal amplification by the action of the conjugated enzyme such as alkaline phosphatase or horseradish peroxidase (HRP) when adding a certain substrate [161, 162].

3.9.1 Release of HMGB1 from JM1 and B16F1 cells

JM1 and B16F1 cells were seeded in 6-well plates at a density of 2.0 x 10^5 cells per well in a volume of 2 ml (culture media) and allowed to adhere overnight. Cells were either treated with either the 2 x IC_{50}^{4h} or 4 x IC_{50}^{4h} value of LTX-401 (54 μM and 108 μM, respectively) for different time points (10, 30, 60, 90, 120 and 240 min). Serum-free RPMI 1640 was used as negative control. Cells were washed twice with 2 ml serum-free RPMI 1640 before being

incubated with LTX-401. Supernatants were directly transferred to 1.5 ml centrifuge tubes and centrifuged at 5000g for 3 min to remove remaining cell debris before being up-concentrated using Amicon Ultra-0.5 Centrifugal Filter units with Ultracel-50 membrane (Milipore, Norway). Cell lysates were washed once with 2 mL serum-free RPMI 1640 and subjected to 160 µl lysis buffer (mastermix) containing 2x NuPAGE LDS Sample buffer, a 1x NuPAGE Sample Reducing Agent (DTT) and 50 % sterile H_20 (table 3.1). Next, lysates were harvested with a sterile cell scraper and transferred to 1.5 ml centrifuge tubes. Both lysates and supernatants were stored at -20 °C until used in western blots. All samples were on the day of use diluted to the same concentration using reducing NuPAGE LDS sample buffer and NuPAGE Sample Reducing Agent before being boiled at 70 °C for 10 min. Lysate samples were additionally sonicated for 8 cycles at 20 sec each. The samples (20 µl), together with a molecular marker and a protein standard (5 µl), were then loaded and immediately run on NuPAGE Novex 4-12% Bis-Tris Gels at 200 V for 40 min in the presence of a running buffer. After gel electrophoresis the gel cassettes were carefully opened to expose the gels before removing their lower part (edge) and wells. The gels were then assembled in a so-called transfer sandwich together with blotting pads, filter papers and PDVF membranes (Immobilon®-P Transfer Membrane). Both blotting pads and filter papers were pre-soaked in blotting buffer while PDVF membranes were wet in methanol for 10 sec to activate its protein binding capacity. The transfer sandwich was sealed tightly and brought together in the XCell SureLock™ Mini-Cell chamber where it was covered with blotting buffer before proceeding with electrotransfer at 25 V for 1.5 h. The rest of the chamber surrounding the transfer sandwich was filled with water. After blotting, the membranes were moved to 50 ml tubes and washed once with ~3 ml TBS-T before being blocked with 3 ml 5 % non-fat dry milk in TBS-T for 1 h at room temperature and further incubated with primary antibody overnight at 4 °C. The following day, membranes were washed for a total of 5 times with ~3 ml TBS-T, and further incubated with horseradish peroxidase conjugated secondary antibody for an additional two hours at room temperature. Both primary and secondary antibodies were diluted in 5 % non-fat dry milk in TBS-T (See table 2.3 for specific antibody dilutions). All blots were developed by with the western blotting luminol reagent kit according to the manufacturer's instructions and imaged/scanned using ImageQuant LAS 4000 and ImageQuant software (GE Healthcare, USA). The HMBG1 protein is approximately 30 kilodalton (kDa). A graphical illustration showing its correlation to the MagicMark™ XP

Western Protein Standard (protein ladder) and blots developed by the supplier of the anti-HMGB1 antibody (Abcam™) is provided in figure 3.3.

Table 3.1. Lysis buffer for cell harvesting

Reagents	Amount for six wells
4x NuPAGE LDS buffer	384 µl
1x NuPAGE DTT	96 µl
ddH_2O	480 µl
Total volume	**960 µL**

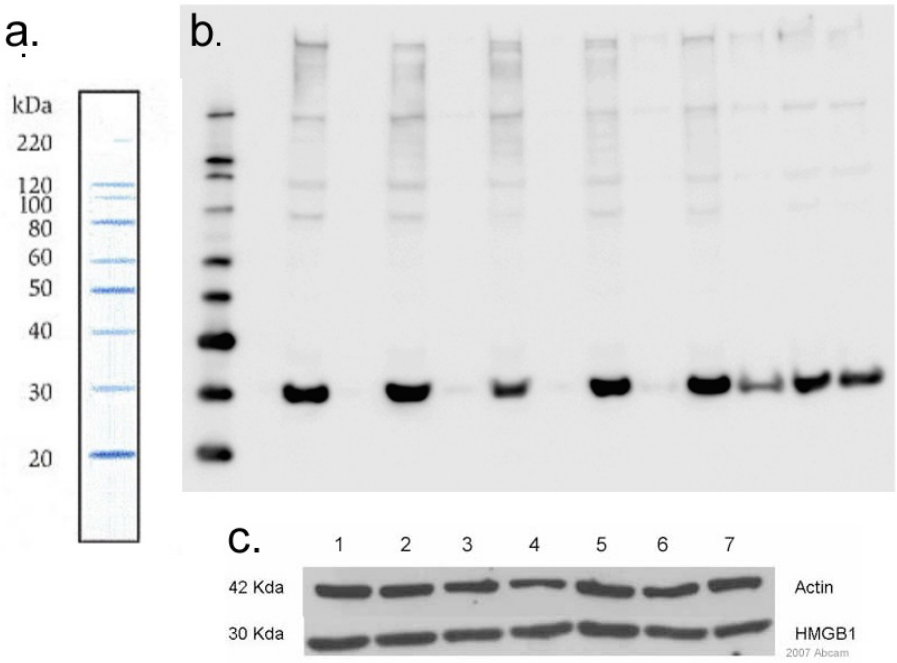

Fig. 3.3. Verification of the HMGB1 protein size. The HMGB1 protein is approximately 30 kilodalton (kDa). An unedited blot/picture **(b)** from this thesis is provided to demonstrate the location of HMGB1 on the PDVF membrane in correlation to the protein standard **(a)** and blots performed by supplier of the anti-HMGB1 antibody **(c).** Figure **a.** and **c.** are retrieved from [163] and [164], respectively. (HMGB1, high mobility group box 1)

3.10 Release of Cytochrome *c* from JM1 and B16F1 cells

JM1 and B16F1 cells (1 x 10^4 cells/well) were plated onto 96-well culture plates in a volume of 1 ml culture media and left to adhere overnight. Cells were treated with the 4 x IC_{50}^{4h} value of LTX-401 (108 μM) for designated time points (30, 60, 90, 120 and 240 min) before collecting the supernatant for further analysis. Cells incubated with serum-free RPMI1640 served as negative control, while a blank sample consisted of RPMI 1640 alone. Quantification of cytochrome *c* was performed using the Rat/Mouse Cytochrome c Quantikine ELISA kit and all reagents were prepared according to the manufacturer's instructions. The kit offers a sensitivity of 0.5 ng/ml while simultaneously allowing for the absolute detection of both reduced and oxidized forms of natural rat and mouse cytochrome *c.* Antibodies that are pre-coated on a microplate captures cytochrome *c* present in the sample while a secondly added HRP-labeled antibody binds to the captured analyte-antibody complex, which allows for unbound substrate and antibodies to be washed away. After incubation, the substrate tetramethylbenzidine is added to each well that generates a blue colored solution that is proportional to the amount of cytochrome *c* in the sample [165]. Seventy five μl of Rat/Mouse Cytochrome *c* Conjugate was added to each well 10 min before adding 50 μl of standard (Rat/Mouse Cytochrome *c* Standard), controls (Rat/Mouse Cytochrome *c* Control) and samples. All samples were diluted 1/5 in serum-free RPMI 1640 as initial studies showed that the attained values were outside the standard range. The plate was covered with an adhesive strip provided with the kit and incubated for 2 h at room temperature. Next, each well was aspirated and washed for a total of five times with 300 μl of washing buffer before adding 100 μl of Substrate Solution and allowing it to incubate for 30 min (protected from light). Hundred μl of Stop Solution was added to terminate the reaction, yielding a yellow color whose absorbance was measured at 450 nm on a spectrophotometric microtiter plate reader (Thermomax Molecular Devices, NJ, USA).

3.11 The B16 mouse melanoma model

In 1954, a melanoma tumor spontaneously arose in a C57BL/6J mouse at the Jackson Laboratories in Maine [177]. Since then, it has been isolated and maintained *in vitro* as a mixed population of heterogeneous cells consisting of both spindle-shaped and epithelial-like cells [178, 179]. The B16F1 cell line represents the original one, and has later been named

consecutively (e.g F2, F3 etc) according to different subcultures that were developed after a series of passages and isolation from metastatic tumors [177]. The subcutaneous B16 melanoma model is notoriously difficult to treat, and has therefore been widely used in oncology research to evaluate certain anticancer therapies [180]. The murine B16F1 melanoma model is well established in our research group and was therefore chosen to study the *in vivo* effects of LTX-401.

3.11.1 Animals and ethical statement

Female C57BL/6 wild-type mice, 5-6 weeks old, were obtained from Charles River, United Kingdom. All animals were housed in the same room and in cages (containing 2-5 mice) specially designed for mice, with 12h/12h day-night cycle, and allowed *ad libitum* access to high quality food and water. Each cage contained environmental enrichments such as nest material, chewing sticks and house. All experiments were approved by the Norwegian National Animal Research Authority (NARA) and conducted in accordance to local and European Ethical Committee guidelines. **NARA/FOTS approval ID: 6586.**

3.11.2 Private statement

PhD student Liv-Marie Eike and Dr. Ketil A. Camilio had the overall responsibility for the animals experiments. After obtaining the Felasa C certificate that allowed me of handling and working with laboratory animals (see Appendix D), I took part in planning the *in vivo* trials, culturing of cells, performing pre-experimental procedures such as weight measurements, shaving the abdomen and individually marking each animal by ear puncturing. The majority of injections were conducted by Liv-Marie Eike to avoid technical variation, but I occasionally contributed by injecting the non-treated animals with vehicle control (saline solution). Every injection performed by me was monitored and carefully instructed by my co-supervisor, Dr. Ketil A. Camilio.

NOTE! All data from the animal experiments that are presented in this thesis descend from initial pilot studies where the aim was to obtain an optimal dose for LTX-401. The main experiment will be finished in Q3/Q4 2015.

Table. 3.2. Overview of *in vivo* experiments

Groups	Intralesional treatment	LTX-401 concentration
Group 1 (5 animals)	0.25 mg LTX-401 in 50 µl saline (2-3 treatments)	5 mg/ml
Group 2 (5 animals)	0.1 mg LTX-401 in 50 µl saline (2-3 treatments)	2 mg/ml
Group 3 (5 animals)	0.05 mg LTX-401 in 50 µl saline (2-3 treatments)	1 mg/ml
Group 4 (5 animals)	0.025 mg LTX-401 in 50 µl saline (2-3 treatments)	0.5 mg/ml
Group 5 (5 animals)	50 µl/ml vehicle control (saline)	-

n=25 animals

saline = 0.9 % NaCl in sterile H_2O

3.11.3 Preparation, intradermal injection and tumor treatment

In addition to marking and weighing, each animal was prior to intradermal (i.d) injection of B16F1 cells shaved on the abdomen (4 cm^2). Cells were harvested and prepared as previously described in section 3.2, but additionally washed in serum-free RPMI 1640 before being diluted to a final concentration of 1 million cells/ml in a cryotube. After gentle mixing to avoid sedimentation of cells, they were injected i.d in the right hand side of the abdomen (5×10^4 B16F1 cells per mouse/50 µl RPMI 1640) using an insulin syringe (Braun Omnican 50). Leftover cells from i.d injection were occasionally brought back to the cell lab to test for cell viability. After reaching a size of around 20-30 mm^2, palpable tumors were injected intralesionally with single doses of LTX-401 dissolved in saline (0.025-0.25 mg LTX-401/50 µl saline) (table. 3.2) once a day for 3 consecutive days. Vehicle control was saline only (0.9 % NaCl in sterile H_2O). Tumor size was monitored by caliper measurements along the length and width of the tumors and expressed as the area of an ellipse [(maximum dimension/2) × (minimum dimension/2) × π].

3.11.4 Secondary tumor challenge

Animals demonstrating complete regression of established B16 melanoma tumors after treatment with LTX-401 were 4-5 weeks later given a second i.d tumor challenge (5×10^4 B16F1 cells per mouse/50 µl RPMI 1640) on the left hand side of the abdomen (contralateral to primary tumor position).

3.11.5 Monitoring of animals and Human endpoint-criteria

All mice were the following days after initial i.d inoculation monitored for tumor growth, body weight and overall physical condition, which were noted on a score scheme (Appendix C). The following Human endpoint-criteria (as stated in the FOTS/NARA application) were implemented in this study;

- Weightloss < 10 %
- Tumor exceeding a diameter of 12-13 mm or 130 mm^2
- Excessive wounds in the area of the tumor
- General signs of discomfort including rouch hair coat and hunched posture

If any of these criteria were met, or if metastasis was evident, the animal was euthanized.

3.12 Statistical analysis

Statistical analysis was performed using GraphPad Prism® software, version 6.0 for Mac. Results are presented as mean ± standard error of mean (SEM) or standard deviation (SD) of at least two or three independent experiments. Data from both ATP bioluminescence and cytochrome *c* assays was compared using Tukey's Multiple Comparison Test, while animal survival curves (Kaplan-Meier Plot) were compared using a Log-rank (Mantel-Cox) test. $P<0.05$ was considered statistically significant.

4. Results

4.1 LTX-401 displays cytotoxic activity against several cancer cell lines

The cell viability assay (MTT) was adopted in order to evaluate the cytotoxic activity of LTX-401 against a panel of both transformed and non-malignant cell lines, and elucidate whether LTX-401 displayed selective killing of tumor cells. A recent study by Hansen and colleagues demonstrated that similar $\beta^{2,2}$-amino acid derivatives of LTX-401 showed high anticancer potency with selective killing of the human Burkitt's lymphoma cell line Ramos compared to RBCs and MRC-5 cells [153]. As a result of the reported cytotoxic activity by these small amphipatic molecules, a continued investigation was conducted on two selected $\beta^{2,2}$-amino acid derivatives, notably BAA-1 (now LTX-401) and BAA-2, for screening of anticancer activity [156]. By employing a rezasurin based cell viability assay to assess the cytotoxic activity against Ramos cells, the authors concluded that LTX-401 displayed anticancer activity comparable with the commonly used chemotherapeutic drug doxorubicin.

In this study, LTX-401 effectively reduced the viability of several tumor cell lines *in vitro*, with a similar degree of cytotoxicity against non-malignant cells (table 4.1). In fact, the minimal cytotoxic activity of LTX-401 was observed against the hepatocellular carcinoma cell line HEPG2 (35.4 μM), while demonstrating almost twice the activity against the human endothelial cell line HUV-EC-C (18.4 μM). For the remaining cell lines, LTX-401 exhibited similar IC_{50} values varying slightly in the range of 22-30 μM, including the non-malignant cell line MRC-5. No *in vitro* hemolytic activity against RBCs was observed using high dosages of LTX-401 (400 μg/ml = 1087 μM), but a slight increase of hemolysis was observed at the maximum concentration tested (500 μg/ml = 1358 μM) (fig. 4.1). Overall, these results indicate that LTX-401 is capable of killing a wide range of cancer cell lines independent of their proliferative status as shown by similar IC_{50} values. Moreover, LTX-401 is also active against non-malignant cells, with the exception of erythrocytes.

Table 4.1. *In vitro* cell viability assay of LTX-401 against cancer cell lines and non-malignant cells. Cells were treated with concentrations ranging from 1-100 μg/ml for 4 hours. IC_{50} values are converted and given in micro molar (μM). Data are presented as mean and are representative of two or three independent experiments.

Cell line	Origin	LTX-401 IC_{50}[1] ± SD (μM)
JM1	Rat hepatocellular carcinoma	22.8 ± 3.3
HEPG2	Human hepatocellular carcinoma	35.4 ± 0.6
BEL7402	Human hepatocellular carcinoma	26.7 ± 0.4
HT-29	Human colorectal adenocarcinoma	31.7 ± 2.9
B16F1	Murine skin malignant melanoma	23.3 ± 3.9
A375	Human skin malignant melanoma	30 ± 0.9
SK-N-AS	Human neuroblastoma	30.6 ± 0
MRC-5	Human lung fibroblasts	22.9 ± 1.4
HUVEC	Human vascular endothelium	18.4 ± 1.9
RBC	Human	>1087[2]

[1] The peptide concentration killing 50 % of the cells

[2] Highest tested concentration of peptide before 50 % lysis of RBCs was 400 μg/ml (1087 μM)

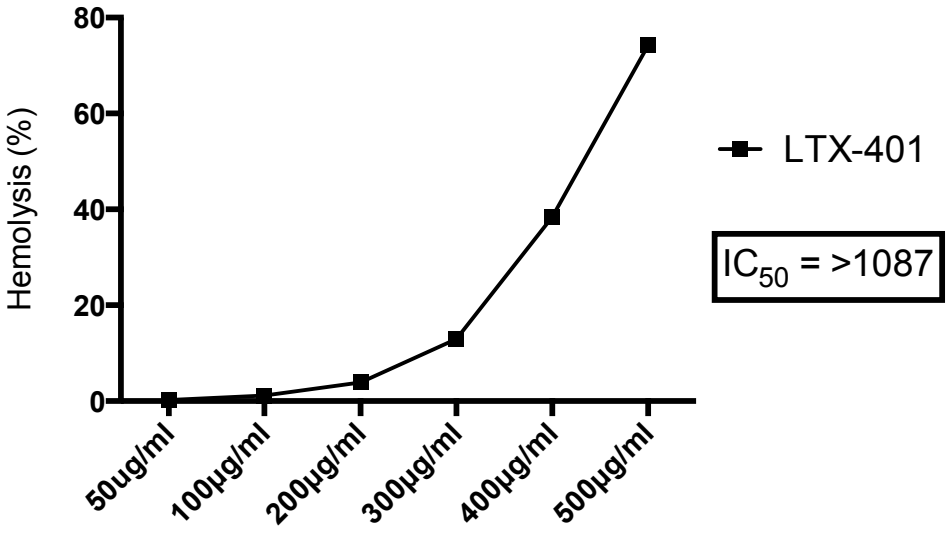

Fig. 4.1. *In vitro* hemolytic activity of LTX-401. Freshly isolated hRBCs were incubated with increasing concentrations of LTX-401 (50 – 500 μg/ml) for 1 h before the absorbance of the supernatant was measured at 405 nm. Cells incubated with PBS and 10 % Triton solution alone served as negative and positive control, respectively. (hRBCs, human red blood

4.2 Time course of killing by LTX-401 against JM1 and B16F1 cells

One of the main advantages of ACPs is their ability to induce rapid killing of tumors cells by facilitating membrane destabilization resulting in loss of its integrity. Kinetic experiments were in this thesis carried out to determine the time dependency of killing by LTX-401 against JM1 hepatocellular carcinoma cells and B16F1 melanoma cells. Two different concentrations representing the 2 x IC_{50}^{4h} and 4 x IC_{50}^{4h} of LTX-401, i.e 54 μM and 108 μM, respectively, were chosen on the background of previously determined IC_{50} values of LTX-401 (~26-27 μM). Figure 4.2 shows that treatment with both 54 μM and 108 μM of LTX-401 against JM1 cells display similar kinetics up to 30 min, with a kill ratio just beneath 50 %. Within 90 min, all JM1 cells were dead when treated with 108 μM, while a small fraction of cells (~10 %) still remained metabolically active after 240 min when stimulated with 54 μM of LTX-401. B16F1 cells treated with 108 μM of LTX-401 exhibited similar killing kinetics as JM1 cells with a kill ratio of 50 % after 15 min, followed by nearly 100 % cell death two hours after start of treatment. In contrast, cells incubated with 54 μM of LTX-401 followed a gradual inhibition of cell viability with 50 % cell survival after two hours.

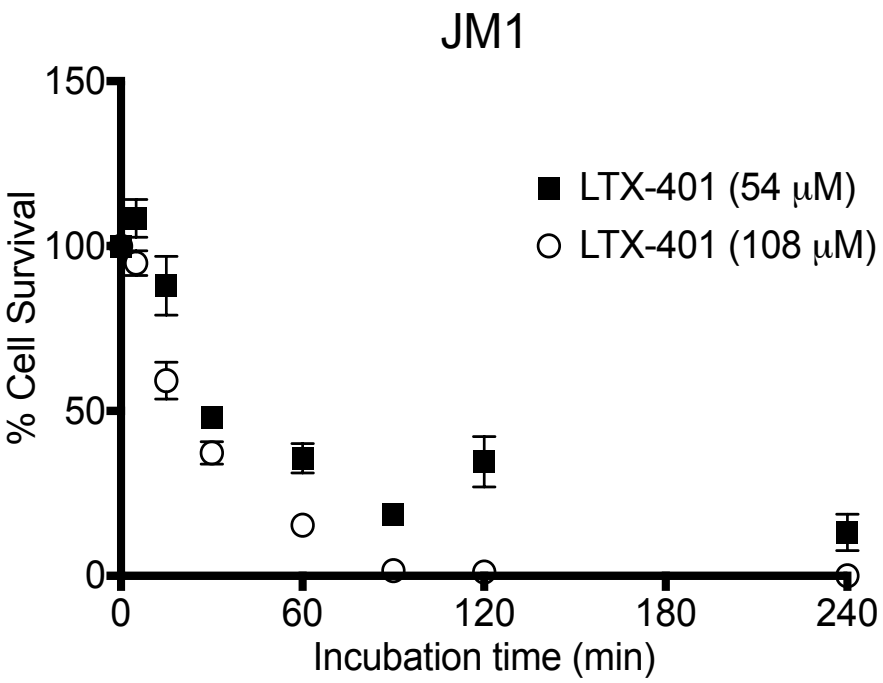

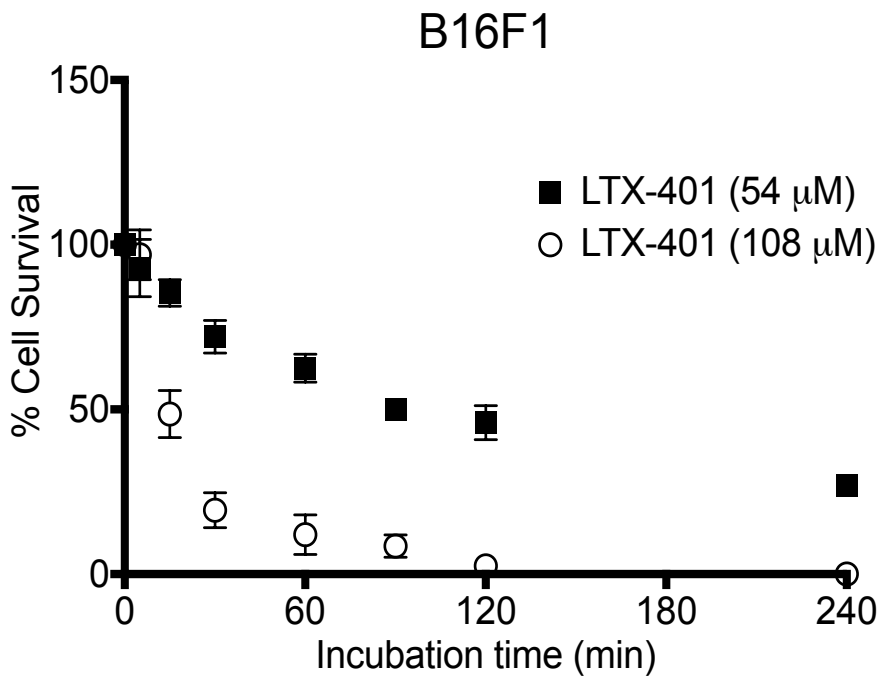

Fig. 4.2 Killing kinetics of JM1 hepatocellular carcinoma and B16F1 melanoma cells treated with LTX-401. Cells were treated with 54 and 108 μM of LTX-401 for designated time points (5, 15, 30, 60, 90, 120 and 240 min). Both concentrations represent the 2 x IC_{50}^{4h} and 4 x IC_{50}^{4h} of LTX-401, respectively. Data represent the mean ± SEM of three independent experiments with duplicates for each.

4.3 Treatment with LTX-401 lead to ultrastructural changes in JM1 and B16F1 cells

To further investigate the mechanism of action underlying the cytotoxic activity of LTX-401, both JM1 and B16F1 cells were incubated with the 4 x IC_{50}^{4h} of LTX-401 (108 μM) for 5, 15, 30 and 60 min. Untreated cells served as control and were incubated in serum-free RPMI 1640 until the experimental end-point (60 min). After incubation, all cells were fixed and prepared for TEM studies. Electron microscopic examination of untreated JM1 cells (fig. 4.3a and b) revealed a rough cell surface provided with many microvillous-like pseudopods indicating highly active cells. The cytoplasm contained a relatively large amount of mitochondria with clearly visible morphology as seen by the normal cristae structure (fig. 4.3g). A majority of the cells had a nucleus mainly consisting of euchromatin with little or no apparent heterochromatin. By contrast, JM1 cells treated with LTX-401 displayed several ultrastructural differences that after 5 min manifested itself in loss or reduction of cell surface (microvillous-like structures) and a moderate increase in cell volume due to swelling (fig. 4.3c and d). After 60 min, TEM micrographs showed massive vacuolization of treated cells with clearly diminished plasma membrane integrity conferring to an almost "boiling-like" appearance (fig. 4.3e, f and h). In addition, cells treated with LTX-401 showed no significant alterations in chromatin appearance/structure. Higher magnification also revealed clear changes in mitochondrial morphology (fig. 4.3g compared to fig. 4.3h), which included swelling of the internal compartment and overall loss of cristae structure. The majority of treated cells had the appearance of the single cell presented in figure. 4.3f, but TEM micrographs also revealed a small portion of cells with disrupted plasma membranes and leakage of cellular content (images not shown). Of note, cells that have lost their adhesion are likely to be washed away during sample preparation, which could help explain the low occupancy of cells with the endpoint morphology typical for necrosis.

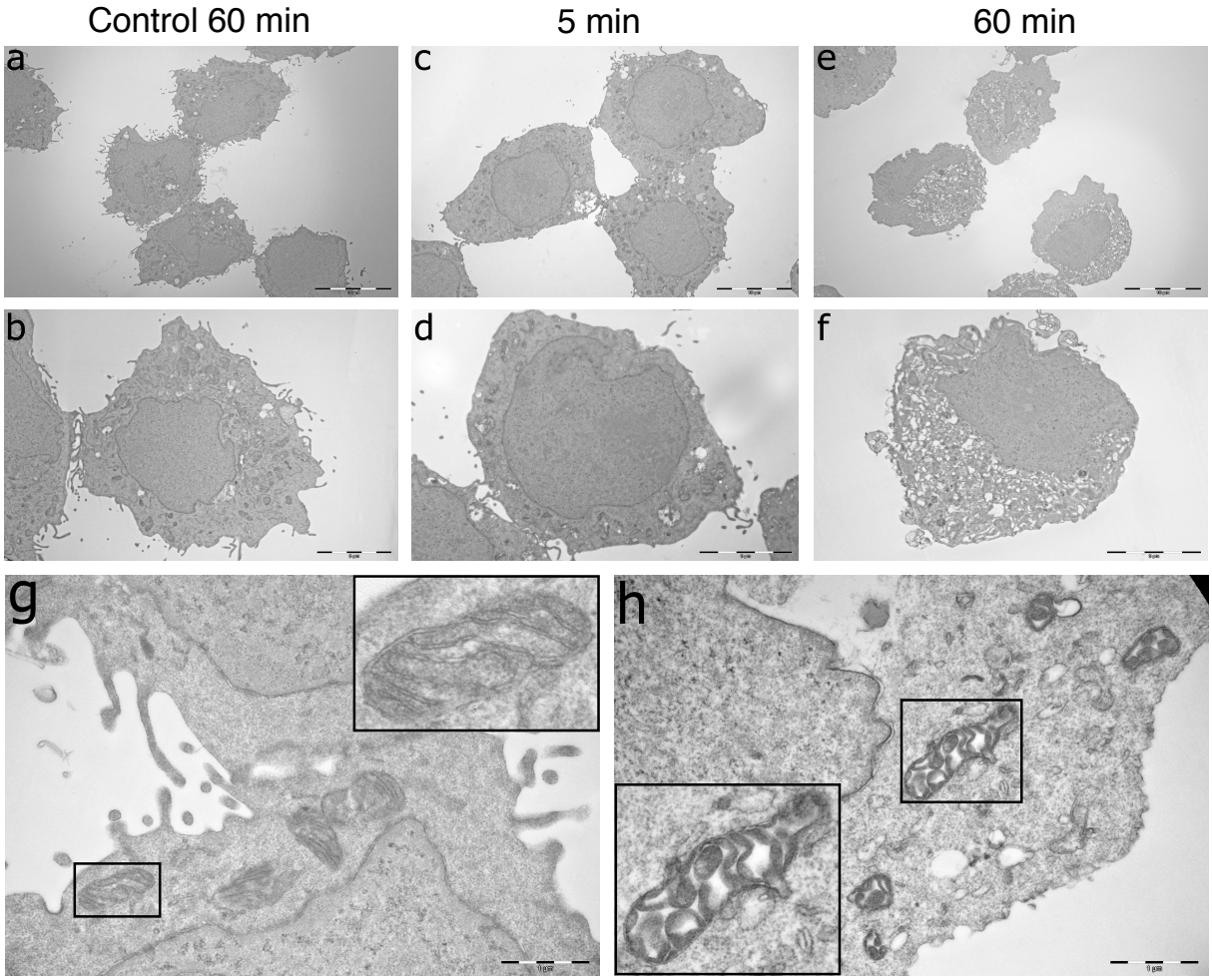

Fig. 4.3. Representative TEM micrographs of JM1 hepatocellular carcinoma cells treated with LTX-401. Cells were seeded at a density of 1.0 x 10^4 in 35 mm tissue culture dishes and allowed to reach confluence of ~80 % before being treated with the 4 x IC_{50}^{4h} of LTX-401 (108 μM) for various time points (5, 15, 30 and 60 min), and finally fixed in a PHEM buffered malachite green fixative containing 0.05 % malachite green, 0.5 % glutaraldehyde and 4 % formaldehyde. Untreated control cells (**a, b**) were kept in serum-free RPMI 1640 until experimental end-point (60 min) and compared with cells treated for 5 min (**c, d**) and 60 min (**e, f**). Morphology of mitochondria in control cells (**g**) was compared to LTX-401 treated cells (**h**). Scale bares = 10 μm for **a**, **c**, **e**, 5 μm for **b**, **d**, **f** and 1 μm for **g** and **h**.

TEM images of untreated B16F1 cells also revealed a rough surface characterized by frequent microvillous-like protrusions on the plasma membrane. The cytoplasm consisted of several electron-dense mitochondria while also having visible smooth ER and Golgi apparatus. As with JM1 cells, the nucleus of B16F1 cells was primarily composed of euchromatin (fig. 4.4a and b). A small population of LTX-401 treated cells lost their surface morphology after 5 min (image not shown), but the majority of cells were without significant alterations except slight

vacuolization of the cytoplasm (fig. 4.4c and d). At experimental end-point (60 min), TEM images demonstrated a heterogeneous population/mixture of cells including both heavily vacuolated and large non-vacuolated cells. A relatively large portion of cells was necrotic as clearly seen by the loss of plasma membrane integrity and leakage of cell constituents into the extracellular space (fig. 4.4e and f). While chromatin structure was more or less unaffected by LTX-401 treatment (albeit slightly condensed in some), a relatively large portion of cells displayed nuclear envelope invaginations, some even reaching deep into the nucleoplasm. Furthermore, higher magnification revealed no significant ultrastructural changes in mitochondria of the majority of LTX-401 treated cells (fig. 4.4h) compared to control (fig. 4.4g), except containing more electron-dense cristae. In addition, images taken at 140,000x magnification (not shown) even exposed intact inner and outer mitochondrial membranes. Cells that were examined close to end-point treatment, however, contained mitochondria with some degree of swelling although these were difficult to image and interpret due to an even more electron-dense appearance. Overall, these observations demonstrate that LTX-401 kills via a lytic/disruptive mode of action, and that cell death is accompanied by cellular swelling and massive vacuolization of the cytoplasm in both JM1 and B16F1 cells but varies with respect to morphology of certain organelles (i.e. mitochondria).

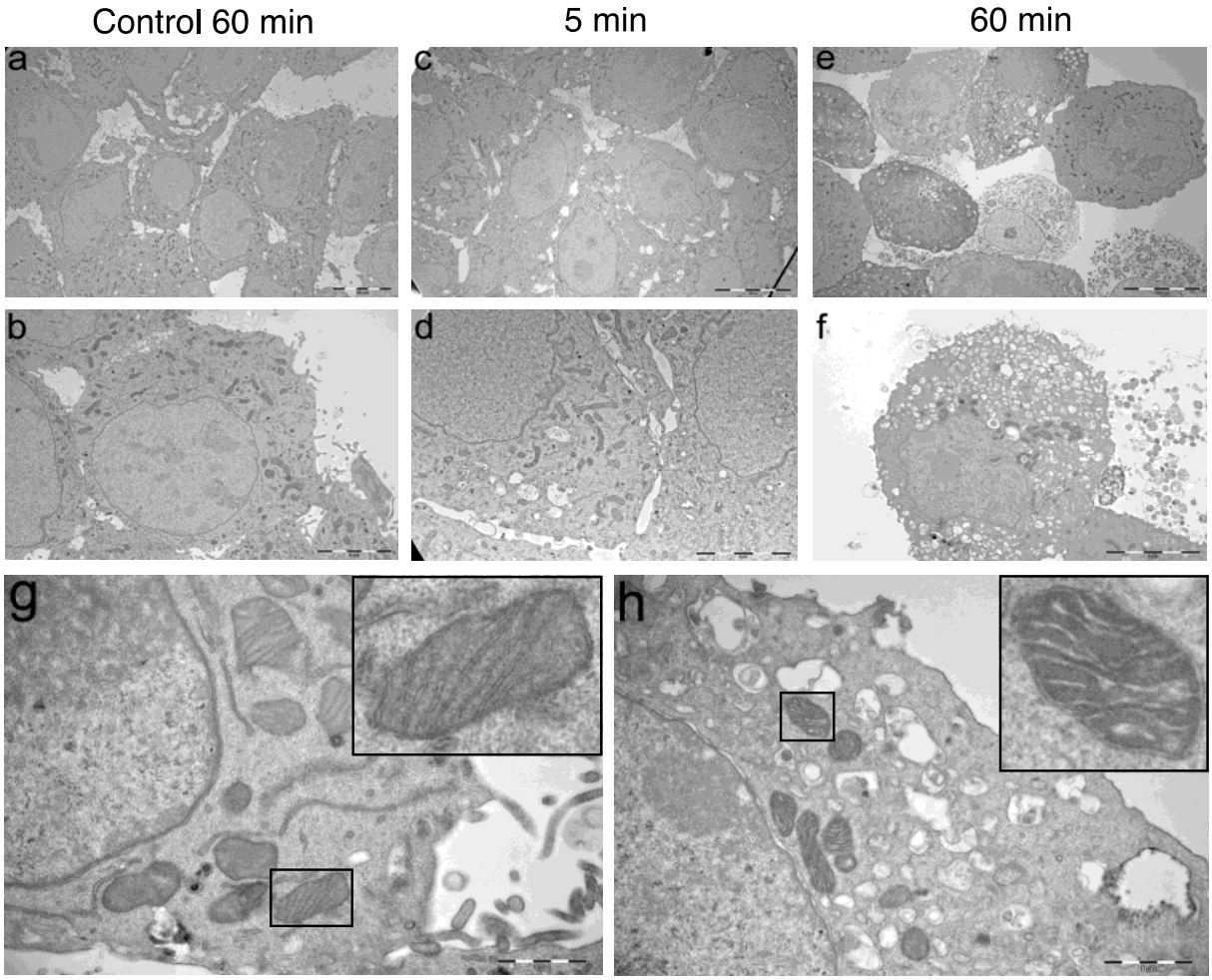

Fig. 4.4. Representative TEM micrographs of B16F1 melanoma cells treated with LTX-401. Cells were seeded at a density of 1.0 x 10^4 in 35 mm tissue culture dishes and allowed to reach confluence of ~80 % before being treated with the 4 x IC_{50}^{4h} of LTX-401 (108 μM) for various time points (5, 15, 30 and 60 min), and finally fixed in a PHEM buffered malachite green fixative containing 0.05 % malachite green, 0.5 % glutaraldehyde and 4 % formaldehyde. Untreated control cells (**a, b**) were kept in serum-free RPMI 1640 until experimental end-point (60 min) and compared with cells treated for 5 min (**c, d**) and 60 min (**e, f**). Morphology of mitochondria in control cells (**g**) was compared to LTX-401 treated cells (**h**). Scale bares = 10 μm for **a**, **c**, **e**, 5 μm for **b**, **d**, **f** and 1 μm for **g** and **h**.

4.4 Morphological study by phase-contrast microscopy imaging

Phase-contrast imaging was employed to substantiate electron microscopy studies and to study morphology of LTX-401 treated cells. After treated for 15 min, JM1 cells had lost their elongations/cell tips and started to appear more vacuolated and necrotic after 30 min. At experimental end-point (60 min), the majority of cells were lysed as seen by the presence of necrotic cell bodies and cellular debris (fig. 4.5). B16F1 cells followed similar morphological

changes, but seemed more viable after 15 compared to JM1 cells. After 30 min, B16F1 cells had lost their overall morphology and some necrotic cell bodies were observed. At 60 min, the majority cells were no longer capable of retaining membrane integrity, and thus succumbed to necrosis (fig. 4.6). Interestingly, B16F1 cells were, compared to JM1 cells, not only more adherent to the surface after 60 min of LTX-401 treatment, but also adherent to each other.

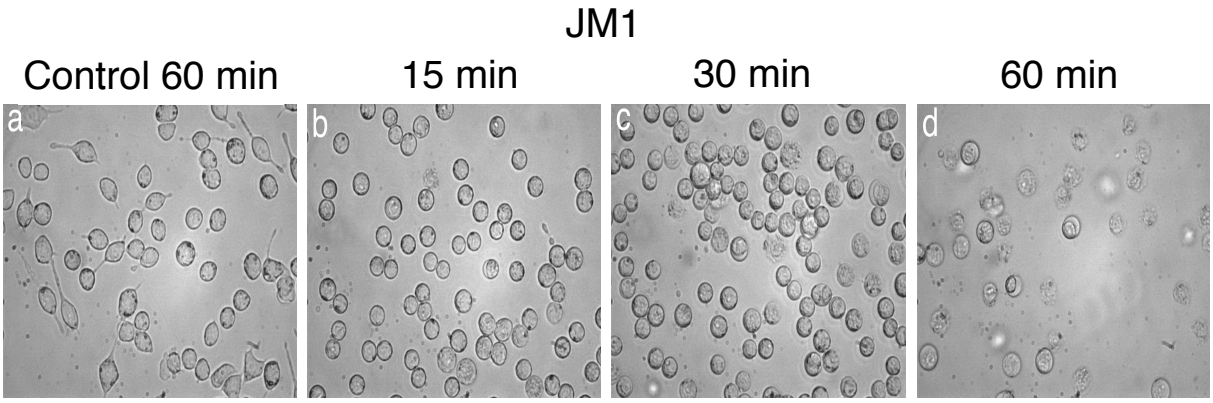

Fig. 4.5. Phase-contrast imaging of JM1 hepatocellular carcinoma cells treated with LTX-401. Cells were seeded at a density of 2.0 x 10^5 cells/well on 6-well plates and treated with the 4 x IC_{50}^{4h} of LTX-401 (108 μM) for 15 (**b**), 30 (**c**) and 60 (**d**) min and compared with non-treated control cells (**a**) incubated in serum-free RPMI 1640. All images were taken at 40x magnification.

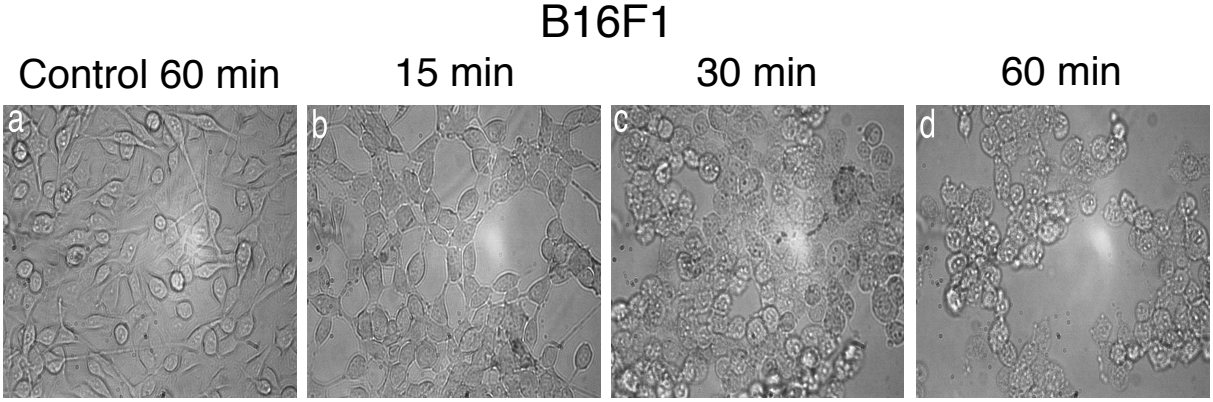

Fig. 4.6. Phase-contrast imaging of B16F1 melanoma cells treated with LTX-401. Cells were seeded at a density of 2.0 x 10^5 cells/well on 6-well plates and treated with the 4 x IC_{50}^{4h} of LTX-401 (108 μM) for 15 (**b**), 30 (**c**) and 60 (**d**) min and compared with non-treated control cells (**a**) incubated in serum-free RPMI 1640 for 60 min. All images were taken at 40x magnification.

4.5 JM1 and B16F1 cells release ATP when treated with LTX-401 *in vitro*

ATP is reported to have immunogenic properties when released from dying and/or stressed cells, including cancer cells succumbing to conventional chemotherapy [181], and has thus become one of the main determinants of ICD. To investigate whether LTX-401 was able to induce the release of ATP from JM1 and B16F1 cells a luciferin-luciferase based reaction assay was employed. In JM1 cells, the extracellular concentration of ATP quickly increased after 60 min of LTX-401 treatment (fig. 4.6a) while, contrary to B16F1 cells, peaked at 90 min before the signal dropped after 120 min. The signal obtained at 120 min, however, was still significantly higher than control cells. As with JM1 cells, the extracellular concentration of ATP by B16F1 cells quickly rose 60 min after initiating treatment with a gradual increase towards 120 min (fig. 4.6b). Since all experiments were conducted during a two-hour period, a diminished signal was not observed as it was with JM1 cells. It is noteworthy that B16F1 cells display a 5-fold higher release of ATP than JM1 cells at time points 120 min and 90 min, respectively. Taken together, these observations indicate that LTX-401 induced cell death of JM1 and B16F1 cells is accompanied by the extracellular release of ATP into the culture supernatant and that the relative amount is dependent on cell type.

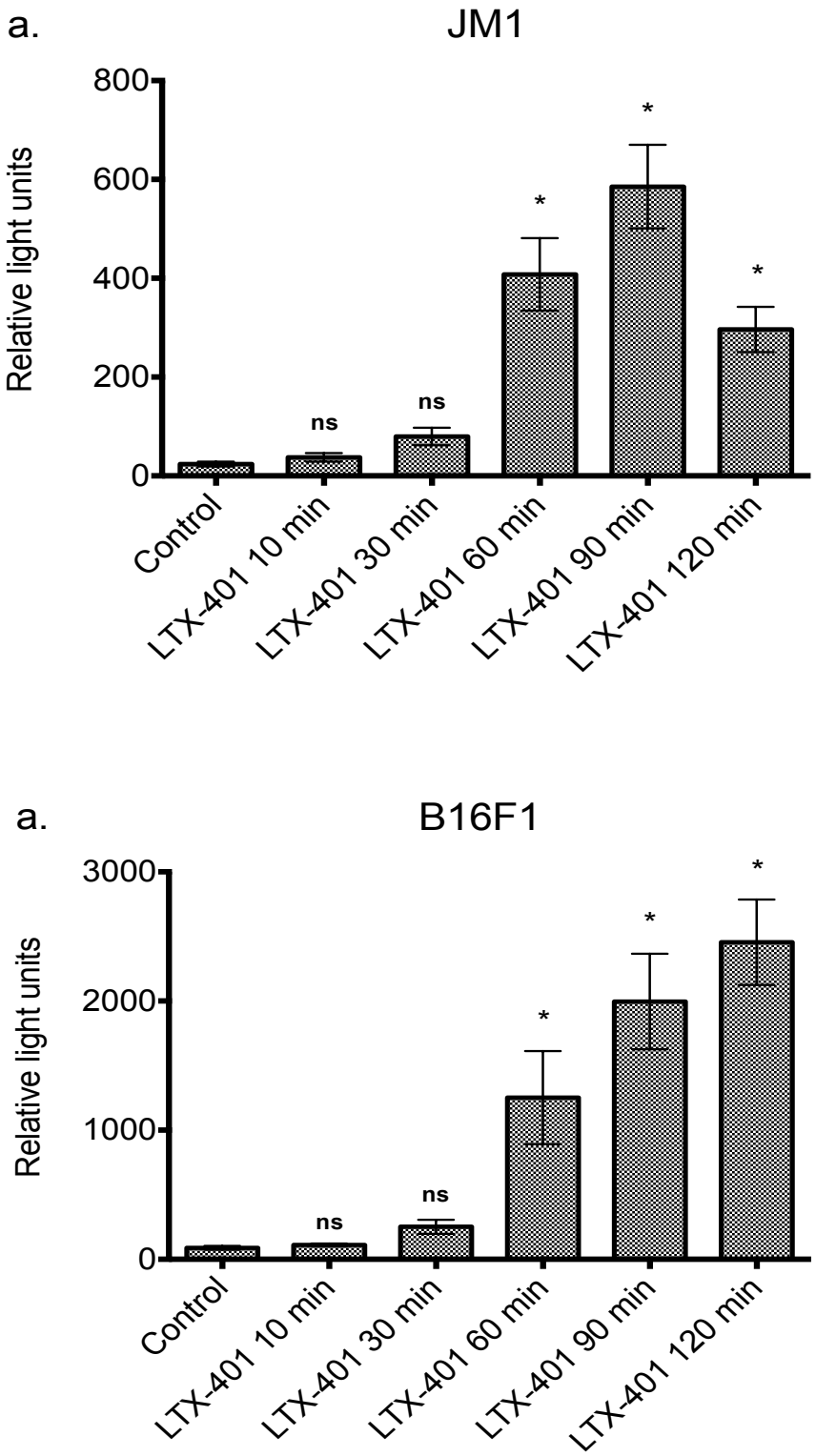

Fig. 4.6. Extracellular ATP levels following treatment with LTX-401. Both **(a)** JM1 hepatocellular carcinoma and **(b)** B16F1 melanoma cells were seeded (1 x 10^4 cells/well) in 96-well plates and left to adhere overnight in a cell incubator before being incubated with 2 x IC_{50}^{4h} value of LTX-401 (54 μM) for designated time points (10, 30, 60, 90 and 120 min). Cells preserved in serum-free RPMI 1640 for equal time points served as control. NB! Data from controls were gathered and organized into one single column. Culture supernatants were collected at end of treatment and subjected to an rLuciferase/Luciferin (rL/L) reagent to facilitate the chemiluminescent reaction. At the highest peak, release of ATP is 5-fold higher in B16F1 cells **(b)** compared to JM1 cells **(a)**. Values are expressed in relative light units (RLU) and represent the mean (with SEM) of duplicate samples from three representative experiments on each cell line. *Statistical significance (treated vs control), was determined using Tukeys

4.6 JM1 and B16F1 cells release HMGB1 when treated with LTX-401 *in vitro*

As with ATP, the cytokine-like DAMP activities of secreted HMGB1 from stressed and/or dying cells is also crucial in mounting an immunogenic response [182]. To further characterize the ability of LTX-401 to induce ICD, the release of HMGB1 from JM1 and B16F1 into cell culture supernatants was assessed by western blot analysis. Using a dosage of 54 μM LTX-401 (2 x IC_{50}^{4h}) over 2 h induced a late release of HMGB1 from JM1 cells, as seen by the translocation of the protein from the lysate to the supernatant (fig. 4.7a). LTX-401 failed to stimulate HMGB1 translocation in B16F1 cells (fig. 4.7b), indicating that the response is cell type-specific.

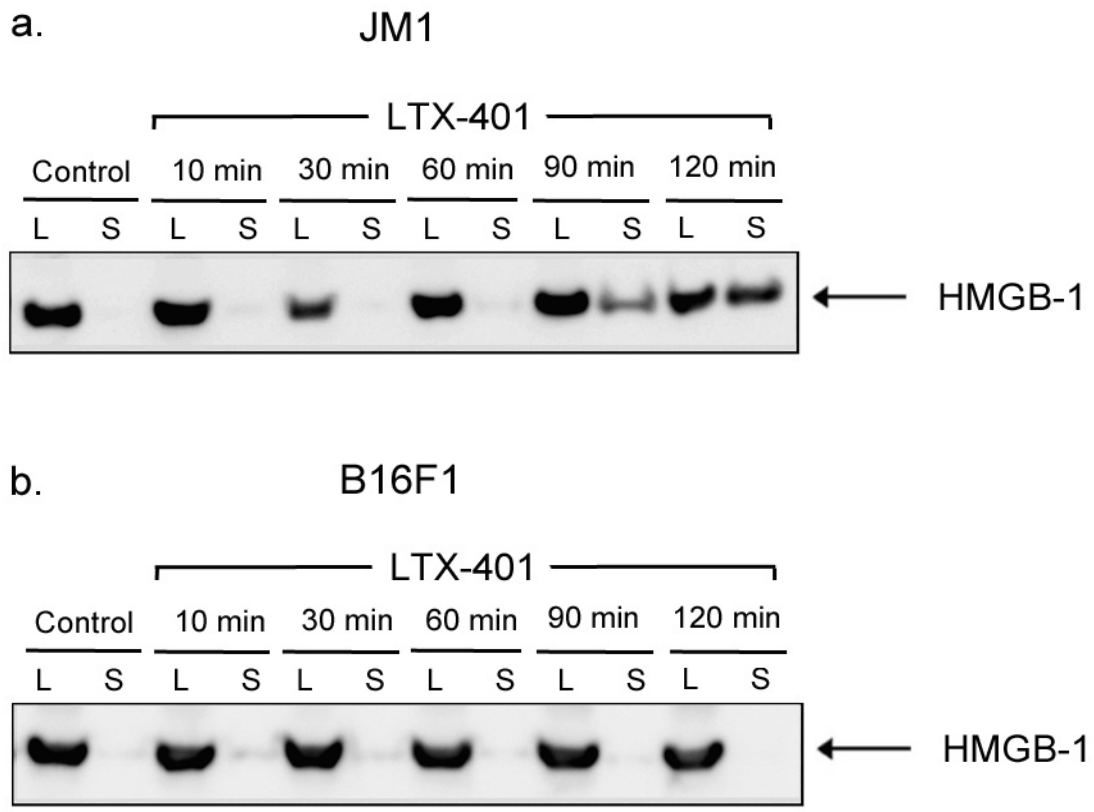

Fig. 4.7. Western blot analysis of HMGB1 following treatment with LTX-401. JM1 hepatocellular carcinoma **(a)** and B16F1 melanoma cells **(b)** were seeded in 6-well plates (2.0 x 10^5 cells per well) and treated with the 2 x IC_{50}^{4h} value of LTX-401 (54 μM) for designated time points (10, 30, 60, 90 and 120 min). Control cells were during the whole experiment (120 min) preserved in serum-free RPMI 1640 medium only. The translocation of HMGB1 from the JM1 cell lysate **(L)** to the supernatant **(S)** is seen at 90 min while continuing/increasing in signal strength towards 120 min. For B16F1 cells, no translocation of HMGB1 was observed using a dosage of 54 μM LTX-401. The figure is a representative image of several western blots attained for experimental validation. (HMGB1, high mobility group box 1)

To explore whether higher dosages of LTX-401 managed to induce release of HMGB1 from B16F1 cells, an experimental setup using increasingly higher concentrations of LTX-401 in the range of 12.5 μg/ml – 200 μg/ml (34-543 μM) with a fixed time period of 4 h was employed. Indeed, LTX-401 stimulated B16F1 cells to release HMGB1 in a dose-dependent manner (fig. 4.8), in which translocation of the protein was initiated at a concentration of 25 μg/ml (68 μM). The following concentrations all induced complete translocation of HMGB1 from the lysate to the supernatant.

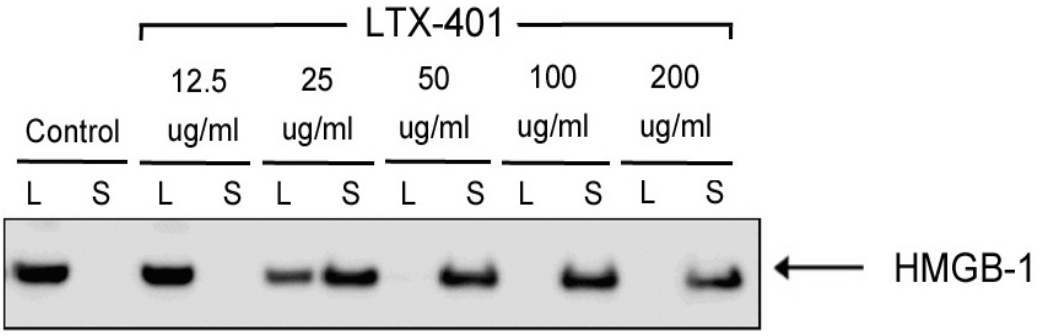

Fig. 4.8. LTX-401 induces the release of HMGB1 from B16F1 melanoma cells in a dose-dependent manner. B16F1 melanoma cells were seeded at a density of 2.0 x 10^5 cells per well in a volume of 2 ml medium in 6 well tissue culture plates and treated with increasing doses of LTX-401 (12.5 – 200 μg/ml) during a 4 h period. B16F1 cells attained in serum-free RPMI 1640 alone served as a control. Western blot analysis of lysates (L) and supernatants (S) show the HMGB1 protein starting to appear in supernatants of cells treated with 25 μg/ml of LTX-401. Following doses of LTX-401 all show translocation of HMGB1 from cell lysate to supernatant. The figure is a representative image of several western blot analysis attained for experimental validation. (HMGB1, high mobility group box 1)

As these experimental data indicated the need of higher concentrations of LTX-401 to induce complete release of HMBG1 into cell culture supernatants, additional experiments were performed on both JM1 and B16F1 cells. Using twice the 4 x IC_{50}^{4h} value of LX-401 (108 μM) and increased time points as in preliminary studies, LTX-401 was able to stimulate a complete release of HMGB1 into the supernatant in both JM1 (fig. 4.9a) and B16F1 cells (fig. 4.9b). Furthermore, the translocation was initially faster in B16F1 cells compared to JM1 cells with release of HMGB1 occurring at 30 and 60 min, respectively. In contrast to earlier findings, it was interesting to observe a quicker release of HMGB1 in B16F1 cells compared to JM1 cells,

suggesting that not only is the release cell type-specific, but the inherent capability of LTX-401 to induce such is dependent on the concentration. Untreated control cells displayed no release of HMGB1 into the supernatant, as seen by the complete retainment of the protein within the lysates in all experiments.

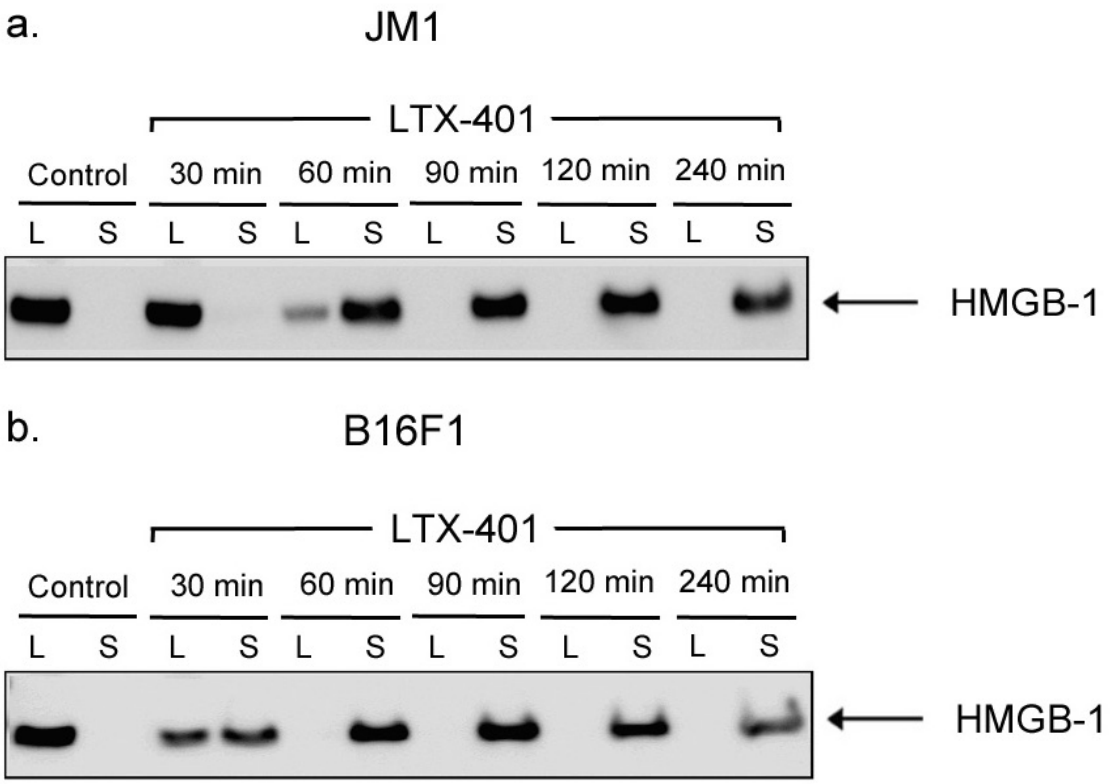

Fig. 4.9. Western blot analysis of HMGB1 following treatment with LTX-401. JM1 hepatocellular carcinoma **(a)** and B16F1 melanoma cells **(b)** were seeded in 6-well plates and treated with the 4 x IC_{50}^{4h} of LTX-401 (108 μM) for designated time points (30, 60, 90, 120 and 240 min). Control cells were during the whole experiment (240 min) preserved in serum-free RPMI 1640 medium only. HMGB1 translocates from the cell lysate **(L)** to the supernatant **(S)** after 60 min for JM1 cells, while displaying slightly accelerated release into the supernatant for B16F1 cells after 30 min. The figure is a representative image of several western blot analysis attained for experimental validation. (HMGB1, high mobility group box 1)

4.7 JM1 and B16F1 cells release cytochrome *c* when treated with LTX-401 *in vitro*

Although not typically associated with ICD, cytochrome *c* still marks one of the early events during apoptotic cell death where its release from the mitochondrial intermembrane space into the cytosol controls the assembly of the apoptosome and activation of procaspase-9 [183, 184]. To study whether LTX-401 was able to induce release of cytochrome *c* from the mitochondria of JM1 and B16F1 cells, an ELISA assay was employed to measure the amounts of cytochrome *c* in the cell culture medium after treatment. Quantitative analysis demonstrated that cytochrome *c* was found in the supernatants of JM1 and B16F1 cells as early as 30 min into treatment with the 4 x IC_{50}^{4h} value of LTX-401 (108 μM) (fig. 4.10). The absolute amount of cytochrome *c* was not, however, statistically significant when compared to control cells until 90 min into treatment for JM1 cells and 120 min for B16F1 cells. The release of cytochrome *c* from B16F1 cells followed a gradual increase over time, reaching a peak of around 40 ng/ml at experimental endpoint (fig. 4.10b). LTX-401 induced a slightly different pattern of cytochrome c release in JM1 cells displaying a drop after peaking at 90 min, before yet increasing at 240 min (fig. 4.10a). However, calculations (using Tukey's multiple comparisons test, data not shown) revealed that the value obtained for 120 min was not statistically different compared to values obtained for 90 min and 120 min, respectively. As with ATP-release from JM1 and B16F1 cells after treatment with LTX-401, the release of cytochrome *c* is also cell type-specific as demonstrated by the 2-fold higher amount released from JM1 cells contrary to B16F1 cells. These data suggests that LTX-401 might traverse the plasma membrane and induce mitochondrial membrane permeabilization and/or swelling, leading to the release of cytochrome *c* into the cytosol, while later eventuating in the extracellular space as plasma membrane integrity becomes lost.

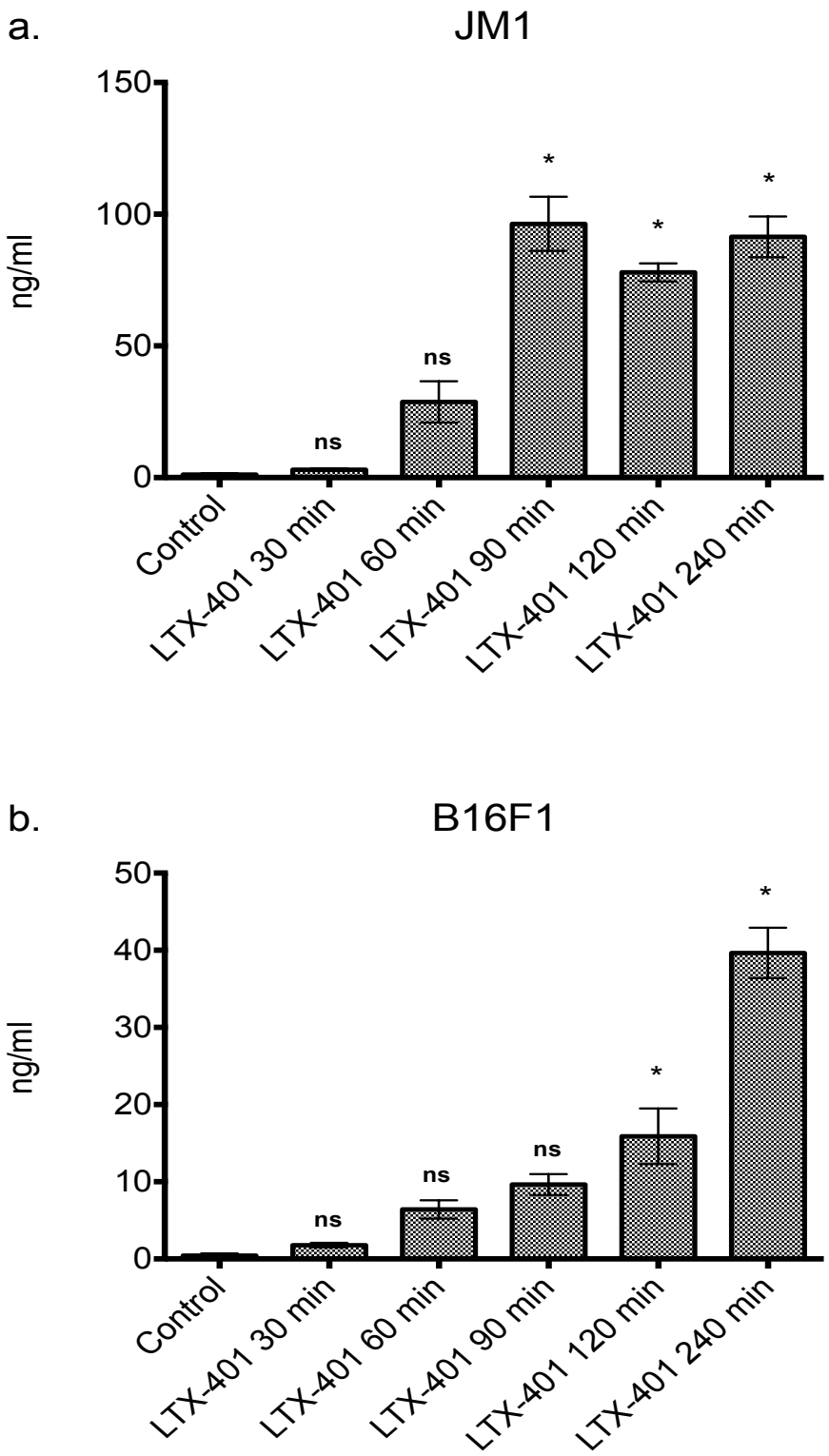

Fig. 4.10. Quantitative analysis of cytochrome *c* in cell culture supernatants after treatment with LTX-401. JM1 hepatocellular carcinoma **(a)** and B16F1 melanoma cells **(b)** were incubated with the 4 x IC_{50}^{4h} of LTX-401 (108 μM) for different time points (30, 60, 90, 120 and 240 min) before evaluating the amount of cytochrome *c* in supernatants using the 'Rat/Mouse Cytochrome c Quantikine®ELISA' kit. Untreated cells incubated in RMPI 1640 served as a control. Values are expressed as ng/ml of cytochrome *c* and represent the mean (with SEM) of duplicate samples from two representative experiments on each cell line. *Statistical significance (treated vs control), was determined using Tukeys multiple comparisons test where $P<0.05$. **ns**=not significant

4.8 LTX-401 induces complete regression of B16 melanomas

In order to identify the optimal dosage of LTX-401 in the murine B16 melanoma model, a pilot study was conducted using 5 groups of animals, in which four received different doses (0.5 mg/ml – 5 mg/ml) of LTX-401, while the final group served as a vehicle-injected group. Mice with i.d established B16 melanomas were injected intralesionally with 50 µl of either vehicle control (n = 5), 5 mg/ml LTX-401 (n = 5) 2 mg/ml LTX-401 (n=3), 1 mg/ml LTX-401 (n=5) or 0,5 mg/ml LTX-401 (n = 5) for three consecutive days (fig. 4.11a). In the group receiving 2 mg/ml of LTX-401 only 3 animals were treated due to lack of primary tumor growth in 2 of the animals. Tumors in both the control group and group receiving 0.5 mg/ml of LTX-401 grew rapidly and all mice were euthanized due to excessive tumor growth (130 mm^2) within 22 days after tumor challenge. Likewise, all animals in the group receiving 1 mg/ml of LTX-401 had to be euthanized due to tumor burden, albeit slightly prolonged survival in one individual who was not euthanized until 25 days after tumor challenge. Only one animal injected with a dosage of 2 mg/ml survived while the remaining two were euthanized after 15 and 17 days, respectively. All animals receiving the highest concentration of LTX-401 (5 mg/ml) displayed complete regression of tumors and showed no signs of relapse throughout the observation period of 4 weeks after treatment.

Following the hypothesis that the durable response of LTX-401 was based on adaptive immune responses, cured animals (n=5), along with untreated control animals (n=2), were given a second i.d tumor challenge of 5×10^4 viable B16F1 cells in their abdomen contralateral to the primary tumor site (seven weeks post primary tumor challenge). As presented in figure 4.11c, tumor growth was only observed in one individual while being completely absent in the remaining animals. In addition, tumor reoccurrence was not observed within the observation period of 50 days after secondary tumor challenge indicating protective immune responses. It should be noted, however, that this finding was not statistically significant as shown by a log-rank (Mantel-Cox) test (data not shown), due to few animals in the control group as the current study was designed to test "proof-of-principle". In contrast, all control animals developed tumor (fig. 4.11b).

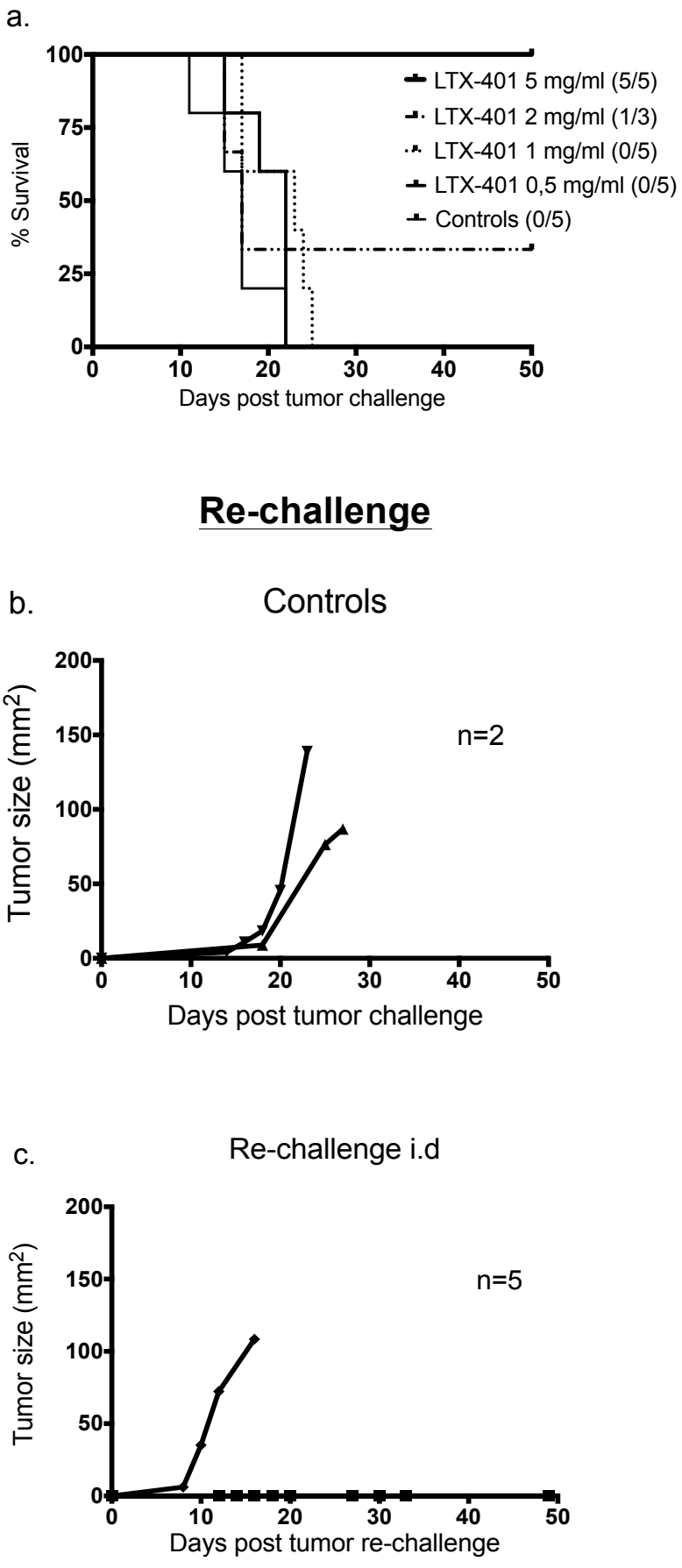

Fig. 4.11. Anti-tumor activity of LTX-401 in i.d established murine B16 melanomas. Palpable melanoma tumors syngeneic with C57BL/6 mice were treated intralesionally with various concentrations of LTX-401 or with vehicle control (0.9 % NaCl) **(a),** presented as Kaplan-Meier survival curves, and analyzed using a log-rank (Mantel-Cox) test ($P < 0.05$). Mice that were previously cured using a concentration of 5 mg/ml LTX-401 were given a second i.d challenge (5×10^4 B16F1 cells contralateral to primary tumor site) (**c**) and compared with non-treated control animals receiving vehicle control (saline solution only (**b**). (i.d, intradermal).

5. Discussion

The present study aimed to investigate the mechanisms underlying the anticancer effect of the synthetic $\beta^{2,2}$-amino acid derivative LTX-401. A central question to be answered was whether LTX-401 displayed cytotoxic activity against cancer cell lines other than the ones previously reported and if this effect was selective compared to non-cancerous cells. There are several reports on both naturally occurring and synthetic anticancer peptides (ACPs) with the capacity of selective killing [85, 93, 185], a property believed to derive from the fact that cancer cells often carry a higher net negative charge on their plasma membrane compared to non-transformed cells. This may in turn help facilitate binding and aggregation of cationic ACPs on the surface of cancer cells, thus causing membrane destabilization and lysis of the cell. Non-transformed cells are less likely to be targeted by ACPs as their plasma membrane is predominantly composed of electrically neutral (zwitterionic) molecules such as sphingomyelin and phosphatidylcholine [48, 49]. By contrast, the plasma membrane of cancer cells has been shown to carry a higher net negative charge due to a higher than normal amount of anionic molecules including phosphatidylserine [43, 44], sulfated glycosaminoglycans like heparin sulfate [45, 46] and O-glycosylated mucins [45, 47]. In addition to differences in membrane net charge, cancer and normal mammalian cells also vary with respect to membrane fluidity and increased surface area of cancer cells due to a higher number of microvilli [50, 51], which may increase their susceptibility to ACPs.

As presented in this study, LTX-401 exhibited anticancer activity against a wide range of human cancer cell lines (HEPG2, BEL7402, HT-29, A375, SK-N-AS), as well as a rat hepatocellular carcinoma (JM1) and murine melanoma cell line (B16F1). However, despite the effectiveness in killing tumor cells, LTX-401 is equally potent against non-malignant cells as demonstrated by the IC_{50} value obtained on human fibroblasts and human umbilical cord endothelial cells. Our group has previously, through structure-activity relationship studies on bovine lactoferricin (LfcinB) derivatives, designed 9-mer peptides (the LTX-300 series) with a net positive charge of +6. Both LTX-302 and LTX-315 have the potential to adopt an α-helical coil structure (predicted by the Garnier-Osguthorpe-Robson V method [186]) and have been shown to kill cancer cells more effectively than the naturally occurring LfcinB (25-mer), both *in vitro* and *in vivo* [110, 111]. LTX-315 is, however, thought to be less selective than LTX-302 due to the slightly larger aromatic sector, thus conferring it an overall higher hydrophobicity.

This notion is supported by recent observations in which α-ACPs with greater hydrophobicity were less selective and exhibited more cytotoxicity against normal cells [85, 187]. Such a structural parameter may (partly) help explain the lack of selectivity and hence an unspecific targeting of non-malignant cells by LTX-401 as the two aromatic side chains governs it a high hydrophobicity, thus making it more prone to interact with phospholipid bilayers. Furthermore, it is likely that the low positive charge of LTX-401 (+2) reduces its capacity of binding strongly to anionic surface components on cancer cells via electrostatic forces. It is plausible that a higher cationicity would render non-malignant cells less susceptible to killing, but since LTX-401 was designed for the local treatment of solid tumors, the selectivity against cancer cells is less important in contrast to anticancer drugs designed for systemic use.

Despite being efficient in killing several cancer cell lines at low micromolar concentrations, LTX-401 displays insignificant IC_{50} hemolytic activity against human red blood cells (fig. 4.1). A number of ACPs are in fact ineffective against erythrocytes, which is believed to derive from both elevated levels of cholesterol in their membranes and a high content of zwitterionic plasma membrane components [188-191]. Studies have also indicated that increased hydrophobicity of ACPs correlates with an increase of hemolytic activity, which is consistent with membrane discrimination mechanisms on eukaryotic cells [85, 187, 192]. Due to its highly hydrophobic side chains, and overall amphipatic structure, it is likely that LTX-401 is capable of penetrating deep into, and even transverse cancer cell membranes. Whether cell death as induced by LTX-401 is accompanied by pore formation remains elusive, but chances are that the molecule is of insufficient size to initiate such events and may thereby constitute a new and unknown mechanism of action that needs to be further elucidated.

Kinetic experiments were conducted in order to study the impact of different concentrations of LTX-401 against JM1 hepatocellular carcinoma cells and B16F1 melanoma cells over time. Both concentrations represented the 2 x IC_{50}^{4h} and 4 x IC_{50}^{4h} value (approximately). Surprisingly, both 2 x IC_{50}^{4h} and 4 x IC_{50}^{4h} value of LTX-401 caused a similar degree of reduced cell viability in JM1 cells while having a more severe impact on B16F1 cells (fig. 4.2). The cellular survival was, however, reduced to an absolute minimum in both cell lines after 90-120 min using the 4 x IC_{50}^{4h} value (108 μM). In contrast, commonly used chemotherapeutics are known to require much longer incubation periods to exert significant

anticancer effects due to its intercalating mode of action by targeting susceptible phases of the cell cycle. In addition, the use of chemotherapy alone is seldom effective and curative in solid tumors [193].

Electron microscopy was employed to study morphological changes of LTX-401-treated cancer cells, but also to verify and substantiate further bioassay based results (i.e release of DAMPs). These studies revealed an early loss of surface morphology and slight vacuolization of the cytoplasm in both JM1 and B16F1 cells, albeit to a different extent in the two cell lines (fig. 4.3 and 4.4). An increase in cell size (i.e oncosis) was also evident shortly after start of LTX-401 treatment. The latter is regarded as an early morphological characteristic of necrosis, while the phenomenon of cells rounding-up is considered a morphological aspect of apoptosis [194]. By prolonging the incubation period (to 60 min) of treated cells, transmission electron microscopy (TEM) images demonstrated that cells were killed via a lytic mode of action resulting in loss of cell membrane integrity and subsequent leakage of intracellular contents into the extracellular milieu. Apoptotic cell bodies were not observed in either cell line treated with LTX-401. Cell death by necrosis was also observed by Ausbacher et al., in which LTX-401 was tested against human Burkitt's lymphoma (Ramos cells) [154]. Necrotic cell death was, however, more apparent in TEM micrographs of B16F1 cells compared to JM1 cells, which could reflect a shortcoming in the microwave assisted procedure; since both pre- and post-fixation is carried out *en bloc* with several washing steps in between, it is reasonable to believe that a considerable amount of dead (and detached) cells are washed away during the process. Considering the equal experimental setup for both cell lines, one explanation as to why there are more B16F1 cells with endpoint morphology typical for necrosis than JM1 cells could derive from differences in adherence between the two cell lines, or that JM1 cells reach endpoint earlier than B16F1 cells. Moreover, phase-contrast imaging revealed that a substantial portion of JM1 cells were in fact necrotic, and detached cells appeared floating in the culture medium (fig. 4.5).

Kroemer et al. has defined massive vacuolization of the cytoplasm (and absence of chromatin condensation) as a morphological aspect of autophagic cell death [194], a notion that is also supported in other literature [195, 196]. The contribution of autophagy to cell death is still somewhat controversial [197], but in this context, the formation of vacuoles containing

cytoplasmic material could perhaps constitute a transitional state in which cells respond to acute intracellular stress exerted by LTX-401 on different organelles. At higher magnification, TEM micrographs revealed that a substantial portion of LTX-401-treated JM1 cells contained significantly affected mitochondria, which was clearly seen by excessive swelling and loss of normal cristae structure (fig. 4.3h). In contrast, the mitochondria of B16F1 cells seemed less affected by treatment (fig. 4.4h), but swelling and formation of electron dense cristae was still evident. The observed differences could account for cell-specific (plasma membrane) differences that allows for quicker internalization of LTX-401 in JM1 cells compared to B16F1 cells, and is thus given more time to act on organelles such as mitochondria before cellular lysis and death. The B16F1 cell line is moreover known to consist of a heterogeneous population of both spindle-shaped and epithelial like cells [178, 179, 198], which could respond differently to treatment with anticancer substances, including LTX-401.

One of the major drawbacks of conventional cancer regiments is their inability to eradicate all tumor cells due to high heterogeneity of the tumor and thereby its non-targeted mode of action. Moreover, cell death as induced by many commonly used chemotherapeutics proceeds by triggering downstream events that ultimately results in programmed cell death (apoptosis). The latter is often regarded as a non-stimulatory event and may recreate an immunosuppressive environment that is detrimental to any potential anti-tumor immune responses [101, 122, 199, 200]. After the introduction of the concept of immunogenic cell death (ICD), it has become increasingly evident that the mode of cancer cell death represents a larger role in determining the outcome and success of selected anticancer therapies than previously anticipated [112, 122, 201]. The activation of potent anti-tumor immune responses has been shown to rely on a series of cellular and biochemical events culminating in the emission of Damage-Associated Molecular Pattern molecules (DAMPs) from dying and/or stressed tumor cells, including surface exposed calreticulin (CRT), secreted adenosine triphosphate (ATP) and passively released High Mobility Group Box-1 protein (HMGB1), which are among the requirements for cell death to be perceived as immunogenic. When interacting with their respective receptors, DAMPs (along with tumor antigens) orchestrate the recruitment and activation of dendritic cells (DCs) into the tumor bed, which may later home to draining lymph nodes to active tumors-specific $CD8^+$ T cells [131-133]. In the present project, JM1 hepatocellular and B16F1 melanoma cells were screened for the release of

ATP and HMGB1 using a modified luciferase assay and western blot analysis, respectively, when treated with LTX-401 *in vitro*. All preliminary experiments were carried out using the 2 x IC_{50}^{4h} value of LTX-401 (54 μM) over a total time period of 1 h, which were parameters chosen based on the background of previously determined IC_{50} values of LTX-401. Accordingly, if the release of DAMPs from dying cancer cells was absent after treatment with LTX-401, the concentration was increased.

Results showed that LTX-401 induced the release of ATP and HMGB1 from JM1 and B16F1 cells (fig. 4.6 and 4.9). When rapidly released or secreted into the extracellular matrix by dying and/or stressed tumor cells, ATP has been shown to act on purinergic receptors to facilitate the recruitment of immune phagocytes and DCs into the tumor bed [134]. Furthermore, when binding to P_2X_7 receptors on DCs, ATP stimulates the assembly of NLRP3 inflammasome causing a series of downstream events that ultimately result in the production and release of IL-1β, a cytokine required for the priming of IFN-γ producing tumor-specific $CD8^+$ T cells [138, 202, 203]. The release of ATP was 5-fold higher in B16F1 cells compared to JM1 cells during the 2h treatment period with LTX-401 (54 μM). In addition, while extracellular levels of ATP continue to increase in B16F1 cells, an opposite trend was observed for JM1 cells. These observations may account for cell-specific, and perhaps, metabolic differences between the two cell lines. Moreover, due to the presence of extracellular ATP-degrading enzymes [204], the extracellular levels of ATP are expected to drop after a given time period. Accordingly, by expanding the time course of the experiment, a drop in signal would probably have been observed for B16F1 as well. Interestingly, a similar pattern of ATP-release from JM1 cells has been observed by treatment with a nonamer lytic peptide LTX-315 (unpublished data/manuscript), in which extracellular ATP levels increased before gradually diminishing. These observations are consistent with results obtained with LTX-401, where an identical experimental setup was employed.

The translocation of HMGB1 from the intracellular compartment to the extracellular space (supernatant) was also observed when treating JM1 and B16F1 cells with LTX-401, which is likely to have occurred after the disruption of the plasma membrane (confirmed by TEM studies). The extracellular release of HMGB1 from post-apoptotic and/or necrotic cells is capable of sustaining and augmenting an anti-tumorigenic environment by the attraction of

inflammatory leukocytes and stimulation of pro-inflammatory cytokines such as TNF-α and IL-6 [145, 205]. In addition, HMGB1 serves a pivotal role in the maturation of DCs and favors both processing and presentation of tumor antigens to naïve T cells, thus establishing a link between innate and adaptive anti-tumor immune responses [122, 206, 207]. However, the release of HMGB1 from dying cancer cells is not solely consistent with establishment of anti-tumor immune responses as redox modifications induced either by the cell or the extracellular milieu might alter and even attenuate its DAMP activities [208, 209].

A cytochrome *c* ELISA assay was performed to further assess the capability of LTX-401 to release mitochondrial DAMPs. The release of cytochrome *c* into the cytoplasm is considered one of the key initiative steps of the intrinsic apoptotic pathway [210, 211]. However, the extracellular functions of cytochrome *c* are less known, but evidence suggests that it may directly modulate the production of pro-inflammatory cytokines and chemokines via activation of the NF-κB pathway [212]. In this thesis, LTX-401 was shown to induce the extracellular release of cytochrome *c* from both JM1 hepatocellular carcinoma and B16F1 melanoma cells, *in vitro* (fig. 4.10). Again, both cell lines displayed intrinsic differences as reflected by the 2-fold higher release of cytochrome *c* from JM1 cells compared to B16F1 cells. The observed variation could derive from the more adverse impact LTX-401 exercise on the mitochondria of JM1 cells (confirmed by TEM studies), thus releasing more cytochrome *c* into the cytosol which can be detected after the loss of plasma membrane integrity. In addition, while TEM micrographs confirmed the lysis of B16F1 cells after 60 min, the release of cytochrome *c* was not significantly different from controls until after 120 min, which could indicate that the mitochondria is still somewhat intact and continue to retain its cytochrome *c* a while after cellular dissolution. Altogether, the findings in this thesis suggest an ICD-inducing role of LTX-401, as demonstrated by the release of ATP, HMGB1 and cytochrome *c* from cancer cells *in vitro.* Moreover, the potential cytotoxic effect exerted by LTX-401 on normal cells may lead to an augmentation of the immune response due to an increase in the amount of DAMPs being released, which ultimately results in an immune response against the more immunogenic tumor antigens.

It has recently been proposed that inducers of ICD can be classified based on their ability to trigger apoptosis via induction of endoplasmic reticulum (ER) stress [112]. Notably, type II ICD inducers such as hypercin-based photodynamic therapy specifically target the ER, while type I inducers including anthracyclines (e.g doxorubicin and mitoxantrone), oxaliplatin and cyclophosphamide primarly target cytosolic proteins, components of the plasma membrane or nucleic proteins [112, 182]. Many studies have demonstrated *in vivo* anticancer effects of both type I and II ICD inducers, mainly through prophylactic tumor vaccination models with transplantable tumors [182]. However, little attention has been given to ACPs in the context of ICD and cancer therapy. This is despite reports on inhibition of tumor growth and metastasis [89, 90, 107], which indicates a potential involvement of the immune system.

As the work conducted in this thesis indicated the potential use of LTX-401 in a therapeutic setting, our group conducted a pilot-study ('proof-of-principle') to assess the anticancer effects against the highly aggressive and poorly immunogenic murine B16 melanomas. Mice that were given the highest dosage of LTX-401 (5 mg/ml) once a day for 3 consecutive days all displayed complete regression of intradermally (i.d) established B16 melanoma tumors (fig. 4.11a). To assess whether this effect was systemic, all cured animals were subjected to a second tumor challenge with live tumor cells (seven weeks after primary tumor challenge), but this time inoculated at a different site on the abdomen. Interestingly, 80 % of previously cured animals displayed no signs of tumor growth, meaning that B16F1 cells were rejected (fig. 4.11c). All control animals, however, developed tumors (fig. 4.11b). Accordingly, this indicates that treatment with LTX-401 induced a secondary (adaptive) immune response with persistence of anti-tumor immunity, thus demonstrating an *in situ* vaccination effect. Histological examinations of tumors treated with LTX-401 revealed increased infiltration of $CD3^+$ T cells (*Prof. B. Sveinbjørnsson, personal communication*), which also correlates with activation of an immune response established by ICD. Therefore, the cytolytic effect exerted by LTX-401 may provide a favourable immunogenic environment due to the release of several DAMPs along with tumor antigens, which together orchestrate long-lasting tumor immune protection. A failure to induce the release of endogenous adjuvants in the form of DAMPs will abolish the perception of ICD by the immune system and hence compromise the immune response [213]. Our group has previously demonstrated that complete regression and systemic protection against rechallenge of i.d established murine A20 lymphomas after

treatment with the lytic ACPs LTX-302, is dependent on the involvement of both $CD4^+$ and $CD8^+$ T cells [111]. As the mechanism of action by LTX-401 is similar to LTX-302, it strongly suggests a T-cell based immunity, which is consistent with the model of ICD [214].

6. Conclusions and future perspectives

The work of this thesis has attempted to investigate the mechanisms underlying the anticancer activity of the $\beta^{2,2}$-amino acid derivative LTX-401. This was achieved by utilizing biological assays followed by a 'proof-of-principle' study in the B16 mouse melanoma model to assess its clinical potential for use in solid tumors. *In vitro* cytotoxicity studies demonstrated that LTX-401 displays potent activity against several cancer cell lines. Further analysis revealed a lytic mechanism of action by LTX-401 that is accompanied by the release of DAMPs such as ATP, HMGB1 and cytochrome *c*. Moreover, mice that were treated intralesionally with LTX-401 displayed complete regression of tumors and were protected against relapse of the cancer. The combined observations (both *in vitro* and *in vivo*) suggest that the therapeutic effect of LTX-401 is achieved by two distinct modalities. First, LTX-401 exerts a direct cytotoxic effect against cancer cells that ultimately leads to the irreversible loss of plasma membrane integrity, thus releasing intracellular content. Second, as a result of the direct effect, the extracellular milieu becomes enriched with tumor antigens and DAMPs that initiates the activation and maturation of antigen-presenting cells. This may lead to cross-priming of tumor-specific $CD8^+$ cytotoxic T lymphocytes and subsequent generation of protective antitumor immunity.

In conclusion, the obtained results support LTX-401 as a novel and promising drug candidate for the treatment of solid tumors.

To further study the role of LTX-401 as an anticancer- and ICD-inducing agent, complementary studies should be aimed at investigating the potential role of other DAMPs *in vitro,* including surface exposure of CRT but also newly discovered contributors to the immunogenicity of cell death such as interferon-α and various chaperones of the heat-shock protein family. While the latter can be studied by using Western Blot analysis on cells treated with LTX-401, assays for the evaluation of ICD *in vivo* are naturally more demanding, and also limited to the number of syngeneic tumor models. As of today, the primary approach to

assess ICD *in vivo* consists of prophylactic vaccination assays with *ex vivo* treated cancer cells. Nonetheless, assays that monitors cell death-associated parameters and patterns of pro-inflammatory cytokines will strengthen the hypothesis of LTX-401 functioning as an inducer of ICD. Finally, it would also be of great interest to study the effects of LTX-401 in combination with other anticancer regiments to improve the chances of therapeutic success.

7. References

1. Hancock, R.E. and Diamond, G. 2000. The role of cationic antimicrobial peptides in innate host defences. *Trends in microbiology*. 8, 9 (Oct. 2000), 402–10.
2. Hancock, R.E.W. and Sahl, H.-G. 2006. Antimicrobial and host-defense peptides as new anti-infective therapeutic strategies. *Nature biotechnology*. 24, 12 (Dec. 2006), 1551–7.
3. Seo, M.-D., Won, H.-S., Kim, J.-H., Mishig-Ochir, T. and Lee, B.-J. 2012. Antimicrobial peptides for therapeutic applications: a review. *Molecules (Basel, Switzerland)*. 17, 10 (Oct. 2012), 12276–86.
4. Nijnik, A. and Hancock, R. 2012. Host defence peptides: antimicrobial and immunomodulatory activity and potential applications for tackling antibiotic-resistant infections. *Emerging health threats journal*. 2, (Mar. 2012), e1.
5. Steinstraesser, L., Kraneburg, U.M., Hirsch, T., Kesting, M., Steinau, H.-U., Jacobsen, F. and Al-Benna, S. 2009. Host defense peptides as effector molecules of the innate immune response: a sledgehammer for drug resistance? *International journal of molecular sciences*. 10, 9 (Oct. 2009), 3951–70.
6. Boman, H.G. 1996. Peptide antibiotics: holy or heretic grails of innate immunity? *Scandinavian journal of immunology*. 43, 5 (Jun. 1996), 475–82.
7. Ganz, T. and Lehrer, R.I. 1998. Antimicrobial peptides of vertebrates. *Current opinion in immunology*. 10, 1 (May. 1998), 41–4.
8. http://aps.unmc.edu/AP/main.php
9. Hancock, R.E. and Scott, M.G. 2000. The role of antimicrobial peptides in animal defenses. *Proceedings of the National Academy of Sciences of the United States of America*. 97, 6 (Sep. 2000), 8856–61.
10. van 't Hof, W., Veerman, E.C., Helmerhorst, E.J. and Amerongen, A.V. 2001. Antimicrobial peptides: properties and applicability. *Biological chemistry*. 382, 4 (Jun. 2001), 597–619.

11. Stark, M., Liu, L.-P. and Deber, C.M. 2002. Cationic hydrophobic peptides with antimicrobial activity. *Antimicrobial agents and chemotherapy*. 46, 11 (Oct. 2002), 3585–90.

12. Jenssen, H., Hamill, P. and Hancock, R.E.W. 2006. Peptide antimicrobial agents. *Clinical microbiology reviews*. 19, 3 (Jul. 2006), 491–511.

13. Sitaram, N. and Nagaraj, R. 2000. Interaction of antimicrobial peptides with biological and model membranes: structural and charge requirements for activity. *Biochimica et biophysica acta*. 1462, 1-2 (Feb. 2000), 29–54.

14. Yeaman, M.R. and Yount, N.Y. 2003. Mechanisms of antimicrobial peptide action and resistance. *Pharmacological reviews*. 55, 1 (Mar. 2003), 27–55.

15. Teixeira, V., Feio, M.J. and Bastos, M. 2012. Role of lipids in the interaction of antimicrobial peptides with membranes. *Progress in lipid research*. 51, 2 (Feb. 2012), 149–77.

16. Park, S.-C., Park, Y. and Hahm, K.-S. 2011. The role of antimicrobial peptides in preventing multidrug-resistant bacterial infections and biofilm formation. *International journal of molecular sciences*. 12, 9 (Oct. 2011), 5971–92.

17. Hassan, M., Kjos, M., Nes, I.F., Diep, D.B. and Lotfipour, F. 2012. Natural antimicrobial peptides from bacteria: characteristics and potential applications to fight against antibiotic resistance. *Journal of applied microbiology*. 113, 4 (Sep. 2012), 723–36.

18. Fernebro, J. 2011. Fighting bacterial infections-future treatment options. *Drug resistance updates : reviews and commentaries in antimicrobial and anticancer chemotherapy*. 14, 2 (May. 2011), 125–39.

19. Brogden, K.A. 2005. Antimicrobial peptides: pore formers or metabolic inhibitors in bacteria? *Nature reviews. Microbiology*. 3, 3 (Mar. 2005), 238–50.

20. Guilhelmelli, F., Vilela, N., Albuquerque, P., Derengowski, L. da S., Silva-Pereira, I. and Kyaw, C.M. 2013. Antibiotic development challenges: the various mechanisms of action of antimicrobial peptides and of bacterial resistance. *Frontiers in microbiology*. 4, (Dec. 2013), 353.

21. Vizioli, J. and Salzet, M. 2002. Antimicrobial peptides from animals: focus on invertebrates. *Trends in pharmacological sciences*. 23, 11 (Nov. 2002), 494–6.

22. Shin, S.Y., Kang, J.H., Lee, M.K., Kim, S.Y., Kim, Y. and Hahm, K.S. 1998. Cecropin A - magainin 2 hybrid peptides having potent antimicrobial activity with low hemolytic effect. *Biochemistry and molecular biology international*. 44, 6 (Aug. 1998), 1119–26.

23. Dürr, U.H.N., Sudheendra, U.S. and Ramamoorthy, A. 2006. LL-37, the only human member of the cathelicidin family of antimicrobial peptides. *Biochimica et biophysica acta*. 1758, 9 (Oct. 2006), 1408–25.

24. De Smet, K. and Contreras, R. 2005. Human antimicrobial peptides: defensins, cathelicidins and histatins. *Biotechnology letters*. 27, 18 (Oct. 2005), 1337–47.

25. Sato, H. and Feix, J.B. 2006. Peptide-membrane interactions and mechanisms of membrane destruction by amphipathic alpha-helical antimicrobial peptides. *Biochimica et biophysica acta*. 1758, 9 (Oct. 2006), 1245–56.

26. Ganz, T. 2003. Defensins: antimicrobial peptides of innate immunity. *Nature reviews. Immunology*. 3, 9 (Sep. 2003), 710–20.

27. Yang, D., Biragyn, A., Hoover, D.M., Lubkowski, J. and Oppenheim, J.J. 2004. Multiple roles of antimicrobial defensins, cathelicidins, and eosinophil-derived neurotoxin in host defense. *Annual review of immunology*. 22, (Mar. 2004), 181–215.

28. Greer, A., Zenobia, C. and Darveau, R.P. 2013. Defensins and LL-37: a review of function in the gingival epithelium. *Periodontology 2000*. 63, 1 (Aug. 2013), 67–79.

29. Ebenhan, T., Gheysens, O., Kruger, H.G., Zeevaart, J.R. and Sathekge, M.M. 2014. Antimicrobial peptides: their role as infection-selective tracers for molecular imaging. *BioMed research international*. 2014, (Sep. 2014), 867381.

30. Friedrich, C.L., Rozek, A., Patrzykat, A. and Hancock, R.E. 2001. Structure and mechanism of action of an indolicidin peptide derivative with improved activity against gram-positive bacteria. *The Journal of biological chemistry*. 276, 26 (Jun. 2001), 24015–22.

31. Hiemstra, P.S., Fernie-King, B.A., McMichael, J., Lachmann, P.J. and Sallenave, J.-M. 2004. Antimicrobial peptides: mediators of innate immunity as templates for the development of novel anti-infective and immune therapeutics. *Current pharmaceutical design*. 10, 23 (Sep. 2004), 2891–905.

32. Bowdish, D.M.E., Davidson, D.J. and Hancock, R.E.W. 2005. A re-evaluation of the role of host defence peptides in mammalian immunity. *Current protein & peptide science*. 6, 1 (Jan. 2005), 35–51.

33. Yang, D., Biragyn, A., Kwak, L.W. and Oppenheim, J.J. 2002. Mammalian defensins in immunity: more than just microbicidal. *Trends in immunology*. 23, 6 (Jun. 2002), 291–6.

34. Hilchie, A.L., Wuerth, K. and Hancock, R.E.W. 2013. Immune modulation by multifaceted cationic host defense (antimicrobial) peptides. *Nature chemical biology*. 9, 12 (Nov. 2013), 761–8.

35. Zhang, M., Zhao, J. and Zheng, J. 2014. Molecular understanding of a potential functional link between antimicrobial and amyloid peptides. *Soft matter*. 10, 38 (Sep. 2014), 7425–51.

36. Fox, J.L. 2013. Antimicrobial peptides stage a comeback. Nat Biotechnol. 2013 May;31(5):379-82. doi: 10.1038/nbt.2572.

37. Silva, O.N., Mulder, K.C.L., Barbosa, A.E.A.D., Otero-Gonzalez, A.J., Lopez-Abarrategui, C., Rezende, T.M.B., Dias, S.C. and Franco, O.L. 2011. Exploring the pharmacological potential of promiscuous host-defense peptides: from natural screenings to biotechnological applications. *Frontiers in microbiology*. 2, (Nov. 2011), 232.

38. Gaspar, D., Veiga, A.S. and Castanho, M.A.R.B. 2013. From antimicrobial to anticancer peptides. A review. *Frontiers in microbiology*. 4, (Oct. 2013), 294.

39. Mader, J.S. and Hoskin, D.W. 2006. Cationic antimicrobial peptides as novel cytotoxic agents for cancer treatment. *Expert opinion on investigational drugs*. 15, 8 (Jul. 2006), 933–40. Zheng, L.-H., Wang, Y.-J., Sheng, J., Wang, F., Zheng, Y., Lin, X.-K. and Sun, M. 2011. Antitumor peptides from marine organisms. *Marine drugs*. 9, 10 (Nov. 2011), 1840–59.

41. Hoskin, D.W. and Ramamoorthy, A. 2008. Studies on anticancer activities of antimicrobial peptides. *Biochimica et biophysica acta*. 1778, 2 (Jan. 2008), 357–75.

42. Tyagi, A., Tuknait, A., Anand, P., Gupta, S., Sharma, M., Mathur, D., Joshi, A., Singh, S., Gautam, A. and Raghava, G.P.S. 2015. CancerPPD: a database of anticancer peptides and proteins. *Nucleic acids research*. 43, Database issue (Jan. 2015), D837–43.

43. Utsugi, T., Schroit, A.J., Connor, J., Bucana, C.D. and Fidler, I.J. 1991. Elevated expression of phosphatidylserine in the outer membrane leaflet of human tumor cells and recognition by activated human blood monocytes. *Cancer research*. 51, 11 (Jun. 1991), 3062–6.

44. Riedl, S., Rinner, B., Asslaber, M., Schaider, H., Walzer, S., Novak, A., Lohner, K. and Zweytick, D. 2011. In search of a novel target - phosphatidylserine exposed by non-apoptotic tumor cells and metastases of malignancies with poor treatment efficacy. *Biochimica et biophysica acta*. 1808, 11 (Aug. 2011), 2638–45.

45. Varki A, Kannagi R, Toole BP. Glycosylation Changes in Cancer. In: Varki A, Cummings RD, Esko JD, et al., editors. Essentials of Glycobiology. 2nd edition. Cold Spring Harbor (NY): Cold Spring Harbor Laboratory Press; 2009. Chapter 44. Available from: http://www.ncbi.nlm.nih.gov/books/NBK1963/

46. Smorenburg, S.M. and Van Noorden, C.J. 2001. The complex effects of heparins on cancer progression and metastasis in experimental studies. *Pharmacological reviews*. 53, 1 (Feb. 2001), 93–105.

47. Yoon, W.H., Park, H.D., Lim, K. and Hwang, B.D. 1996. Effect of O-glycosylated mucin on invasion and metastasis of HM7 human colon cancer cells. *Biochemical and biophysical research communications*. 222, 3 (Jul. 1996), 694–9.

48. Chiu, M.H., Wan, C.-P.L., Weers, P.M.M. and Prenner, E.J. 2009. Apolipophorin III interaction with model membranes composed of phosphatidylcholine and sphingomyelin using differential scanning calorimetry. *Biochimica et biophysica acta*. 1788, 10 (Oct. 2009), 2160–8.

49. Ohvo-Rekilä, H., Ramstedt, B., Leppimäki, P. and Slotte, J.P. 2001. Cholesterol interactions with phospholipids in membranes. *Progress in lipid research*. 41, 1 (Nov. 2001), 66–97.

50. Riedl, S., Zweytick, D. and Lohner, K. 2011. Membrane-active host defense peptides--challenges and perspectives for the development of novel anticancer drugs. *Chemistry and physics of lipids*. 164, 8 (Nov. 2011), 766–81.

51. Huang, W., Seo, J., Willingham, S.B., Czyzewski, A.M., Gonzalgo, M.L., Weissman, I.L. and Barron, A.E. 2014. Learning from host-defense peptides: cationic, amphipathic peptoids with potent anticancer activity. *PloS one*. 9, 2 (Mar. 2014), e90397.

52. Won, A., Ruscito, A. and Ianoul, A. 2012. Imaging the membrane lytic activity of bioactive peptide latarcin 2a. *Biochimica et biophysica acta*. 1818, 12 (Sep. 2012), 3072–80.

53. Llaverias, G., Danilo, C., Mercier, I., Daumer, K., Capozza, F., Williams, T.M., Sotgia, F., Lisanti, M.P. and Frank, P.G. 2011. Role of cholesterol in the development and progression of breast cancer. *The American journal of pathology*. 178, 1 (Jan. 2011), 402–12.

54. Palmer, C.P., Mahen, R., Schnell, E., Djamgoz, M.B.A. and Aydar, E. 2007. Sigma-1 receptors bind cholesterol and remodel lipid rafts in breast cancer cell lines. *Cancer research*. 67, 23 (Dec. 2007), 11166–75.

55. Li, Y.C., Park, M.J., Ye, S.-K., Kim, C.-W. and Kim, Y.-N. 2006. Elevated levels of cholesterol-rich lipid rafts in cancer cells are correlated with apoptosis sensitivity induced by cholesterol-depleting agents. *The American journal of pathology*. 168, 4 (Mar. 2006), 1107–18; quiz 1404–5.

56. Zhang, Y., Lima, C.F. and Rodrigues, L.R. 2014. Anticancer effects of lactoferrin: underlying mechanisms and future trends in cancer therapy. *Nutrition reviews*. 72, 12 (Dec. 2014), 763–73.

57. van Zoggel, H., Carpentier, G., Dos Santos, C., Hamma-Kourbali, Y., Courty, J., Amiche, M. and Delbé, J. 2012. Antitumor and angiostatic activities of the antimicrobial peptide dermaseptin B2. *PloS one*. 7, 9 (Oct. 2012), e44351.

58. Chan, S.C., Hui, L. and Chen, H.M. 1999. Enhancement of the cytolytic effect of anti-bacterial cecropin by the microvilli of cancer cells. *Anticancer research*. 18, 6A (Feb. 1999), 4467–74.

59. Suttmann, H., Retz, M., Paulsen, F., Harder, J., Zwergel, U., Kamradt, J., Wullich, B., Unteregger, G., Stöckle, M. and Lehmann, J. 2008. Antimicrobial peptides of the Cecropin-family show potent antitumor activity against bladder cancer cells. *BMC urology*. 8, (Mar. 2008), 5.

60. Wu, W.K.K., Wang, G., Coffelt, S.B., Betancourt, A.M., Lee, C.W., Fan, D., Wu, K., Yu, J., Sung, J.J.Y. and Cho, C.H. 2010. Emerging roles of the host defense peptide LL-37 in human cancer and its potential therapeutic applications. *International journal of cancer. Journal international du cancer*. 127, 8 (Aug. 2010), 1741–7.

61. Lehmann, J., Retz, M., Sidhu, S.S., Suttmann, H., Sell, M., Paulsen, F., Harder, J., Unteregger, G. and Stöckle, M. 2006. Antitumor activity of the antimicrobial peptide magainin II against bladder cancer cell lines. *European urology*. 50, 1 (Jun. 2006), 141–7.

62. Wang, C., Li, H.-B., Li, S., Tian, L.-L. and Shang, D.-J. 2012. Antitumor effects and cell selectivity of temporin-1CEa, an antimicrobial peptide from the skin secretions of the Chinese brown frog (Rana chensinensis). *Biochimie*. 94, 2 (Jan. 2012), 434–41.

63. Nakamura, T., Furunaka, H., Miyata, T., Tokunaga, F., Muta, T., Iwanaga, S., Niwa, M., Takao, T. and Shimonishi, Y. 1988. Tachyplesin, a class of antimicrobial peptide from the hemocytes of the horseshoe crab (Tachypleus tridentatus). Isolation and chemical structure. *The Journal of biological chemistry*. 263, 32 (Dec. 1988), 16709–13.

64. Chen, Y., Xu, X., Hong, S., Chen, J., Liu, N., Underhill, C.B., Creswell, K. and Zhang, L. 2001. RGD-Tachyplesin inhibits tumor growth. *Cancer research*. 61, 6 (Apr. 2001), 2434–8.

65. Tian, W., Li, B., Zhang, X., Dang, W., Wang, X., Tang, H., Wang, L., Cao, H. and Chen, T. 2012. Suppression of tumor invasion and migration in breast cancer cells following delivery of siRNA against Stat3 with the antimicrobial peptide PR39. *Oncology reports*. 28, 4 (Sep. 2012), 1362–8.

66. Agerberth, B., Lee, J.Y., Bergman, T., Carlquist, M., Boman, H.G., Mutt, V. and Jörnvall, H. 1992. Amino acid sequence of PR-39. Isolation from pig intestine of a new member of the family of proline-arginine-rich antibacterial peptides. *European journal of biochemistry / FEBS*. 202, 3 (Feb. 1992), 849–54.

67. Epand, R.F., Maloy, L., Ramamoorthy, A. and Epand, R.M. 2010. Amphipathic helical cationic antimicrobial peptides promote rapid formation of crystalline states in the presence of phosphatidylglycerol: lipid clustering in anionic membranes. *Biophysical journal*. 98, 11 (Jun. 2010), 2564–73.

68. Zemel, A., Fattal, D.R. and Ben-Shaul, A. 2003. Energetics and self-assembly of amphipathic peptide pores in lipid membranes. *Biophysical journal*. 84, 4 (Apr. 2003), 2242–55.

69. Hall, K., Lee, T.-H., Mechler, A.I., Swann, M.J. and Aguilar, M.-I. 2014. Real-time measurement of membrane conformational states induced by antimicrobial peptides: balance between recovery and lysis. *Scientific reports*. 4, (Jun. 2014), 5479.

70. Strandberg, E., Tiltak, D., Ehni, S., Wadhwani, P. and Ulrich, A.S. 2013. Lipid shape is a key factor for membrane interactions of amphipathic helical peptides. *Biochimica et biophysica acta*. 1818, 7 (May. 2013), 1764–76.

71. Bechinger, B. and Lohner, K. 2006. Detergent-like actions of linear amphipathic cationic antimicrobial peptides. *Biochimica et biophysica acta*. 1758, 9 (Oct. 2006), 1529–39.

72. Mihajlovic, M. and Lazaridis, T. 2010. Antimicrobial peptides in toroidal and cylindrical pores. *Biochimica et biophysica acta*. 1798, 8 (Jun. 2010), 1485–93.

73. Yang, L., Harroun, T.A., Weiss, T.M., Ding, L. and Huang, H.W. 2001. Barrel-stave model or toroidal model? A case study on melittin pores. *Biophysical journal*. 81, 3 (Aug. 2001), 1475–85.

74. Ludtke, S.J., He, K., Heller, W.T., Harroun, T.A., Yang, L. and Huang, H.W. 1996. Membrane pores induced by magainin. *Biochemistry*. 35, 43 (Dec. 1996), 13723–8.

75. Wiesner, J. and Vilcinskas, A. 2010. Antimicrobial peptides: the ancient arm of the human immune system. *Virulence*. 1, 5 (Dec. 2010), 440–64.

77. Miteva, M., Andersson, M., Karshikoff, A. and Otting, G. 2000. Molecular electroporation: a unifying concept for the description of membrane pore formation by antibacterial peptides, exemplified with NK-lysin. *FEBS letters*. 462, 1-2 (Jan. 2000), 155–8.

78. Chan, D.I., Prenner, E.J. and Vogel, H.J. 2006. Tryptophan- and arginine-rich antimicrobial peptides: structures and mechanisms of action. *Biochimica et biophysica acta*. 1758, 9 (Oct. 2006), 1184–202.

79. Woo, H.-J. and Wallqvist, A. 2011. Spontaneous buckling of lipid bilayer and vesicle budding induced by antimicrobial peptide magainin 2: a coarse-grained simulation study. *The journal of physical chemistry. B*. 115, 25 (Jun. 2011), 8122–9.

80. Golstein, P. and Kroemer, G. 2007. Cell death by necrosis: towards a molecular definition. *Trends in biochemical sciences*. 32, 1 (Jan. 2007), 37–43.

81. Papo, N. and Shai, Y. 2005. Host defense peptides as new weapons in cancer treatment. *Cellular and molecular life sciences : CMLS*. 62, 7-8 (May. 2005), 784–90.

82. Davitt, K. et al. 2014. The anti-cancer peptide, PNC-27, induces tumor cell necrosis of a poorly differentiated non-solid tissue human leukemia cell line that depends on expression of HDM-2 in the plasma membrane of these cells. *Annals of clinical and laboratory science*. 44, 3 (Aug. 2014), 241–8.

83. Hansel, W., Leuschner, C., Gawrońska, B. and Enright, F. 2003. Targeted destruction of prostate cancer cells and xenografts by lytic peptide-betaLH conjugates. *Reproductive biology*. 1, 1 (Dec. 2003), 20–32.

84. Al-Benna, S., Shai, Y., Jacobsen, F. and Steinstraesser, L. 2011. Oncolytic activities of host defense peptides. *International journal of molecular sciences*. 12, 11 (Dec. 2011), 8027–51.

85. Huang, Y.-B., Wang, X.-F., Wang, H.-Y., Liu, Y. and Chen, Y. 2011. Studies on mechanism of action of anticancer peptides by modulation of hydrophobicity within a defined structural framework. *Molecular cancer therapeutics*. 10, 3 (Mar. 2011), 416–26.

86. Bhutia, S.K. and Maiti, T.K. 2008. Targeting tumors with peptides from natural sources. *Trends in biotechnology*. 26, 4 (Mar. 2008), 210–7.

87. Giuliani A, Pirri G, Nicoletto SF. Antimicrobial peptides: An overview of a promising class of therapeutics. Cent Eur J Biol 2007;2:1–33.

88. Longhi, C., Conte, M.P., Bellamy, W., Seganti, L. and Valenti, P. 1994. Effect of lactoferricin B, a pepsin-generated peptide of bovine lactoferrin, on Escherichia coli HB101 (pRI203) entry into HeLa cells. *Medical microbiology and immunology*. 183, 2 (Nov. 1994), 77–85.

89. Eliassen, L.T., Berge, G., Sveinbjørnsson, B., Svendsen, J.S., Vorland, L.H. and Rekdal, Ø. 2003. Evidence for a direct antitumor mechanism of action of bovine lactoferricin. *Anticancer research*. 22, 5 (Jan. 2003), 2703–10.

90. Eliassen, L.T., Berge, G., Leknessund, A., Wikman, M., Lindin, I., Løkke, C., Ponthan, F., Johnsen, J.I., Sveinbjørnsson, B., Kogner, P., Flaegstad, T. and Rekdal, Ø. 2006. The antimicrobial peptide, lactoferricin B, is cytotoxic to neuroblastoma cells in vitro and inhibits xenograft growth in vivo. *International journal of cancer. Journal international du cancer*. 119, 3 (May. 2006), 493–500.

91. Li, W.Y., Li, Q.W., Han, Z.S., Jiang, Z.L., Yang, H., Li, J. and Zhang, X.B. 2011. Growth suppression effects of recombinant adenovirus expressing human lactoferrin on cervical cancer in vitro and in vivo. *Cancer biotherapy & radiopharmaceuticals*. 26, 4 (Aug. 2011), 477–83.

92. Yoo, Y.C., Watanabe, S., Watanabe, R., Hata, K., Shimazaki, K. and Azuma, I. 1997. Bovine lactoferrin and lactoferricin, a peptide derived from bovine lactoferrin, inhibit tumor metastasis in mice. *Japanese journal of cancer research : Gann*. 88, 2 (Apr. 1997), 184–90.

93. Mader, J.S., Salsman, J., Conrad, D.M. and Hoskin, D.W. 2005. Bovine lactoferricin selectively induces apoptosis in human leukemia and carcinoma cell lines. *Molecular cancer therapeutics*. 4, 4 (Apr. 2005), 612–24.

94. Park, C.B., Yi, K.S., Matsuzaki, K., Kim, M.S. and Kim, S.C. 2000. Structure-activity analysis of buforin II, a histone H2A-derived antimicrobial peptide: the proline hinge is responsible for the cell-penetrating ability of buforin II. *Proceedings of the National Academy of Sciences of the United States of America*. 97, 15 (Aug. 2000), 8245–50.

95. Lee, H.S., Park, C.B., Kim, J.M., Jang, S.A., Park, I.Y., Kim, M.S., Cho, J.H. and Kim, S.C. 2008. Mechanism of anticancer activity of buforin IIb, a histone H2A-derived peptide. *Cancer letters*. 271, 1 (Oct. 2008), 47–55.

96. Michelakis, E.D. 2008. Mitochondrial medicine: a new era in medicine opens new windows and brings new challenges. *Circulation*. 117, 19 (May. 2008), 2431–4.

97. http://www.who.int/mediacentre/factsheets/fs297/en/

98. Bignold, L.P. 2006. Alkylating agents and DNA polymerases. *Anticancer research*. 26, 2B (Apr. 2006), 1327–36.

99. Abdulkareem, I.H. and Zurmi, I.B. 2012. Review of hormonal treatment of breast cancer. *Nigerian journal of clinical practice*. 15, 1 (Mar. 2012), 9–14.

100. Galm, U., Hager, M.H., Van Lanen, S.G., Ju, J., Thorson, J.S. and Shen, B. 2005. Antitumor antibiotics: bleomycin, enediynes, and mitomycin. *Chemical reviews*. 105, 2 (Feb. 2005), 739–58.

101. Green, D.R., Ferguson, T., Zitvogel, L. and Kroemer, G. 2009. Immunogenic and cell death. *Nature reviews. Immunology*. 9, 5 (Apr. 2009), 353–63.

102. Zitvogel, L., Casares, N., Péquignot, M.O., Chaput, N., Albert, M.L. and Kroemer, G. 2004. Immune response against dying tumor cells. *Advances in immunology*. 84, (Jul. 2004), 131–79.

103. Kim, H.J., Zheng, H., Liu, X., Du, Q., Zhang, L., Li, X. and Ma, X. 2013. Breaking the immune tolerance to apoptotic cancer cells ingested by phagocytes. *J Immunol Clin Res 1: 1001.*

104. Devocelle, M. 2012. Targeted antimicrobial peptides. *Frontiers in immunology*. 3, (Oct. 2012), 309.

105. Camilio, K.A., Rekdal, O. and Sveinbjörnsson, B. 2014. LTX-315 (Oncopore™): A short synthetic anticancer peptide and novel immunotherapeutic agent. *Oncoimmunology*. 3, (Aug. 2014), e29181.

106. Hilchie, A.L,. Coombs M.R.P. and Hoskin, D.W. 2012. Obstacles and Solutions to the Use of Cationic Antimicrobial Peptides in the Treatment of Cancer. *Small Wonders: Peptides for Disease Control.* January 1, 61-78

107. Papo, N., Seger, D., Makovitzki, A., Kalchenko, V., Eshhar, Z., Degani, H. and Shai, Y. 2006. Inhibition of tumor growth and elimination of multiple metastases in human prostate and breast xenografts by systemic inoculation of a host defense-like lytic peptide. *Cancer research*. 66, 10 (May. 2006), 5371–8.

108. Leuschner, C. and Hansel, W. 2005. Targeting breast and prostate cancers through their hormone receptors. *Biology of reproduction*. 73, 5 (Oct. 2005), 860–5.

109. Kuriyama, I., Miyazaki, A., Tsuda, Y., Yoshida, H. and Mizushina, Y. 2012. Inhibitory effect of novel somatostatin peptide analogues on human cancer cell growth based on the selective inhibition of DNA polymerase β. *Bioorganic & medicinal chemistry*. 21, 2 (Dec. 2012), 403–11.

110. Camilio, K.A., G., Ravuri, C.S., Rekdal, O. and Sveinbjørnsson, B. 2014. Complete regression and systemic protective immune responses obtained in B16 melanomas after treatment with LTX-315. *Cancer immunology, immunotherapy : CII*. 63, 6 (May. 2014), 601–13.

111. Berge, G., Eliassen, L.T., Camilio, K.A., Bartnes, K., Sveinbjørnsson, B. and Rekdal, O. 2010. Therapeutic vaccination against a murine lymphoma by intratumoral injection of a cationic anticancer peptide. *Cancer immunology, immunotherapy : CII*. 59, 8 (May. 2010), 1285–94.

112. Inoue, H. and Tani, K. 2013. Multimodal immunogenic cancer cell death as a consequence of anticancer cytotoxic treatments. *Cell death and differentiation*. 21, 1 (Dec. 2013), 39–49.

113. Matzinger, P. 1994. Tolerance, danger, and the extended family. *Annual review of immunology*. 12, (Jul. 1994), 991–1045.

114. Matzinger, P. 2002. The danger model: a renewed sense of self. *Science (New York, N.Y.)*. 296, 5566 (Apr. 2002), 301–5.

115. Thierry, A., Giraud, S., Robin, A., Barra, A., Bridoux, F., Ameteau, V., Hauet, T., Girard, J.-P., Touchard, G., Gombert, J.-M. and Herbelin, A. 2014. The alarmin concept applied to human renal transplantation: evidence for a differential implication of HMGB1 and IL-33. *PloS one*. 9, 2 (Mar. 2014), e88742.

116. Tveita, A.A. 2010. The danger model in deciphering autoimmunity. *Rheumatology (Oxford, England)*. 49, 4 (Mar. 2010), 632–9.

117. Pradeu, T. and Cooper, E.L. 2012. The danger theory: 20 years later. *Frontiers in immunology*. 3, (Jan. 2012), 287.

118. Kaczmarek, A., Vandenabeele, P. and Krysko, D.V. 2013. Necroptosis: the release of damage-associated molecular patterns and its physiological relevance. *Immunity*. 38, 2 (Feb. 2013), 209–23.

119. Jounai, N., Kobiyama, K., Takeshita, F. and Ishii, K.J. 2013. Recognition of damage-associated molecular patterns related to nucleic acids during inflammation and vaccination. *Frontiers in cellular and infection microbiology*. 2, (Jan. 2013), 168.

120. Newton, K. and Dixit, V.M. 2012. Signaling in innate immunity and inflammation. *Cold Spring Harbor perspectives in biology*. 4, 3 (Mar. 2012).

121. Iwasaki, A. and Medzhitov, R. 2010. Regulation of adaptive immunity by the innate immune system. *Science (New York, N.Y.)*. 327, 5963 (Jan. 2010), 291–5.

122. Palombo, F., Focaccetti, C. and Barnaba, V. 2014. Therapeutic implications of immunogenic cell death in human cancer. *Frontiers in immunology*. 4, (Jan. 2014), 503.

123. Garg, A.D. et al. 2012. A novel pathway combining calreticulin exposure and ATP secretion in immunogenic cancer cell death. *The EMBO journal*. 31, 5 (Mar. 2012), 1062–79.

124. Casares, N. et al. 2005. Caspase-dependent immunogenicity of doxorubicin-induced tumor cell death. *The Journal of experimental medicine*. 202, 12 (Dec. 2005), 1691–701.

125. Galluzzi, L., Maiuri, M.C., Vitale, I., Zischka, H., Castedo, M., Zitvogel, L. and Kroemer, G. 2007. Cell death modalities: classification and pathophysiological implications. *Cell death and differentiation*. 14, 7 (Jun. 2007), 1237–43.

126. Sauter, B., Albert, M.L., Francisco, L., Larsson, M., Somersan, S. and Bhardwaj, N. 2000. Consequences of cell death: exposure to necrotic tumor cells, but not primary tissue cells or apoptotic cells, induces the maturation of immunostimulatory dendritic cells. *The Journal of experimental medicine*. 191, 3 (Apr. 2000), 423–34.

127. Kershaw, M.H., Devaud, C., John, L.B., Westwood, J.A. and Darcy, P.K. 2013. Enhancing immunotherapy using chemotherapy and radiation to modify the tumor microenvironment. *Oncoimmunology*. 2, 9 (Dec. 2013), e25962.

128. Duffy, A.G. and Greten, T.F. 2013. Immunological off-target effects of standard treatments in gastrointestinal cancers. *Annals of oncology : official journal of the European Society for Medical Oncology / ESMO*. 25, 1 (Dec. 2013), 24–32.

129. Ha, T.-Y. 2010. The role of regulatory T cells in cancer. *Immune network*. 9, 6 (Feb. 2010), 209–35.

130. Kroemer, G., Galluzzi, L., Kepp, O. and Zitvogel, L. 2013. Immunogenic cell death in cancer therapy. *Annual review of immunology*. 31, (Mar. 2013), 51–72.

131. Krysko, O., Løve Aaes, T., Bachert, C., Vandenabeele, P. and Krysko, D.V. 2013. Many faces of DAMPs in cancer therapy. *Cell death & disease*. 4, (May. 2013), e631.

132. Bianchi, M.E. 2013. Killing cancer cells, twice with one shot. *Cell death and differentiation*. 21, 1 (Dec. 2013), 1–2.

133. Kepp, O., Galluzzi, L., Martins, I., Schlemmer, F., Adjemian, S., Michaud, M., Sukkurwala, A.Q., Menger, L., Zitvogel, L. and Kroemer, G. 2011. Molecular determinants of immunogenic cell death elicited by anticancer chemotherapy. *Cancer metastasis reviews*. 30, 1 (Feb. 2011), 61–9.

134. Elliott, M.R., Chekeni, F.B., Trampont, P.C., Lazarowski, E.R., Kadl, A., Walk, S.F., Park, D., Woodson, R.I., Ostankovich, M., Sharma, P., Lysiak, J.J., Harden, T.K., Leitinger, N. and Ravichandran, K.S. 2009. Nucleotides released by apoptotic cells act as a find-me signal to promote phagocytic clearance. *Nature*. 461, 7261 (Sep. 2009), 282–6.

135. Baroja-Mazo, A., Barberà-Cremades, M. and Pelegrín, P. 2013. P2X7 receptor activation impairs exogenous MHC class I oligopeptides presentation in antigen presenting cells. *PloS one*. 8, 8 (Aug. 2013), e70577.

136. Ghiringhelli, F. et al. 2009. Activation of the NLRP3 inflammasome in dendritic cells induces IL-1beta-dependent adaptive immunity against tumors. *Nature medicine*. 15, 10 (Oct. 2009), 1170–8.

137. Martins, I., Tesniere, A., Kepp, O., Michaud, M., Schlemmer, F., Senovilla, L., Séror, C., Métivier, D., Perfettini, J.-L., Zitvogel, L. and Kroemer, G. 2009. Chemotherapy induces ATP release from tumor cells. *Cell cycle (Georgetown, Tex.)*. 8, 22 (Nov. 2009), 3723–8.

138. Aymeric, L., Apetoh, L., Ghiringhelli, F., Tesniere, A., Martins, I., Kroemer, G., Smyth, M.J. and Zitvogel, L. 2010. Tumor cell death and ATP release prime dendritic cells and efficient anticancer immunity. *Cancer research*. 70, 3 (Feb. 2010), 855–8.

139. Gombault, A., Baron, L. and Couillin, I. 2013. ATP release and purinergic signaling in NLRP3 inflammasome activation. *Frontiers in immunology*. 3, (Jan. 2013), 414.

140. Raucci, A., Palumbo, R. and Bianchi, M.E. 2007. HMGB1: a signal of necrosis. *Autoimmunity*. 40, 4 (May. 2007), 285–9.

141. Andersson, U., Erlandsson-Harris, H., Yang, H. and Tracey, K.J. 2002. HMGB1 as a DNA-binding cytokine. *Journal of leukocyte biology*. 72, 6 (Dec. 2002), 1084–91.

142. Wang, H. et al. 1999. HMG-1 as a late mediator of endotoxin lethality in mice. *Science (New York, N.Y.)*. 285, 5425 (Jul. 1999), 248–51.

143. Chen, G.Y. and Nuñez, G. 2010. Sterile inflammation: sensing and reacting to damage. *Nature reviews. Immunology*. 10, 12 (Nov. 2010), 826–37.

144. Vanden Berghe, T., Linkermann, A., Jouan-Lanhouet, S., Walczak, H. and Vandenabeele, P. 2014. Regulated necrosis: the expanding network of non-apoptotic cell death pathways. *Nature reviews. Mol. cell biology*. 15, 2 (Jan. 2014), 135–47.

145. Lotze, M.T. and Tracey, K.J. 2005. High-mobility group box 1 protein (HMGB1): nuclear weapon in the immune arsenal. *Nature reviews. Immunology*. 5, 4 (Apr. 2005), 331-42.

146. Kim, S., Kim, S.Y., Pribis, J.P., Lotze, M., Mollen, K.P., Shapiro, R., Loughran, P., Scott, M.J. and Billiar, T.R. 2013. Signaling of high mobility group box 1 (HMGB1) through 4 in macrophages requires CD14. *Molecular medicine (Cambridge, Mass.)*. 19, (May. 2013), 88–98.

147. Apetoh, L. et al. 2007. Toll-like receptor 4-dependent contribution of the immune system to anticancer chemotherapy and radiotherapy. *Nature medicine*. 13, 9 (Sep. 2007), 1050–9.

148. Yamazaki, T., Hannani, D., Poirier-Colame, V., Ladoire, S., Locher, C., Sistigu, A., Prada, N., Adjemian, S., Catani, J.P.P., Freudenberg, M., Galanos, C., André, F., Kroemer, G. and Zitvogel, L. 2013. Defective immunogenic cell death of HMGB1-deficient tumors: compensatory therapy with TLR4 agonists. *Cell death and differentiation*. 21, 1 (Dec. 2013), 69–78.

149. Sims, G.P., Rowe, D.C., Rietdijk, S.T., Herbst, R. and Coyle, A.J. 2010. HMGB1 and RAGE in inflammation and cancer. *Annual review of immunology*. 28, (Mar. 2010), 367–88.

150. Yanai, H., Ban, T. and Taniguchi, T. 2012. High-mobility group box family of proteins: ligand and sensor for innate immunity. *Trends in immunology*. 33, 12 (Nov. 2012), 633–40.

151. Jube, S., Rivera, Z.S., Bianchi, M.E., Powers, A., Wang, E., Pagano, I., Pass, H.I., Gaudino, G., Carbone, M. and Yang, H. 2012. Cancer cell secretion of the DAMP protein HMGB1 supports progression in malignant mesothelioma. *Cancer research*. 72, 13 (Jul. 2012), 3290–301.

152. Zhao, C.-B., Bao, J.-M., Lu, Y.-J., Zhao, T., Zhou, X.-H., Zheng, D.-Y. and Zhao, S.-C. 2014. Co-expression of RAGE and HMGB1 is associated with cancer progression and poor patient outcome of prostate cancer. *American journal of cancer research*. 4, 4 (Jul. 2014), 369–77.

153. Hansen, T., Ausbacher, D., Zachariassen, Z.G., Anderssen, T., Havelkova, M. and Strøm, M.B. 2012. Anticancer activity of small amphipathic $\beta^{2,2}$-amino acid derivatives. *European journal of medicinal chemistry*. 58, (Dec. 2012), 22–9.

154. Strøm, M.B., Haug, B.E., Skar, M.L., Stensen, W., Stiberg, T. and Svendsen, J.S. 2003. The pharmacophore of short cationic antibacterial peptides. *Journal of medicinal chemistry*. 46, 9 (Apr. 2003), 1567–70.

155. Midura-Nowaczek, K. and Markowska, A. 2014. Antimicrobial peptides and their analogs: searching for new potential therapeutics. *Perspectives in medicinal chemistry*. 6, (Nov. 2014), 73–80.

156. Ausbacher, D., Svineng, G., Hansen, T. and Strøm, M.B. 2012. Anticancer mechanisms of action of two small amphipathic β(2,2)-amino acid derivatives derived from antimicrobial peptides. *Biochimica et biophysica acta*. 1818, 11 (Aug. 2012), 2917–25.

157. Mosmann, T. 1984. Rapid colorimetric assay for cellular growth and survival: application to proliferation and cytotoxicity assays. *Journal of immunological methods*. 65, 1-2 (Feb. 1984), 55–63.

158. Riss T.L., Moravec R.A., Niles A.L., Benink H.A., Worzella T.J. and Minor, L. 2013. Cell Viability Assays. Assay Guidance Manual [Internet]. Bethesda (MD): Eli Lilly & Company and the National Center for Advancing Translational Sciences; 2004 http://www.ncbi.nlm.nih.gov/books/NBK144065/

159. McELROY, W.D. and KIPNIS, D.M. 1948. The mechanism of inhibition of bioluminescence by nephthoquinones. *Journal of cellular physiology*. 30, 3 (Dec. 1948), 359–80.

160. http://www.nature.com/app_notes/nmeth/2006/063006/full/an1755.html#References

161. Mahmood, T. and Yang, P.-C. 2012. Western blot: technique, theory, and trouble shooting. *North American journal of medical sciences*. 4, 9 (Oct. 2012), 429–34.

162. Jensen, E.C. 2012. The basics of western blotting. *Anatomical record (Hoboken, N.J. : 2007)*. 295, 3 (Feb. 2012), 369–71.

163. https://www.lifetechnologies.com/no/en/home/life-science/protein-biology/protein-gel electrophoresis/protein-standards-ladders/western-blot-protein-ladders.html

164. http://www.abcam.com/hmgb1-antibody-chip-grade-ab18256.html

165. http://www.rndsystems.com/Products/mctc0/Citations

166. Bozzola JJ, Russell LD: Specimen Preparation for Transmission Electron Microscopy. In Electron Microscopy. Principles and Techniques for Biologists. Volume 2. 2nd edition. Edited by Bozzola JJ, Russell LD. Sudbury, MA: Jones and Bartlett Publishers; 1998:17–47.

167. Hopwood, D. 1970. A comparison of the crosslinking abilities of glutaraldehyde, formaldehyde and alpha-hydroxyadipaldehyde with bovine serum albumin and casein. *Histochemie. Histochemistry. Histochimie*. 17, 2 (Feb. 1970), 151–61.

168. Kiernan JA. Formaldehyde, formalin, paraformaldehyde and glutaraldehyde: what they are and what they do. Microsc Today. 2000;00–1:8–12.

169. Ellis, E.A. 2013. Staining sectioned biological specimens for transmission electron microscopy: conventional and en bloc stains. *Methods in molecular biology (Clifton, N.J.)*. 1117, (Dec. 2013), 57–72.

170. Goldberg, M. and Septier, D. 1986. Improved lipid preservation by malachite green-glutaraldehyde fixation in rat incisor predentine and dentine. *Archives of oral biology*. 30, 10 (Feb. 1986), 717–26.

171. Stirling, J.W. 1993. Use of tannic acid and silver enhancer to improve staining for electron microscopy and immunogold labeling. *The journal of histochemistry and cytochemistry : official journal of the Histochemistry Society*. 41, 4 (Apr. 1993), 643–8.

172. Leonard, J.B. and Shepardson, S.P. 1994. A comparison of heating modes in rapid fixation techniques for electron microscopy. *The journal of histochemistry and cytochemistry : official journal of the Histochemistry Society*. 42, 3 (Mar. 1994), 383–91.

173. Webster, P. 2013. Microwave-assisted processing and embedding for transmission electron microscopy. *Methods in molecular biology (Clifton, N.J.)*. 1117, (Dec. 2013), 21–37.

174. Giberson, R.T. and Demaree, R.S. 1996. Microwave fixation: understanding the variables to achieve rapid reproducible results. *Microscopy research and technique*. 32, 3 (Feb. 1996), 246–54.

175. Tinling, S.P., Giberson, R.T. and Kullar, R.S. 2004. Microwave exposure increases bone demineralization rate independent of temperature. *Journal of microscopy*. 215, Pt 3 (Aug. 2004), 230–5.

176. Cocchiaro, J.L., Kumar, Y., Fischer, E.R., Hackstadt, T. and Valdivia, R.H. 2008. Cytoplasmic lipid droplets are translocated into the lumen of the Chlamydia trachomatis parasitophorous vacuole. *Proceedings of the National Academy of Sciences of the United States of America*. 105, 27 (Jul. 2008), 9379–84.

177. Teicher, B.A. 2002. Tumor models in cancer research. *Second edition. Humana Press. Pp. 84-85, Alvarez. E.*

178. Chiang, E.Y., Henson, M. and Stroynowski, I. 2003. Correction of defects responsible for impaired Qa-2 class Ib MHC expression on melanoma cells protects mice from tumor growth. *Journal of immunology (Baltimore, Md.: 1950)*. 170, 9 (Apr. 2003), 4515–23.

179. http://www.lgcstandards-atcc.org/products/all/CRL-6323.aspx?geo_country=no

180. Overwijk, W.W. and Restifo, N.P. 2008. B16 as a mouse model for human melanoma. *Current protocols in immunology / edited by John E. Coligan ... [et al.]*. Chapter 20, (Apr. 2008), Unit 20.1.

181. Martins, I., Michaud, M., Sukkurwala, A.Q., Adjemian, S., Ma, Y., Shen, S., Kepp, O., Menger, L., Vacchelli, E., Galluzzi, L., Zitvogel, L. and Kroemer, G. 2012. Premortem autophagy determines the immunogenicity of chemotherapy-induced cancer cell death. *Autophagy*. 8, 3 (Aug. 2012), 413–5.

182. Krysko, D.V., Garg, A.D., Kaczmarek, A., Krysko, O., Agostinis, P. and Vandenabeele, P. 2012. Immunogenic cell death and DAMPs in cancer therapy. *Nature reviews. Cancer*. 12, 12 (Nov. 2012), 860–75.

183. Goldstein, J.C., Waterhouse, N.J., Juin, P., Evan, G.I. and Green, D.R. 2000. The coordinate release of cytochrome c during apoptosis is rapid, complete and kinetically invariant. *Nature cell biology*. 2, 3 (May. 2000), 156–62.

184. Yang, J., Liu, X., Bhalla, K., Kim, C.N., Ibrado, A.M., Cai, J., Peng, T.I., Jones, D.P. and Wang, X. 1997. Prevention of apoptosis by Bcl-2: release of cytochrome c from mitochondria blocked. *Science (New York, N.Y.)*. 275, 5303 (Mar. 1997), 1129–32.

185. Soballe, P.W., Maloy, W.L., Myrga, M.L., Jacob, L.S. and Herlyn, M. 1995. Experimental local therapy of human melanoma with lytic magainin peptides. *International journal of cancer. Journal international du cancer*. 60, 2 (Feb. 1995), 280–4.

186. Sen, T.Z., Jernigan, R.L., Garnier, J. and Kloczkowski, A. 2005. GOR V server for protein secondary structure prediction. *Bioinformatics (Oxford, England)*. 21, 11 (May. 2005), 2787–8.

187. Huang, Y.-B., He, L.-Y., Jiang, H.-Y. and Chen, Y.-X. 2012. Role of helicity on the anticancer mechanism of action of cationic-helical peptides. *International journal of molecular sciences*. 13, 6 (Jul. 2012), 6849–62.

188. Dennison, S.R., Whittaker, M., Harris, F. and Phoenix, D.A. 2006. Anticancer alpha-helical peptides and structure/function relationships underpinning their interactions with tumour cell membranes. *Cur, prot. & pep. science*. 7, 6 (Dec. 2006),487–99.

189. Srisailam, S., Kumar, T.K., Arunkumar, A.I., Leung, K.W., Yu, C. and Chen, H.M. 2001. Crumpled structure of the custom hydrophobic lytic peptide cecropin B3. *European journal of biochemistry / FEBS*. 268, 15 (Aug. 2001), 4278–84.

190. Simons, K. and Ikonen, E. 2000. How cells handle cholesterol. *Science (New York, N.Y.)*. 290, 5497 (Dec. 2000), 1721–6.

191. Papo, N., Shahar, M., Eisenbach, L. and Shai, Y. 2003. A novel lytic peptide composed of DL-amino acids selectively kills cancer cells in culture and in mice. *The Journal of biological chemistry*. 278, 23 (Jun. 2003), 21018–23.

192. Yang, Q.-Z., Wang, C., Lang, L., Zhou, Y., Wang, H. and Shang, D.-J. 2013. Design of potent, non-toxic anticancer peptides based on the structure of the antimicrobial peptide, temporin-1CEa. *Archives of pharmacal research*. 36, 11 (Nov. 2013), 1302–10.

193. Choy, H. 2001. Taxanes in combined modality therapy for solid tumors. *Critical reviews in oncology/hematology*. 37, 3 (Mar. 2001), 237–47.

194. Kroemer, G. et al. 2008. Classification of cell death: recommendations of the Nomenclature Committee on Cell Death 2009. *Cell death and differentiation*. 16, 1 (Dec. 2008), 3–11.

195. González-Polo, R.-A., Boya, P., Pauleau, A.-L., Jalil, A., Larochette, N., Souquère, S., Eskelinen, E.-L., Pierron, G., Saftig, P. and Kroemer, G. 2005. The apoptosis/autophagy paradox: autophagic vacuolization before apoptotic death. *Journal of cell science*. 118, Pt 14 (Jul. 2005), 3091–102.

196. Levine, B. and Yuan, J. 2005. Autophagy in cell death: an innocent convict? *The Journal of clinical investigation*. 115, 10 (Oct. 2005), 2679–88.

197. Das, G., Shravage, B.V. and Baehrecke, E.H. 2012. Regulation and function of autophagy during cell survival and cell death. *Cold Spring Harbor perspectives in biology*. 4, 6 (Jun. 2012).

198. Khodarev, N.N., Roach, P., Pitroda, S.P., Golden, D.W., Bhayani, M., Shao, M.Y., Darga, T.E., Beveridge, M.G., Sood, R.F., Sutton, H.G., Beckett, M.A., Mauceri, H.J., Posner, M.C. and Weichselbaum, R.R. 2009. STAT1 pathway mediates amplification of metastatic potential and resistance to therapy. *PloS one*. 4, 6 (Jun. 2009), e5821.

199. van der Most, R.G., Robinson, B.W.S. and Lake, R.A. 2010. Combining immunotherapy with chemotherapy to treat cancer. *Discovery medicine*. 5, 27 (Jan. 2010), 265–70.

200. Ménard, C., Martin, F., Apetoh, L., Bouyer, F. and Ghiringhelli, F. 2008. Cancer chemotherapy: not only a direct cytotoxic effect, but also an adjuvant for antitumor immunity. *Cancer immunology, immunotherapy : CII*. 57, 11 (Aug. 2008), 1579–87.

201. Zitvogel, L., Apetoh, L., Ghiringhelli, F., André, F., Tesniere, A. and Kroemer, G. 2008. The anticancer immune response: indispensable for therapeutic success? *The Journal of clinical investigation*. 118, 6 (Jun. 2008), 1991–2001.

202. Liu, Y. and Zeng, G. 2012. Cancer and innate immune system interactions: translational potentials for cancer immunotherapy. *Journal of immunotherapy (Hagerstown, Md. : 1997)*. 35, 4 (Apr. 2012), 299–308.

203. Ayna, G., Krysko, D.V., Kaczmarek, A., Petrovski, G., Vandenabeele, P. and Fésüs, L. 2012. ATP release from dying autophagic cells and their phagocytosis are crucial for inflammasome activation in macrophages. *PloS one*. 7, 6 (Jul. 2012), e40069.

204. Fitz, J.G. 2008. Regulation of cellular ATP release. *Transactions of the American Clinical and Climatological Association*. 118, (Jun. 2008), 199–208.

205. Tang, D., Kang, R., Zeh, H.J. and Lotze, M.T. 2010. High-mobility group box 1 and cancer. *Biochimica et biophysica acta*. 1799, 1-2 (Feb. 2010), 131–40.

206. Ullrich, E., Bonmort, M., Mignot, G., Kroemer, G. and Zitvogel, L. 2007. Tumor stress, cell death and the ensuing immune response. *Cell death and differentiation*. 15, 1 (Dec. 2007), 21–8.

207. Guerriero, J.L., Ditsworth, D., Catanzaro, J.M., Sabino, G., Furie, M.B., Kew, R.R., Crawford, H.C. and Zong, W.-X. 2011. DNA alkylating therapy induces tumor regression through an HMGB1-mediated activation of innate immunity. *Journal of immunology (Baltimore, Md. : 1950)*. 186, 6 (Mar. 2011), 3517–26.

208. Yang, H., Lundbäck, P., Ottosson, L., Erlandsson-Harris, H., Venereau, E., Bianchi, M.E., Al-Abed, Y., Andersson, U., Tracey, K.J. and Antoine, D.J. 2012. Redox modification of cysteine residues regulates the cytokine activity of high mobility group box-1 (HMGB1). *Molecular medicine (Cambridge, Mass.)*. 18, (Apr. 2012), 250–9.

209. Carta, S., Castellani, P., Delfino, L., Tassi, S., Venè, R. and Rubartelli, A. 2009. DAMPs and inflammatory processes: the role of redox in the different outcomes. *Journal of leukocyte biology*. 86, 3 (Sep. 2009), 549–55.

210. Gogvadze, V., Orrenius, S. and Zhivotovsky, B. 2006. Multiple pathways of cytochrome c release from mitochondria in apoptosis. *Biochimica et biophysica acta*. 1757, 5-6 (Jul. 2006), 639–47.

211. Ow, Y.-L.P., Green, D.R., Hao, Z. and Mak, T.W. 2008. Cytochrome c: functions beyond respiration. *Nature reviews. Molecular cell biology*. 9, 7 (Jun. 2008), 532–42.

212. Pullerits, R., Bokarewa, M., Jonsson, I.-M., Verdrengh, M. and Tarkowski, A. 2004. Extracellular cytochrome c, a mitochondrial apoptosis-related protein, induces arthritis. *Rheumatology (Oxford, England)*. 44, 1 (Dec. 2004), 32–9.

213. Kepp, O., Tesniere, A., Zitvogel, L. and Kroemer, G. 2009. The immunogenicity of tumor cell death. *Current opinion in oncology*. 21, 1 (Jan. 2009), 71–6.

214. Kepp, O., Senovilla, L. and Kroemer, G. 2014. Immunogenic cell death inducers as anticancer agents. *Oncotarget*. 5, 14 (Aug. 2014), 5190–1.

Personal communications

Rekdal Ø, Professor II, Molecular inflammation research group, Department of Medical Biology, University of Tromsø

Sveinbjørnsson B, Professor, Molecular inflammation research group, Department of Medical Biology, University of Tromsø

Appendix A - Solutions

Table. A.1. 1x PBS

Solution	Amount
PBS tablets	2
Milli-Q water	1000 ml

Table. A.2. MTT stock solution (5 mg/ml)

Solution	Amount
MTT	50 mg
1X PBS	10.0 ml

Table. A.3. 0.04 M HCl in isopropanol

Solution	Amount
Isopropanol (Absolute)	1 L
HCl (37%, 12.08 M)	0.33 L

Table. A.4. 1x Running Buffer

Solution	Amount
Running buffer (20x)	35.0 ml
dH_2O	675 ml

Table. A.6. Blotting Buffer

Solution	Amount
Tris	5.8 g
Glycin	29 g
MeOH	100 ml
dH_2O	900 ml

Table. A.7. 1x TBS-T

Solution	Amount
1 M Tris (pH 7.5)	20.0 ml
Tween 20	1.0 ml
5 M NaCl	100 ml
dH_2O	879 ml

→ pH was adjusted to 8.4 by adding 37 % HCl

Table. A.8. 5 % Blocking Buffer

Solution	Amount
Low fat milk powder	2.5 g
1x TBS-T	50.0 ml

Table. A.9. 4x PHEM Buffer (for 100 ml), pH 6.9

Solution	Amount
PIPES 240 mM	7.26 g
HEPES 100 mM	2.38 g
$MgCl_2$*$6H_2O$ 8 mM	0.16 g
EGTA 40 mM (Ethylene glycol tetraacetic acid)	1.52 g

→ Since PIPES does not dissolve until pH is raised, drops of NaOH were applied to the solution while mixing to yield pH 6.9 (monitored by pH-meter). A 1x solution (0.1 M) was made by diluting in 300 ml

Table. A.10. 1x Malachite Green fixative

Solution	Amount
1 % Malachite Green	0.2 ml
25 % Glutaraldehyde	0.8 ml
16 % Formaldehyde	1.0 ml
0.1 M PHEM Buffer	2.0 ml

→ The 1 % Malachite Green stock solution was prepared by mixing 0.1 g of the salt in 10.0 ml dH_2O

Table. A.11. Cacodyl buffer (0.2 M), pH 7.4

Solution	Amount
Sodium cacodylate	4.28 g
dH_2O	80 ml

→ pH was adjusted to 7.4 with HCl

Table. A.12. 1 % Osmium reduced ferrocyanide

Solution	Amount
4 % Osmium tetroxide	2.5 ml
4 % Ferrocyanide	2.0 ml
0.2 M Cacodyl buffer	5.0 ml
dH_2O	0.5 ml

→ The 4 % stock solution of ferrocyanide ($K_3Fe(CN)_6$) was prepared by mixing 0.4 g of the salt with 10.0 ml dH_2O. Osmium tetroxide is commercially available as a 4 % solution

Table. A.13. Agar resin

Solution	Amount
Agar 100	10.0 ml
DDSA (dodecenyl succinic anhydride)	6.0 ml
NMA (nadic methyl anhydride)	7.5 ml
DMP-30 (2,4,6-trimethylamine methylphenol)	0.5 ml

Appendix B

Program settings for the *PELCO Biowave® Pro*

Step#	Description	User Prompt (on/off)	Time (Hr:min:sec)	Power (Watts)	Temp (ºC)	Load Cooler (off/auto/on)	Vacuum/ Bubbler Pump (off/ bub/ vac cycle/ vac on/ vap)	SteadyTemp pump (on/off)	SteadyTemp temp (ºC)
Protocol #9 Mal Green Fixation									
1	MalGreen GA fix	Off	0: 2: 0	100	50	Off	vacuum on	On	23
2	MalGreen GA fix	Off	0: 2: 0	0	50	Off	vacuum on	On	23
3	MalGreen GA fix	Off	0: 2: 0	100	50	Off	vacuum on	On	23
4	MalGreen GA fix	Off	0: 2: 0	0	50	Off	vacuum on	On	23
5	MalGreen GA fix	Off	0: 2: 0	100	50	Off	vacuum on	On	23
6	MalGreen GA fix	Off	0: 2: 0	0	50	Off	vacuum on	On	23
7	MalGreen GA fix	Off	0: 2: 0	100	50	Off	vacuum cycle	On	23
	2 bench washes								
8	PHEM Buffer	On	0: 0: 40	250	50	Off	Off	On	23
9	PHEM Buffer	On	0: 0: 40	250	50	Off	Off	On	23
10	Osmium	On	0: 2: 0	100	50	Off	vacuum cycle	On	23
11	Osmium	Off	0: 2: 0	0	50	Off	vacuum on	On	23
12	Osmium	Off	0: 2: 0	100	50	Off	vacuum on	On	23
13	Osmium	Off	0: 2: 0	0	50	Off	vacuum on	On	23
14	Osmium	Off	0: 2: 0	100	50	Off	vacuum on	On	23
15	Osmium	Off	0: 2: 0	0	50	Off	vacuum on	On	23
16	Osmium	Off	0: 2: 0	100	50	Off	vacuum cycle	On	23
	2 bench washes								
17	PHEM Buffer	On	0: 0: 40	250	50	Off	Off	On	23
18	PHEM Buffer	On	0: 0: 40	250	50	Off	Off	On	23
19	Tannic Acid	On	0: 1: 0	150	50	Off	vacuum cycle	On	23
20	Tannic Acid	Off	0: 1: 0	0	50	Off	vacuum on	On	23
21	Tannic Acid	Off	0: 1: 0	150	50	Off	vacuum on	On	23
22	Tannic Acid	Off	0: 1: 0	0	50	Off	vacuum on	On	23
23	Tannic Acid	Off	0: 1: 0	150	50	Off	vacuum on	On	23
24	Tannic Acid	Off	0: 1: 0	0	50	Off	vacuum on	On	23
25	Tannic Acid	Off	0: 1: 0	150	50	Off	vacuum cycle	On	23
	2 bench washes								
26	PHEM Buffer	On	0: 0: 40	250	50	Off	Off	On	23
27	Water	On	0: 0: 40	250	50	Off	Off	On	23
28	Water	On	0: 0: 40	250	50	Off	Off	On	23
	2 bench washes								
29	UA	On	0: 1: 0	150	50	Off	vacuum cycle	On	23
30	UA	Off	0: 1: 0	0	50	Off	vacuum on	On	23
31	UA	On	0: 1: 0	150	50	Off	vacuum on	On	23
32	UA	Off	0: 1: 0	0	50	Off	vacuum on	On	23
33	UA	Off	0: 1: 0	150	50	Off	vacuum on	On	23
34	UA	Off	0: 1: 0	0	50	Off	vacuum on	On	23
35	UA	Off	0: 1: 0	150	50	Off	vacuum cycle	On	23
36	Water	On	0: 0: 40	250	50	Off	Off	On	23
37	Water	On	0: 0: 40	250	50	Off	Off	On	23
38	25% ETOH	On	0: 0: 40	250	50	Off	Off	On	23
39	50% ETOH	On	0: 0: 40	250	50	Off	Off	On	23
40	70% ETOH	On	0: 0: 40	250	50	Off	Off	On	23
41	90% ETOH	On	0: 0: 40	250	50	Off	Off	On	23
42	100% ETOH	On	0: 0: 40	250	50	Off	Off	On	23
43	100% ETOH	On	0: 0: 40	250	50	Off	Off	On	23
44	100% ETOH	On	0: 0: 40	250	50	Off	Off	On	23
Protocol #11 - Resin infiltration									
1	Resin 1:2	On	0: 3: 0	250	50	Off	vacuum cycle	On	23
2	Resin 100	On	0: 3: 0	250	50	Off	vacuum cycle	On	23
3	Resin 100	On	0: 3: 0	250	50	Off	vacuum cycle	On	23

Appendix C – Assessment of human endpoints (*in vivo* experiments)

Score N = **Normal, nothing out of the ordinary**
Score 1 = **Slightly influenced, animals must be followed closely**
Score 2 = **Significantly influenced, animals must be euthanized**

Examples of score 1

- **Weightloss < 10 %**
- **Visible tumor, but less than maximal allowed size (i.e. < 12-13 mm i diameter)**
- **Necrosis, but without ulceration**

Examples of Score 2:

- **Weightloss ≧ 10 %**
- **Tumor ≧ 12-13 mm i diameter**
- **Ulceration of the tumor**
- **Bristling fur, inactivity, hunched posture**

The form is filled out for each animal three times per week, in connection with bodyweight measurements. If any symptoms are observed in between these day by the animal care workers, the local competent person and responsible scientist must be notified.

Prosjekt ID (FOTS nr og lokal forsøksnr):											
Mus nummer (bur og øremerke):											
Start kroppsvekt (dag 0 av forsøket):											
Datoer og tid for injeksjoner:	**Inj. 1:**										
	Inj. 2:										
	Inj. 3										
	Inj. 4										
	Inj. 5										
Vurdering av dyrets tilstand gjennom forsøket (Score N, 1 eller 2)											
Uke nr. i eksperimentet	1	2	3	4	5	6	7	8	9	10	11
Dag av eksperimentet											
Observasjoner (påfør N, 1 eller 2 etter angitte kriterier)											
Uforstyrret aktivitet											
Oppførsel											
Kroppsholdning											
Utseende, pels, egenpleie											
Kroppsvekt (g)											
% av utgangsvekt											
Generell status muskler/fett											
Bukomfang											
Tumorstørrelse											
Tumorutseende											
INITIALER (Observatør)											

Appendix D – Confirmation of Felasa C certificate

NB! Not receiving course diploma/certificate before summer of 2015

Copy of email:

"CONFIDENTIAL FELASA Examination

Jeffrey Roy Needham Add to contacts 4/19/2015
To: Brynjar Mauseth

Dear Brynjar

Congratulations.

I am very happy to be able to inform you that your hard work was worthwhile and you passed the recent FELASA examination.

Well done and good luck in the future.

Best wishes"